Università degli Studi di Cagliari

DOTTORATO DI RICERCA
BIOLOGIA E BIOCHIMICA DELL'UOMO E DELL'AMBIENTE
Ciclo XXVIII

Characterization of Ebola virus VP35-dsRNA binding for drug development against Ebola virus disease.

Settore scientifico disciplinare di afferenza

MICROBIOLOGIA GENERALE (BIO/19)

Presentata da:
Dott. Gian Luca Daino

Relatore:
Prof. Enzo Tramontano

Coordinatore Dottorato:
Prof. Emanuele Sanna

ABSTRACT

The Ebola virus (EBOV) VP35 protein plays an important role in the inhibition of the initial innate immune responses to EBOV infection leading to Ebola virus disease development. In fact, VP35 interaction with the RIG-I like receptors (RLR) cascade components inhibits the interferon (IFN) production, impeding proper host immune response. It has been shown that VP35 is a validate drug target. Full-length His-tagged recombinant VP35 (rVP35) has been previously expressed in prokaryotic system and used to validate a biochemical pull-down assay for the screening of small molecules targeted to the VP35-double strand (ds)-RNA interactions. However, low rVP35 amount of purified protein and the use of radioactive substrate for binding evaluation, strongly limited the screening system. In the present study, a new method for high-yield rVP35 expression and purification, based on denaturation and subsequent protein refolding was established. Subsequently, a novel assay based on the use of Nickel-coated plates using a fluorescent labeled 30mer dsRNA was validated, showing a VP35 K_d value for dsRNA binding around 4 nM, comparable to the one previously reported, and a Z'-factor equal to 0.69, that indicate a good assay.

The use of this biochemical assay to screen the ability of plant extracts and derived compounds to inhibit the rVP35 binding to dsRNA allowed to identified a few small molecules able to inhibit the VP35-dsRNA binding with IC50 values in the low micromolar range. Active plant extracts and derived compounds were also tested in a cellular assay to evaluate their ability to counteract the inhibitory activity of VP35 on the IFN response. We identified a number of compounds able to inhibit the VP35 function in biochemical assay but ineffective in the cellular system. Conversely, some other compound, unable to inhibit rVP35 binding to dsRNA in biochemical assay, subverted VP35 inhibition of IFN production in

cellular assay. These results suggested that the VP35 binding to dsRNA may not be the driving force of the VP35 inhibition of the IFN cascade and that an alternative mechanisms of action could be hypothesized for those compounds not able to inhibit VP35-dsRNA binding but effective against the VP35 IFN inhibitory effect. An interesting compound showed activity in both biochemical and cellular assays, suggesting the possibility that some small molecules interact with VP35 in such way to disrupt its interaction with multiple targets.

In order to understand the relative role of VP35-dsRNA binding in inhibiting the RLR cascade, we studied the effects of the lack of VP35 dimerization, considered essential for VP35 binding to dsRNA. For this purpose, three single point mutations, proposed to be essential for VP35 dimerization, were introduced into the coiled-coil VP35 domain. We confirmed by in silico studies that introduction of these three mutations disrupted coiled-coil dimerization. The importance of VP35 dimerization for VP35-dsRNA binding was confirmed by biochemical assay studies, where the mutant rVP35 showed a reduce ability to bind dsRNA. However, the mutant VP35 expressed in a cellular system showed a limited reduction of the ability of IFN production inhibition compared to the wild-type VP35. These results seem to confirm the hypothesis that VP35 binding to dsRNA is not the main interaction needed for VP35 inhibition of the IFN production and suggested that the VP35 interactions with cellular components do not require VP35 dimerization.

In conclusion, we demonstrated that small molecules interacting with VP35 can subvert its inhibition of the IFN production, possibly inhibiting its interactions with cellular components of RLR pathway and suggested that VP35 binding to dsRNA is not the driving for VP35 inhibition RLR cascade activation.

TABLE OF CONTENTS

1 INTRODUCTION

1.1 Taxonomy

Ebolaviruses is a viral genus comprising a group of five species of filamentous, enveloped with a linear non-segmented single-stranded genome of negative polarity. Because the characteristics of their genome, described above, they have been assigned to the order of *Mononegavirales.* Other main and peculiar characteristics of the members belonging to this order are the following: the genomic RNA is uncapped, not polyadenylated and not covalently linked to any protein; the replication occurs through the synthesis of a complete antigenoma; the gene order within the genome is 3'-UTR-core protein genes-envelope protein gene-polymerase gene-5'-UTR; the formation of helical NCs (Kuhn et al., 2010) (Figure 1).

Furthermore, for their particular morphology, their longer genomes and the fact that their genome encodes for two unusual proteins (VP30 and VP24) they are grouped in *Filoviridae* family, with other two genera *Marburgvirus* and newly assigned *Cuevavirus* (Adams et al., 2014; Kuhn et al., 2010). The family name is derived from the Latin word "filum", that means thread, reflecting the unique filamentous morphology of the family *Filoviridae* members (Figure 2). Marburgviruses and ebolaviruses are the only members of the order *Mononegavirales* that cause viral hemorrhagic fever in human and non-human primates (NHPs).

The genus *Marburgvirus* includes two clades: Marburg virus (MARV) and Ravn virus (RAVV) in a single species *Marburg marburgvirus*, whereas the genus Ebolavirus consists of five distinct species, *Zaire ebolavirus*, *Sudan ebolavirus*, *Taï*

Forest ebolavirus (formerly *Cote d'Ivoire ebolavirus*), *Bundibugyo ebolavirus* and *Reston ebolavirus*. According to the rules for taxon naming established by the International Committee on Taxonomy of Viruses (ICTV), the names of members of species of Ebolavirus genus are respectively Ebola virus (EBOV), Sudan virus (SUDV), Taï Forest virus (TAFV), Bundibugyo virus (BDBV) and Reston virus (RESTV).

The genus *Cuevavirus* includes only one specie *Lloviu cuevavirus*, with the newly found Lloviu virus (LLOV), detected from carcasses of Schreiber's bats in a Europe (Negredo et al., 2011).

Following the last review of taxonomy, the order of *Mononegavirales* include eight families: *Bornaviridae*, *Filoviridae*, *Mymonaviridae*, *Nyamiviridae*, *Paramyxoviridae*, *Pneumoviridae*, *Rhabdoviridae*, *Sunviridae*, together with five non assigned viruses (Afonso et al., 2016).
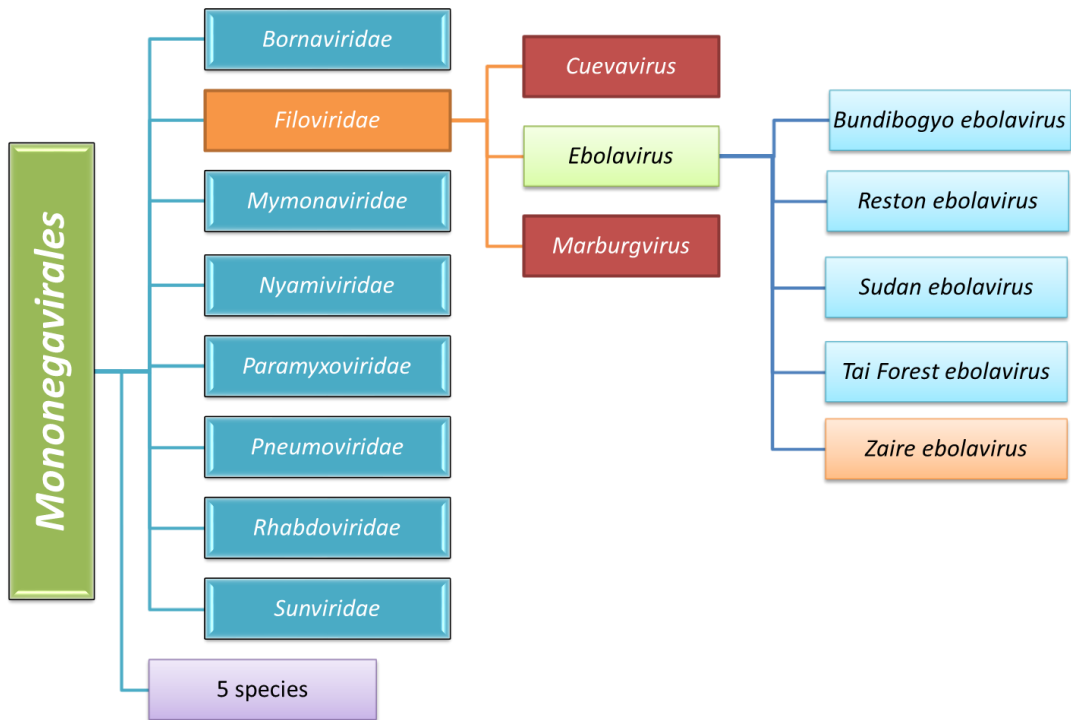
Figure 1 – Taxonomy of *Zaire ebolavirus* specie.
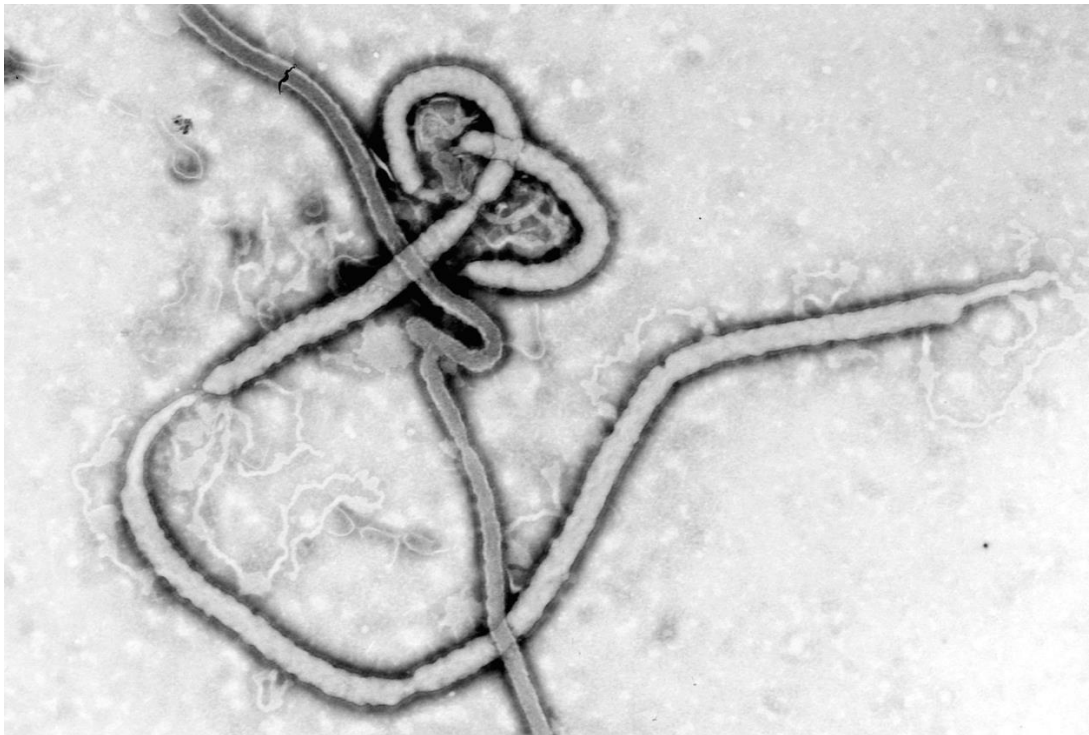
Figure 2 - First electron micrograph of an Ebola viral particle dated 1976, showing the characteristic filamentous structure of a member of family Filoviridae (Murphy, F.A.-CDC)

1.2   Genome, proteins and structure

Most membrane-enveloped viruses have quasi-spherical structure of virion, whereas filovirus particles may appear in several shapes, a biological feature named pleomorphism. These shapes include long, sometimes branched filaments, as well as shorter filaments shaped like a "6", a "U", or a circle (ICTV, 2011). Family *Filoviridae* members differ in length of virions, but are very similar in morphology. In EBOV, virions are rarely straight and show a uniform diameter of about 80 nm, but they vary greatly in length up to 20 μm and more. The most common length of viral particles is around 980 nm The other classes of length found are multiple of this length, revealing that EBOV organization may have the capacity for a modular polyploidy, being able to generate continuous virions, which have two or more genome copies enveloped together. Actually, several different morphologies have been observed (Figure 3): "single" particles, containing a NC) of uniform length (which have been supposed to contain one copy of the genome), ''continuous'' particles, with NCs of a length of the single virion multiplied by an integer of 2 or greater and ''linked'' virions composed of a series single-genome nucleocapsids connected by short sections of empty envelope (Beniac et al., 2012).

As all other mononegaviruses, filoviruses have filamentous helical NCs, but differently from those, they are unique among animal viruses for having the whole virion, not only the NC, highly filamentous, like many plant viruses (Booth et al., 2013). This morphology is unusual for mammalian viruses and is considered characteristic for members of the family (ICTV, 2011).

The genomes of filoviruses consist of a single stranded, non-segmented negative-
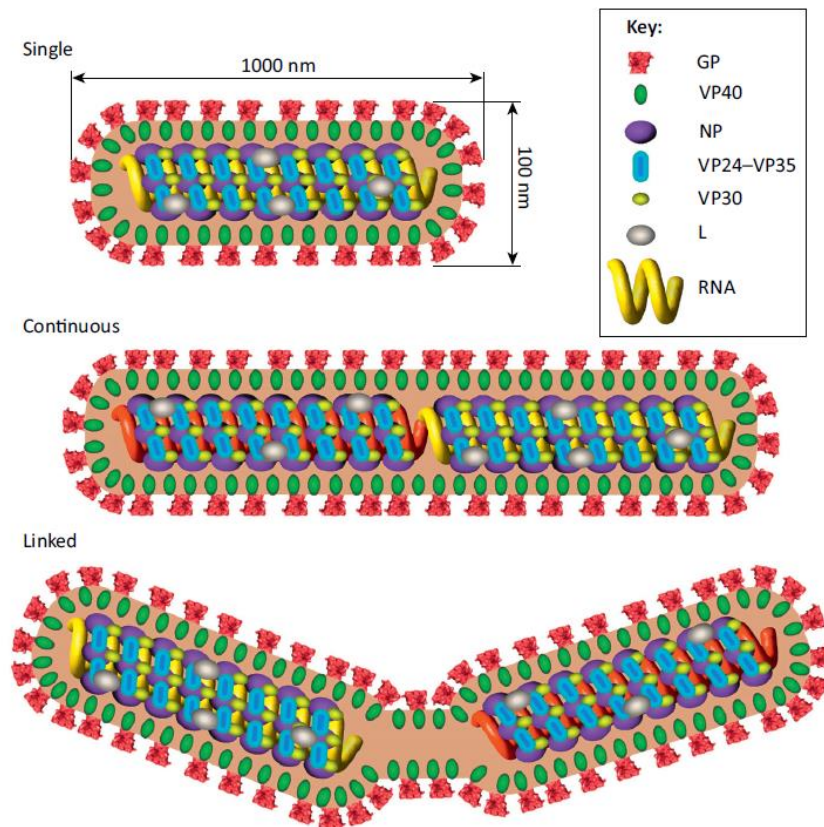
Figure 3- The three different types of EBOV virion structures. Single virions (top) have one copy of the genome; continuous virions (centre) and linked virions (bottom) are polyploid and have two or more copies of the genome. The nucleocapsid consists of NP (nucleoprotein), L ('large', polymerase), and viral proteins VP35, VP30, and VP24, and the envelope has two integral membrane proteins, the VP40 matrix protein on the cytoplasmic side and the externally exposed glycoprotein (GP) spike (Beniac et al., 2012).

sense (NNS) RNA of about 19 kb in length. The EBOV genome contains seven genes in the following order: 3'-NP-VP35-VP40-GP-VP30-VP24-L-5', separated by short intergenic regions (IR) (4–5 non-conserved nucleotides) or overlapping gene sequences (Figure 4). There is only one longer IR: in ebolaviruses it is located between the VP30 and VP24 gene whereas in marburgviruses between the GP and VP30 gene. At the beginning and end of each gene there are highly conserved transcription start and stop signals (Mühlberger, 2007; Sanchez et al., 1993).

EBOV genome presents some other differences with MARV: EBOV noncoding sequences located at the 3' and 5' ends of the viral genomes, called *leader* and *trailer*, are significantly different from MARV for the length. These extragenic regions contain promoters for replication and transcription (Neumann et al., 2009). Furthermore, EBOV genome reveals three gene overlaps, between the VP35 and VP40, the GP and VP30 and the VP24 and L genes whereas the MARV genome contains only one between VP30 and VP24 (Sanchez et al., 1993). The translation of EBOV GP needs the editing activity of the viral polymerase, whereas the GP of MARV is transcribed from a single open reading frame (ORF) (Mühlberger et al., 1999) (Figure 4, Figure 5).

EBOV genome encodes for seven structural viral proteins and two non-structural proteins: the nucleoprotein NP; the polymerase cofactor VP35; the matrix protein VP40; the non-structural soluble glycoprotein (sGP), the structural glycoprotein GP and the small soluble glycoprotein (ssGP) , all encoded by editing from the same GP gene (Figure 5) (Mehedi et al., 2011); VP30; VP24 and the RNA-dependent RNA polymerase L (Mühlberger, 2007).
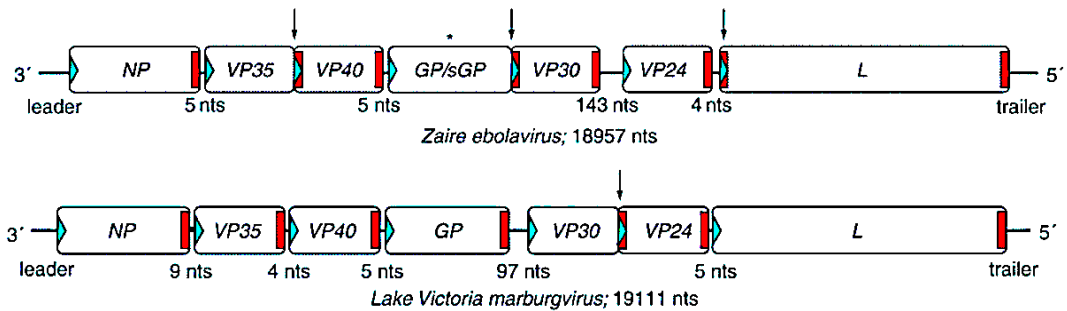
Figure 4 – Genome organization of ebolaviruses and marburgviruses. The genes are depicted as boxes and nontranscribed regions as black horizontal bars (leader, trailer and intergenic regions). Transcription start signals are depicted as green triangles and stop signals as red bars. Gene overlaps are marked by arrows. Asterisk indicates the mRNA editing site within the EBOV GP gene. Below the gene representation is shown the length of the intergenic regions. Note that the EBOV VP24 gene contains two transcription stop signals (Mühlberger, 2007).
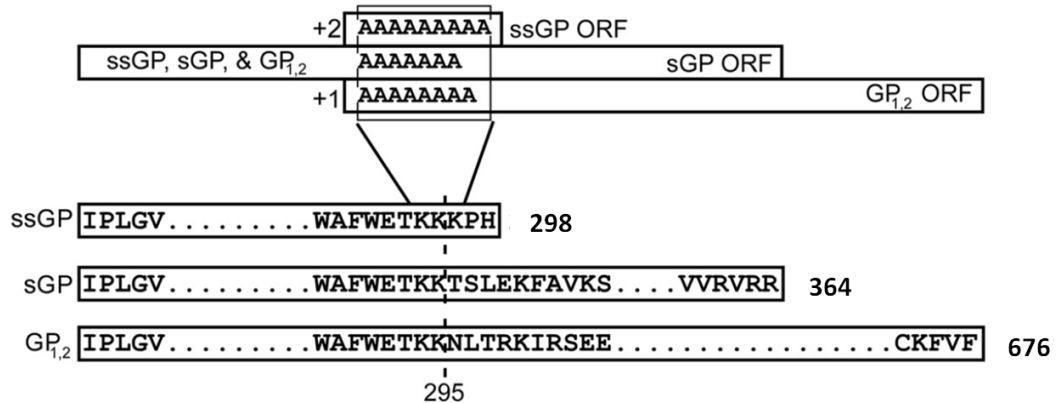
Figure 5 - EBOV glycoprotein gene RNA editing. On the top are depicted the open reading frames for the different GP gene products. On the bottom are shown the primary structures of glycoprotein gene products in relation to the primary amino acid sequences of sGP, $GP_{1,2}$, and ssGP. All three proteins share the first 295 aa but differ in their carboxy-terminal portions (Mehedi et al., 2011 modified).

The coding region of each gene consists of a central open reading frame (ORF) with highly-conserved transcription initiation and termination sequences that contain the pentameric sequence 3'-UAAUU-5' (Mühlberger, 2007).

NP is considered the driving force for the formation of NC. With its primary sequence of 739 amino acid residues and a predicted molecular mass of 83.3 kDa is the largest nucleoprotein of the NNS RNA viruses. It shows two domains: a hydrophobic N-terminal and a hydrophilic C-terminal domain. NP presents O-glycosilation and sialylation, required for its interactions with VP35 and probably important for genome replication. EBOV NP, similarly to other NNS RNA viruses, is able to self-assemble to form helical tubes but these are morphologically different from nucleocapsids. The N-terminal half (from amino acids 1 to 450) is important for NP-NP interactions, while a longer region (from amino acids 1 to 600) is required for the formation of nucleocapsid-like structures and for replication of the viral genome. Lastly, the final 50 amino is thought to be involved in the interaction with VP40 for NC incorporation into virions (Watanabe et al., 2006).

VP35 plays multiple roles during virus infection: actually, VP35 is a component of the viral RNA polymerase complex, a structural/assembly factor and a suppressor of host interferon (IFN) responses (Leung et al., 2009a). EBOV VP35 is a 340 amino acid protein of a 35 kDa mass, that contains an N-terminal coiled coil domain essential for the oligomerization (Reid et al., 2005) and a C-terminal RBD (Hartman et al., 2004; Leung et al., 2009a; Weingartl et al., 2012) (Figure 6A).

Oligomerization of VP35 is important for virus replication, being required for interaction with the L protein (Leung et al., 2009a), and for a full suppression of IFN response (Reid et al., 2005).
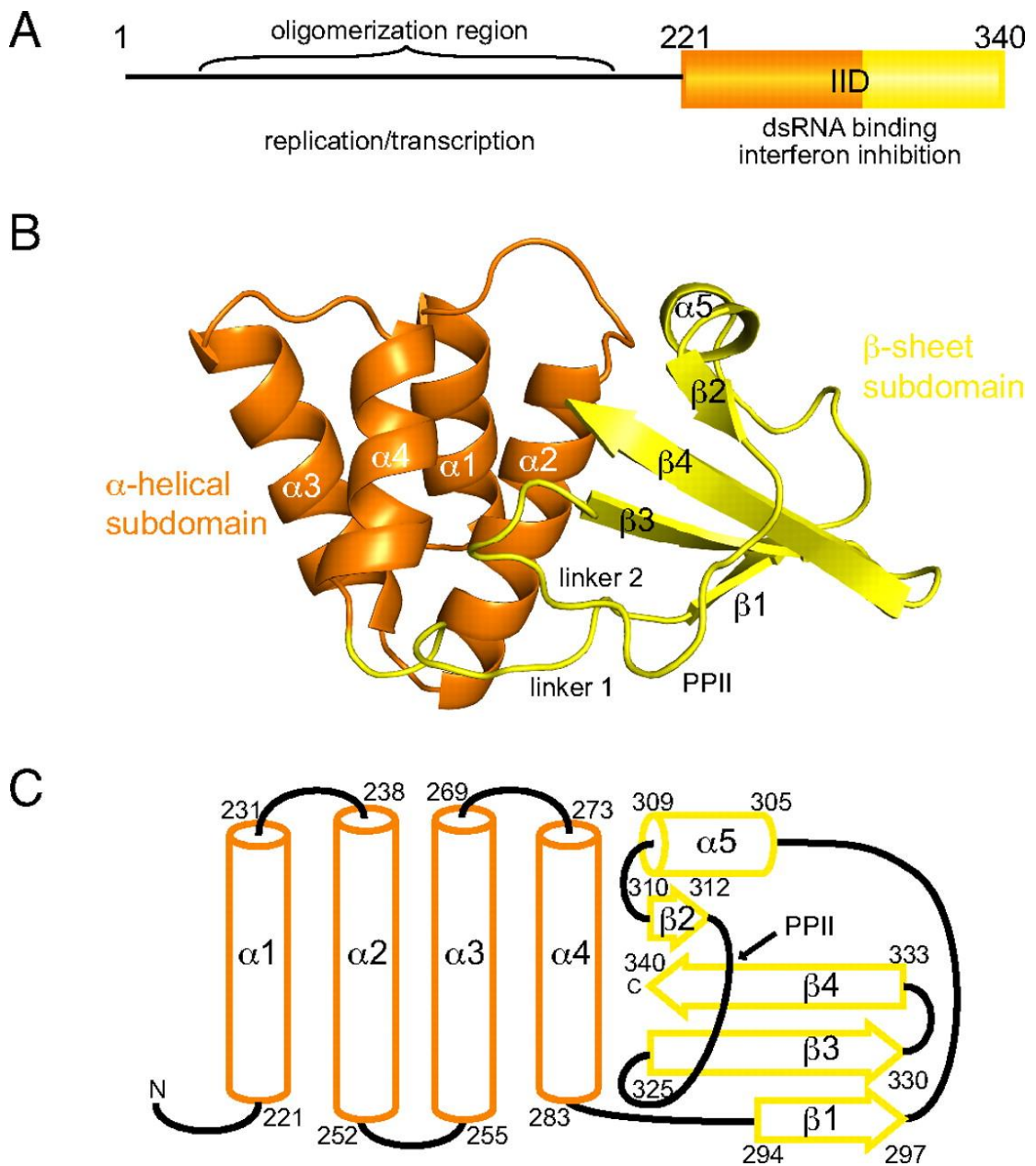
Figure 6 - Crystal structure of VP35 C-terminal IFN-inhibitory domain (IID). (A) Domain organization of full-length VP35. (B) Ribbon representation of VP35 IID. Secondary structural elements that form the α-helical subdomain (orange) and the β-sheet subdomain (yellow). (C) Topology and delimiting sequence markers of VP35 IID (Leung et al., 2009a).

VP35 interacts with L and NP leading to the formation of trimeric complexes in which VP35 serves as a bridge between NP and L (Trunschke et al., 2013). Crystal structure of EBOV full-length VP35 has not yet been determined: are known only the crystal structures of C-terminal RBD (221-340 amino acid residues) (Leung et al., 2009a) (Figure 6B,C) and the structure of C-terminal RBD (215-340 amino acid residues) bound to 8 bases pair (bp) dsRNA, where VP35 forms an asymmetric homodimer and binds both the phosphate backbone of dsRNA (Leung et al., 2010a). VP35 RBD, also called IFN inhibitory domain (IID) because of its role in IFN-antagonist function, consists of two subdomains that form a single independently folded unit: an α-helical subdomain that consists of four α-helix, spanning from residue 221 up to 283, arranged in two layers and a β-sheet subdomain that consists of four-stranded β-sheet with a short helix (residues 294-340). The α-helical and the β-sheet subdomains are connected one to the other by a short, flexible, 10 residues-long linker region (Leung et al., 2009a) (Figure 6). The C-terminal domain of VP35 includes two basic patches: the first basic patch (FBP) is important for interactions with EBOV NP and VP35 polymerase cofactor function (Prins et al., 2010a); the central basic patch (CBP) is important for VP35-dsRNA binding and IFN inhibition (Leung et al., 2009a). Being the VP35 protein the main topic of this work, its structure and functions will be more deeply analyzed in other subsequent parts of the thesis.

The matrix protein VP40 is the most abundant protein in virions and has been shown to be important for EBOV budding and for virus structure and stability. VP40 is made up of 326 amino acids and consists of two domains connected by a flexible linker: even in this case, the N-terminal domain is responsible for oligomerization of

VP40, while the C-terminal domain is required to bind the plasma membrane. It has been shown that for an efficient process of the binding to the membrane and the subsequent particle formation by VP40, its oligomerization is required (Baz-Martínez et al., 2016).

The surface GP protein is the only EBOV structural glycoprotein and is encoded after a process of mRNA editing caused by the slippage of the viral polymerase that insert an extra adenosine (A) (8 instead of 7 consecutive A residues) during transcription of mRNA. Thus, the EBOV GP gene is able to generate three different mRNAs coding for protein precursors pre-sGP, pre-GP and ssGP in a cell type dependent ratio of approximately 14:5:1, respectively (Mehedi et al., 2011). GP consists in 676 amino acid residues and, after translation, undergoes a proteolytic cleavage at the position 324 by host enzyme furin that gives rise to two disulphide-linked heterodimers GP_1 and GP_2. These two proteins are linked by disulfide bonds and form a trimeric chalice structure: the bowl of the chalice, that forms surface spikes on the virion, is shaped by the GP_1 subunits, while GP_2 organizes and anchors the complex to the membrane (Lee et al., 2008; Martin et al., 2016). GP_1 effects attachment to host cells, whereas GP_2 mediates fusion of viral and host membranes (Lee et al., 2008). The unedited transcript of GP gene encodes for a non-structural glycoproteins, the 364 amino acid residues sGP. In the case of a further addition of 1 residue, the editing process inserts 9 adenosines at the editing site and such mRNA encodes for a third GP gene product ssGP (298 amino acid residues) (Figure 5) (Mehedi et al., 2011; Mühlberger, 2007). Pre-sGP undergoes a cleavage at position 324, giving rise to sGP, that is N-glycosylated and secreted as antiparallel orientation homodimer, and a 40 amino acids residues peptide (Δ-peptide) that is O-glycosylated

before to be secreted (Martin et al., 2016; Volchkova et al., 1999). ssGP is N-glycosylated and secreted as a homodimer (Mehedi et al., 2011).

The fifth EBOV gene codes for the viral protein VP30, a 288 amino acid residues protein with a molecular mass of 32 kDa acting as a component of the EBOV NC and is a viral polymerase cofactor important for EBOV transcription. Its structure has been just partially solved and several functional domains have been identified (Kuhn, 2008; Martin et al., 2017). Its C-terminal structure has been solved by X-ray crystallography: it forms a globular structure composed of α-helices that can homodimerize. Furthermore, a basic amino acid cluster has been shown to play a role in interaction with NP and in transcriptional control activity (Hartlieb et al., 2007). In the N-terminal domain different domains have been identified: a hydrophobic leucine-zipper motif involved in hexamerization that represents the active conformation to support viral mRNA transcription (Hartlieb et al., 2007, 2003) and a zinc finger that plays a critical role in transcription activation (Modrof et al., 2003). Phosphorylation of VP30 has been shown to modulate viral transcription and replication as well as interaction of VP30 with the polymerase complex proteins VP35 and NP (Biedenkopf et al., 2013). Even if VP30 is a RNA binding protein (John et al., 2007), it is thought that the effects of VP30 phosphorylation on viral RNA synthesis are triggered by modulation of the VP30-VP35 interaction, which changes the composition of the polymerase complex (Biedenkopf et al., 2013).

The sixth gene codes for VP24, a matrix protein of 251 amino acid residues with a molecular weight of 28.2 kDa. The viral protein VP24 plays a structural role in viral assembly and also in an antagonist of the host innate immune response to viral infection (Kuhn, 2008). The crystal structure of VP24 has been determined, showing

a compact single domain with a triangular pyramidal shape, seven α-helices (α1 and α5-10) and a small, three-stranded, antiparallel β-sheet (β1-3) forming the top of the pyramid with the N-terminus at the apex. A five-stranded antiparallel β sheet (β4-8) forms the center, while a second collection of α helices (α2-4) forms the base. VP24 antagonizes IFN signaling by binding host karyopherin α proteins, preventing in this way the transport of the tyrosine-phosphorylated transcription factor STAT1 to the nucleus, and by binding STAT1 directly, suppressing at least two distinct branches of the IFN pathway (Zhang et al., 2012). Moreover, VP24 plays a role in the assembly of a fully functional ribonucleocapsid complex, contributing to the budding of virus-like particles (VLPs) (Han et al., 2003), and modulates transcription and genome replication when interacting with the ribonucleoprotein complex (Booth et al., 2013).

While several studies have brought insights into the structure/function of NP, VP35 and VP30, much less is known about the essential L protein. No crystal structure of the L protein of filoviruses is available yet. This large protein of about 2200 amino acids has an estimated molecular mass of 250 kDa (Volchkov et al., 1999). Six conserved regions (I to VI) have been identified in all viruses of the order Mononegavirales. They include three enzymatic domains: RNA-dependent RNA polymerase (RdRp) required for replication/transcription and polyadenylation, and polyribonucleotidyltranferase (PRNTase) and methyltransferase (MTase) required for mRNA capping. The determination of the structure of the L protein of vesicular stomatitis virus (VSV), which also belongs to the order Mononegavirales and the analogies with other viral polymerases suggest that RNA synthesis and capping are highly coordinated in mononegaviruses (Martin et al., 2017).

Filoviruses have the most complex NCs of all members of the *Mononegavirales*, being composed by five different proteins: NP, VP30, VP35, VP24 and L together with the 18.9 kb RNA genome, surrounded by a lipid envelope derived from the host-cell plasma membrane.

Using the same methods of investigations (cryoelectron microscopy and cryoelectron tomography to analyze purified and isolated EBOV and EBOV-like structures), two different models of EBOV NC are proposed: curiously for Beniac et al. the EBOV NC is a right-handed double layered helix with an outer diameter of 41 nm, a pitch of is 6.96 nm and a inner hollow channel of 16 nm in diameter (Beniac et al., 2012), whereas for Bharat et al. it is a left-handed helix both for MARV with a pitch of 7.5 nm (Bharat et al., 2011) and for EBOV with a pitch of 7.4 nm (Bharat et al., 2012).

NP, VP30 and VP35 show RNA-binding activity (Booth et al., 2013), whereas VP24 and VP35 both independently associate with NP (Beniac et al., 2012). Three filovirus proteins, VP24, VP35, and NP have been shown to be essential for NC-like structure formation (Huang et al., 2002).

NCs produced by EBOV and those generated by transfection with VP35, VP30, VP24 and NP or with only VP35, VP24 and NP (without VP30) are indistinguishable, showing approximately the same diameter (~50 nm). This indicates that VP30 does not increase the NC diameter (Beniac et al., 2012).
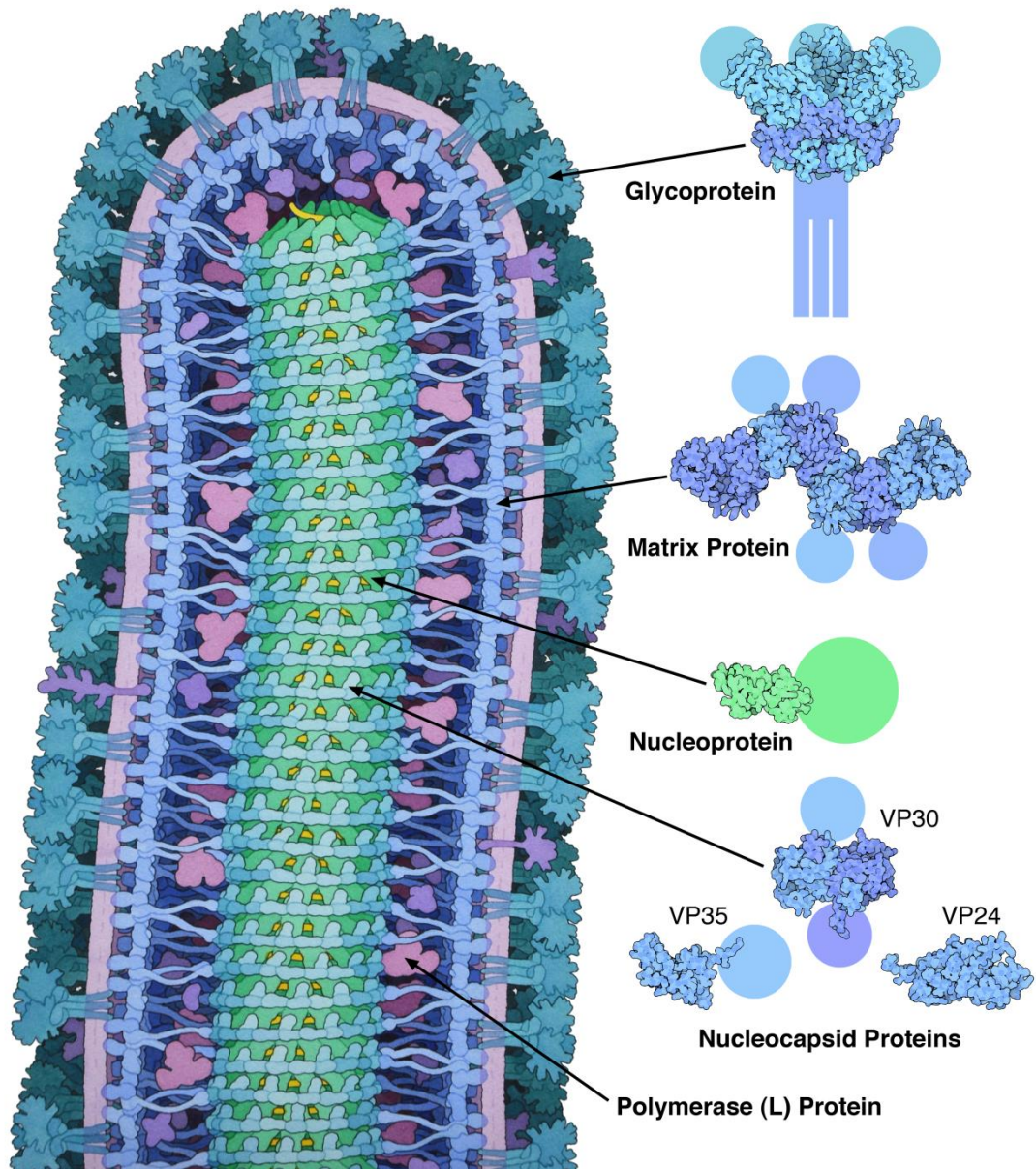
Figure 7 – A watercolor painting illustration of an Ebola virus particle by David Goodsell of The Scripps Research Institute by which he has won the top prize in the 2016 "Wellcome Image Awards". Longitudinal section of ebola virion shows proteins in blue, green and magenta, the RNA genome in yellow, and the membrane in light purple. Atomic structures are shown on the right, with portions that have not been determined shown with schematic circles. GP forms surface spikes on the virion envelope, while VP40 is associated with the inner surface. NP, VP35, VP30, VP24 and L participate to the nucleocapsid formation. The inner canal harbours the RNA genome.

1.3   Epidemiology, ecology and reservoirs

Most of the known filoviruses are pathogenic in primates, including humans, and are endemic in Africa, with the only two exceptions of RESTV, that appears to be pathogenic in NHPs but not in humans and is endemic in the Philippines, and the member of the new species *Lloviu cuevavirus* (Negredo et al., 2011). The firstly identified cases of filoviruses disease occurred in 1967 in Marburg (Germany), during an outbreak in laboratory staff exposed to tissues from African green monkeys (*Cercopithecus aethiops*) imported from Uganda, immediately followed by other cases in Frankfurt (Germany) and in Belgrade (former Yugoslavia). Total cases identified were 31, plus one afterwards detected subsequent serologic investigations, and the dead were 7, with a mortality rate of 23%. Broader epidemics of MARV occur in Watsa, Democratic Republic of Congo (DRC), in 1998-2000 and in Uige, Angola, in 2004-2005 with 149 reported cases with a case fatality rate (CFR) of 83% in DRC and 374 cases with a CFR of 88% in Angola (Sanchez et al., 2007) .

In 1976 two different outbreaks appeared simultaneously in two neighboring regions of the DRC and Sudan with 318 (CFR of 88%) and 284 cases (CFR of 53%), respectively (Table 1). The related etiological agent was names Ebola from the name of a river flowing in northwestern DRC. The fact that these two epidemics were caused by different viruses was determined only some years later by serological investigation: the first mentioned epidemic was caused by EBOV, whereas the second one by SUDV. One year later, a single deadly EBOV case occur in Tandala (DRC) no far from the original site of outbreak of 1976. In 1979, 22 people on 34 cases (CFR 65%) died in Sudan for a SUDV outbreak.

Table 1 – Ebola virus disease (EVD) outbreaks chronology – DRC: Democratic Republic of Congo

Year(s)	Country	Ebola	Number of human cases	Number of deaths among cases	CFR (%)
2014	Multiple villages - DRC	EBOV	66	49	74,2
2014-2016	Multiple countries	EBOV	28652	11325	39,5
2012-2013	Luwero District -Uganda	SUDV	6	3	50,0
2012	Isiro - Province Orientale - DRC	BDBV	36	13	36,1
2012	Kibaale District -Uganda	SUDV	11	4	36,4
2011	Luwero district -Uganda	SUDV	1	1	100,0
2008-2009	Mweka and Luebo -DRC	EBOV	32	15	46,9
2007-2008	Bundibugyo District - Uganda	BDBV	149	37	24,8
2007	Kasai Occidental Province - DRC	EBOV	264	187	70,8
2004	Russia (Lab. contamination)	EBOV	1	1	100,0
2004	Yambio -Sudan (South Sudan)	SUDV	17	7	41,2
2003	Mbomo district - Republic of the Congo	EBOV	35	29	82,9
2002-2003	Mbomo and Kéllé districts - Republic of the Congo	EBOV	143	128	89,5
2001-2002	Republic of the Congo	EBOV	57	43	75,4
2001-2002	Gabon	EBOV	65	53	81,5
2000-2001	Gulu, Masindi, and Mbarara districts - Uganda	SUDV	425	224	52,7
1996	Russia (Lab. contamination)	EBOV	1	1	100,0
1996	Johannesburg -South Africa	EBOV	2	1	50,0
1996-1997	Booué - Gabon	EBOV	60	45	75,0
1996	Mayibout - Gabon	EBOV	37	21	56,8
1995	Kikwit - DRC (formerly Zaire)	EBOV	315	250	79,4
1994	Tai Forest - Republic of Côte d'Ivoire	TAFV	1	0	0
1994	Mékouk - Gabon	EBOV	52	31	59,6
1979	Nzara and Maridi - Sudan (South Sudan)	SUDV	34	22	64,7
1977	Tandala - Zaire	EBOV	1	1	100,0
1976	England (Lab. contamination)	SUDV	1	0	0
1976	Nzara and Maridi - Sudan (South Sudan)	SUDV	284	151	53,2
1976	Yambuku - DRC (formerly Zaire)	EBOV	318	280	88,1

No further cases of viral hemorrhagic fevers caused by ebolaviruses were reported until 1994, when a scientist studying primates was infected by a virus while performing a chimpanzee autopsy. The animal came from a group that had lost several members to an illness later identified as Ebola hemorrhagic fever (Le Guenno et al., 1995). The etiological agent was classified as a new species of ebolavirus originally named *Cote d'Ivoire ebolavirus* and subsequently changed in *Tai Forest ebolavirus* (Kuhn et al., 2010). The most recent ebolavirus classified as new species was discovered in 2007 during a wide epidemic on the west border of Uganda in the town of Bundibugyo, from which the new virus has taken the species name, *Bundibugyo ebolavirus* (Towner et al., 2008).

Reston ebolavirus is the fifth species of the genus Ebolavirus. RESTV is geographically distributed in the Philippines. It was described for the first time in 1989, when an unusually high mortality was noted during quarantine in monkeys imported in the USA from the Philippines. The virus was isolated from the monkey *Macaca fascicularis*. The name of the virus came from Reston in Virginia, where was sited the facility for the animals quarantine. Subsequently, RESTV has been found in the Philippines on several occasions, not only in monkeys but surprisingly even in pigs (Feldmann and Geisbert, 2011).

Further epidemics of ebolaviruses occurred in Africa from 1995 to date, mainly caused by EBOV, except three provoked by SUDV in 2000 (Gulu District in Uganda), 2004 (Yambio County in Sudan) and 2012 (Luwero District in Uganda), with a CFR of 53% (224/425 dead/cases), 41% (7/17) and 50% (3/6) respectively.

Other extensive EBOV outbreaks have been reported in 1995 in Kikwit, 2001 in Mbomo and 2007 in Luebo, all in DRC, showing a CFR of 81% (315/250), 89%

(143/128) and 71% (264/187), respectively (Centers for Disease Control and Prevention, 2016). Kikwit outbreak was hospital-amplified, misdiagnosed clinically as bacterial dysentery, caused the death of a cluster of health care workers infected while assisting, largely unprotected from exposure, at the laparotomies performed on an infected laboratory technician thought to have an acute surgical abdomen. The Kikwit has been the first outbreak involving the media attention and a number of lessons learned from the outbreak led to a reorganization of the international response to infectious disease emergencies (Heymann et al., 1999).

Most of the EBOV epidemics occurred in central Africa except two cases: firstly, the reported infection of two people in South Africa (Joannesburg) in 1996 caused by a medical professional arriving from Gabon after having treated Ebola-infected patients and having been exposed to the virus. He was hospitalized, and a nurse who took care of him became infected and died (Centers for Disease Control and Prevention, 2016; Sanchez et al., 2007); lastly, the largest epidemic caused by filovirus ever happened that occurred in West Africa from 2014 to 2016. The outbreak began in rural Guinea in December 2013 (Elston et al., 2017), and spreads to neighbouring countries of Sierra Leone, Liberia, where also affects urban areas, Senegal, Mali and Nigeria and involving non-African countries as USA, UK, Italy and Spain. Have been reported 28646 cases and 11323 dead, with a CFR of 40% (World Health Organization, 2016a).

The dynamics of epidemic filoviral diseases involves humans, great apes and other primates. Also other mammalian species seems to be susceptible to Ebola virus infection. However, none of these has been reported to be the reservoir species. In fact, several lines of evidence point towards the possibility that fruit bats could be the

EBOV natural reservoir. The detection of viral RNA and anti-EBOV antibodies in three tree-roosting species of fruit bats, *Hypsignathus monstrosus*, *Epomops franqueti*, and *Myonycteris torquata,* provided the first evidences that bats are implicated as reservoirs and vectors for transmission of filoviruses in Africa (Feldmann and Geisbert, 2011). MARV sequences have been subsequently found in fruit (*Rousettus aegyptiacus*) and insectivorous (*Rhinolophus eloquens* and *Miniopterus inflatus*) bats, supporting the hypothesis that bats are reservoir species for filoviruses (Negredo et al., 2011).

Although EBOV has never been isolated from bats in the wild, the possibility that bats are a reservoir for EBOV is also supported by many studies on MARV. An ecological investigation in the Python Cave, Uganda revealed that out of 1622 bats captured and tested between 2008 and 2009, 2.5% were infected with MARV, and infection was present in the lungs, kidneys, colon and reproductive tissues, indicating that the virus could be potentially spread by aerosols, urine, feces and sexually (Amman et al., 2012). In 2009, MARV was detected for the first time in the tissues, in addition to viral RNA and antibodies in the sera, in apparently healthy Egyptian fruit bats caught in the Kitaka cave in western Uganda where in 2007 an outbreak occurred among workers mining for lead and gold. This represented the first time when filoviral antigens were detected in naturally occurring bats (Towner et al., 2007).

Rousettus aegyptiacus is a cave-dwelling fruit bat: the fact that several MARV outbreaks have been associated with caves or mines that are usually heavily infested by bats (Feldmann and Geisbert, 2011) and the discovery of a new filovirus in insectivorous bats of the *Miniopterus schreibersii* species in caves in Europe

(Negredo et al., 2011) lead further support to this idea. Furthermore, has been shown that bats naturally or experimentally infected with ZEBOV or MARV are healthy and shed virus in their feces for up to 3 weeks (Negredo et al., 2011).

To demonstrating direct transmission from putative reservoirs, such as bats, is difficult because of the nature of bat bites, which are often invisible and painless, but evidence for this route, even though circumstantial, is powerful. Consistently, bats host a significantly higher number of viruses per species as compared to rodents, having been implicated in several recent viral outbreaks, including the rabies viruses, the SARS coronavirus, Nipah and Hendra viruses, Rift Valley fever virus, reoviruses and lyssaviruses. It was reported that 85 different viruses have been isolated from or detected in bat tissues (Stein, 2015).

The filoviruses transmission to humans is insufficiently understood. EBOV transmission appears to be unlikely during the incubation period, and the risk increases with the duration of the illness and with the direct contact during the late stages of the infection. Several transmission routes have been proposed to explain transmission to humans, including blood borne transmission, direct contact with infected patients or body fluids, fomites and possibly aerosolisation. During past EBOV epidemics different causes of infection in human population have been determined: reuse of contaminated needles, contact with an ill person, exposure to body fluids, touching a deceased person, butchering of wild animal and consumption of fresh killed bats. EBOV has been demonstrated to be present in the saliva, semen, stool, breast milk and nasal blood. Contact with body fluids emerged as the strongest risk factor, while aerosols are not thought to represent the major transmission route during natural outbreaks. In fact, it has not been demonstrated in humans, even if

there are evidences supporting EBOV transmission by this route between NHPs only under experimental conditions (Feldmann and Geisbert, 2011). This transmission route is facilitated by the stability of filoviruses in aerosols. It is important to note that in all human outbreaks studied to date (with the exception of the last one), the use of standard barrier nursing procedures was able to effectively halt the outbreaks in the hospital settings, and this observation practically rules out aerosol transmission as a major concern for human Ebola virus transmission (Stein, 2015).

Serological studies made on humans found an high seroprevalence to EBOV in apparently healthy individuals, indicating that exposure does not always lead to overt disease, or that may exist EBOV variants that are non-pathogenic or have lower pathogenicity and are antigenically similar to the pathogenic strains. Higher antibody prevalence against EBOV were found in pygmy population of central African rainforest that practice a seminomadic lifestyle based on hunting and gathering natural resources respect to non-pygmy villagers of the same area, practicing subsistence farming, hunting and limited fishing. These results reveal not only that filoviruses circulate, apparently without any clinical manifestations, in human populations living in forest areas in the Central Africa Republic, but also that certain lifestyles, such as hunting, are associated with higher exposure (Stein, 2015) (Figure 8).

EBOV has been detected in the semen of men after their recovery 179 days, or more, after the onset of Ebola virus disease (EVD). Furthermore, sexual transmission of EBOV it has been demonstrated by genomic analysis combined with epidemiologic data (Deen et al., 2015; Mate et al., 2015).
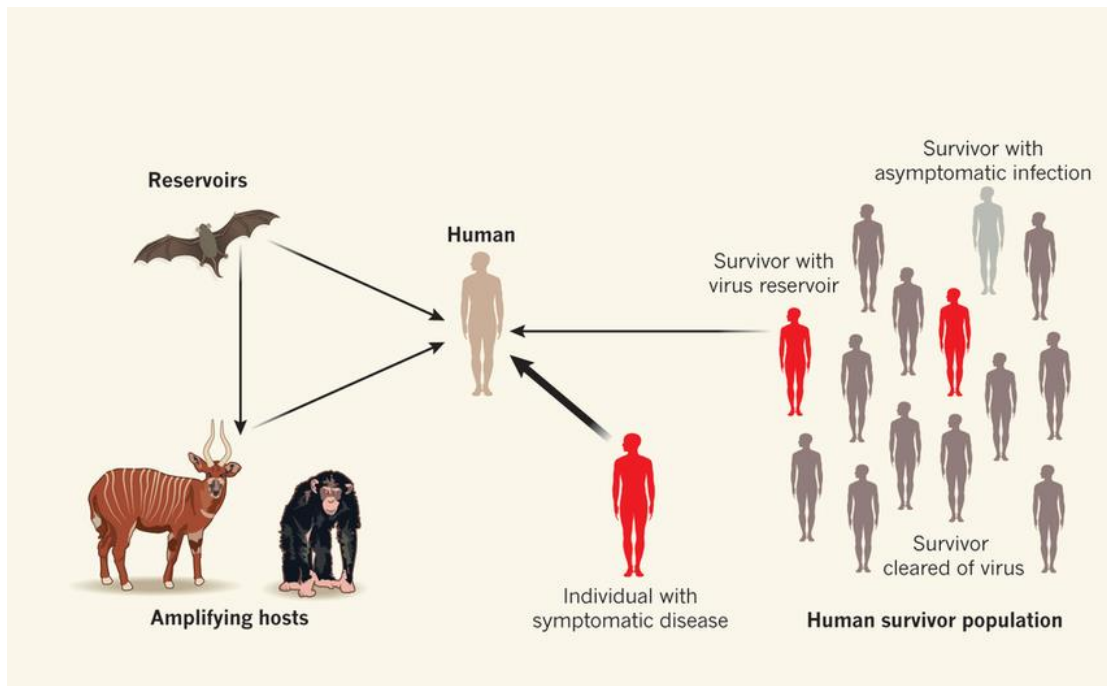
Figure 8 - EBOV infection dynamics in animals and humans. EBOV has been identified in several animal species, including bats, chimpanzees and forest antelopes. Transmission to humans can occur directly from putative reservoir species, in which the virus may persist without causing active infection, or from amplifying host species, in which the virus replicates to high levels, often causing illness and death. Most infected people develop acute EVD and are highly infectious, although some individuals survive exposure and infection without developing symptoms. There is also growing evidence that the virus can persist in the central nervous system and reproductive organs of some survivors of the disease, with the possibility that these survivors could infect others months after resolution of their acute symptoms (Heeney, 2015)

1.4 Clinical manifestations and diagnosis

Infections caused by filoviruses are characterized by a similar disease, which severity and fatality rate depends on infecting viral species. The incubation period of filovirus infections is generally reported to be about 4–10 days, but it may be broader, ranging from 2 to 21 days (Feldmann and Geisbert, 2011). Patients become ill suddenly, initially showing typical flu-like symptoms with fever and chills, headache, muscle pain, nausea, vomiting, abdominal pain, and diarrhea, even if in the last West Africa outbreak the primary clinical presentation was gastrointestinal. The disease can rapidly evolve into a severe state with a rapid clinical decline. This disease phase is characterized by potential hemorrhagic complications and multiple organ failure. About half of patients infected with EBOV develop a purplish-red maculopapular rash on the trunk and shoulders. Some have pharyngitis with a non-productive cough (Goeijenbier et al., 2014; Mahanty and Bray, 2004). Patients commonly show leucopenia and lymphopenia, with a specific decreased neutrophil count, and an increase in liver enzymes, followed by thrombocytopenia and consumptive coagulopathy due to disseminated intravascular coagulation, which contributes to multi-organ failure. Lethal EVD cases generally succumb between day 6 and 16 after the onset of symptoms. Patients die due to shock, hemorrhage and multi-organ failure (Goeijenbier et al., 2014). While fatal illness is associated with high and increasing amounts of virus in the bloodstream, patients who survive infection begin to show a decrease in amounts of circulating virus and clinical improvement around day 7–10. In most cases, this improvement coincides with the appearance of EBOV-specific antibodies (Mahanty and Bray, 2004). For survivors, long-term consequences of

infection may persist as a recurrent hepatitis, spinal cord injury, uveitis, psychosis or hair loss (Goeijenbier et al., 2014).

Since the EBOV is a very dangerous pathogen causing diseases with high morbidity and mortality, viral diagnosis has to be performed only in specialized laboratories with the highest level of biosafety, preferably BSL-4. Methods of diagnosis has to be fast, sensitive and specific, and limit the risks of exposure of people involved in diagnostic methodologies (Zawilińska and Kosz-Vnenchak, 2014). When the index of suspicion for EBOV is low but not negligible, ruling it out becomes a biosafety requirement because the presence of EBOV will lead to changes in the type of patient care needed, such as heightened precautions and limited laboratory testing to reduce exposure risks to medical and laboratory personnel (Sealy et al., 2016).

Since 2000 during the Uganda outbreak, a next-day serology and reverse transcription-polymerase chain reaction (RT-PCR) diagnostics for acute and convalescent case identification is available. Since then, the capability to high-throughput sampling of specimens in secure field laboratory has been progressively improved, creating modular laboratory equipment easily transportable by one or two persons and ensuring a high level of biosecurity and safety for staff during operations. This was the standard of operations in the earliest international laboratories responding to the last West African outbreak, that allowed to perform until to 180 rapid specimen diagnosis per day (Sealy et al., 2016).

Currently, RT-PCR is considered as the most sensitive method, mainly during the acute viremic phase of illness, which allows for detection of the number of viral copies in specimen, although there are other methods of virus identification. With

RT-PCR the presence of viral RNA can be detected by even after 48 hours post onset. However, it should be emphasized that due to continuous virus mutations, RT-PCR method may be unreliable and results should be confirmed by other assay (Wang et al., 2011).

RT-PCR–based techniques are frequently used with serology (IgM and IgG) to track virus-negative but antibody-positive survivors or for surveillance activities in geographic regions previously affected. The timing of specimen collection in regard to symptom onset is a key factor for diagnosis: during symptom onset, blood specimens are usually, but not always, PCR positive; then, in order to avoid false-negative results, a second specimen should be analyzed 72 hours after symptom onset to definitively to exclude infection. Critically ill patients are highly viremic, and virus is readily detectable in oral swabs from deceased persons. In survivors, the humoral immune response begins to manifest toward the end of the second week of disease with transient IgM and rising IgG titers as circulating virus titers decrease.

The most frequently implemented diagnostic tests are based on quantitative RT-PCR (qRT-PCR) targeting conserved domains within genes for the viral polymerase (L) and structural elements (NP, VP40, and GP) of EBOV (Sealy et al., 2016).

1.5   Pathology and pathogenesis

EBOVs enter the human body via mucosal surfaces, abrasions and injuries in the skin or by direct parental transmission. Infection through intact skin is considered unlikely, but not excluded. Although EBOV should be inactivated by cooking the food, ingestion of contaminated food cannot be excluded as possible route of infection. The route of transmission seems to affect the disease outcome; in the early EBOV outbreak in 1976, CFR after transmission by injection was 100% versus 80% in contact exposure cases. This has been confirmed in a NHP model (Feldmann and Geisbert, 2011). Most studies on pathogenesis of EVD have been performed in rodent, guinea pig, primate and in vitro models. Since the virus needs to adapt to cause disease in rodent and guinea pig experimental study models, the most relevant data representing human disease come from NHP studies (Bray et al., 2001). Pathomechanisms of EBOV infection are complex, involving phagocytic cells, released proinflammatory cytokines, chemokines, and growth factors, endothelial cell dysfunction and triggering of coagulopathy, direct damage of cells by viral replication as well as suppression of innate and adoptive immune response.

Mahanty and Bray described six pathogenetic mechanisms that seem to act in combination to cause EVD and divided them in two types: those by which there is a direct damage to tissues and those in which tissue injury is brought about indirectly through interactions between the virus and the innate and adaptive immune systems. In first type they include the capability of virus to bind to widely distributed cell-surface lectins and to induce necrosis in bound cells, maybe through the cytotoxic effects of GP or other viral proteins. Pathogenetic mechanisms that are based on

interactions between filoviruses and the immune system, grouped in the second type, are: systemic dissemination of virus is aided by suppression of innate immune responses in macrophages and dendritic cells; filovirus infection impairs the development of antigen-specific immune responses, by preventing dendritic cells from activating T cells; massive apoptosis of lymphocytes that also contributes to immunosuppression; and, finally, the production by macrophages a range of mediators that induce cell-surface expression of tissue factor, triggering disseminated intravascular coagulation and the release of cytokines and chemokines that induce vascular dysfunction, hypotension, and multiple organ failure (Mahanty and Bray, 2004). Variability in individual innate immune responses is associated with a favourable or unfavourable outcome of disease. Furthermore, the expression of strong proinflammatory cytokine responses early in the disease course facilitates the induction of adaptive responses (Baize et al., 2002).

EBOV shows a broad cell tropism, infecting a wide range of cell types: analysis of tissue from dead patients or from infected NHPs show that monocytes, macrophages, dendritic cells (DCs), endothelial cells, fibroblasts, hepatocytes, adrenal cortical cells and several types of epithelial cells were infected by EBOV viruses, with monocytes, macrophages, DCs as early and preferred replication site of these viruses (Geisbert et al., 2003; Mahanty and Bray, 2004). Likely, viruses spread via monocytes, macrophages and DCs from site of infections through lymphatic system to lymph nodes and through circulatory system to liver and spleen, where the virus can infect resident tissue DCs and macrophages, including Kupffer cells, from which then spread to the rest of the body (Geisbert et al., 2003) (Figure 9).
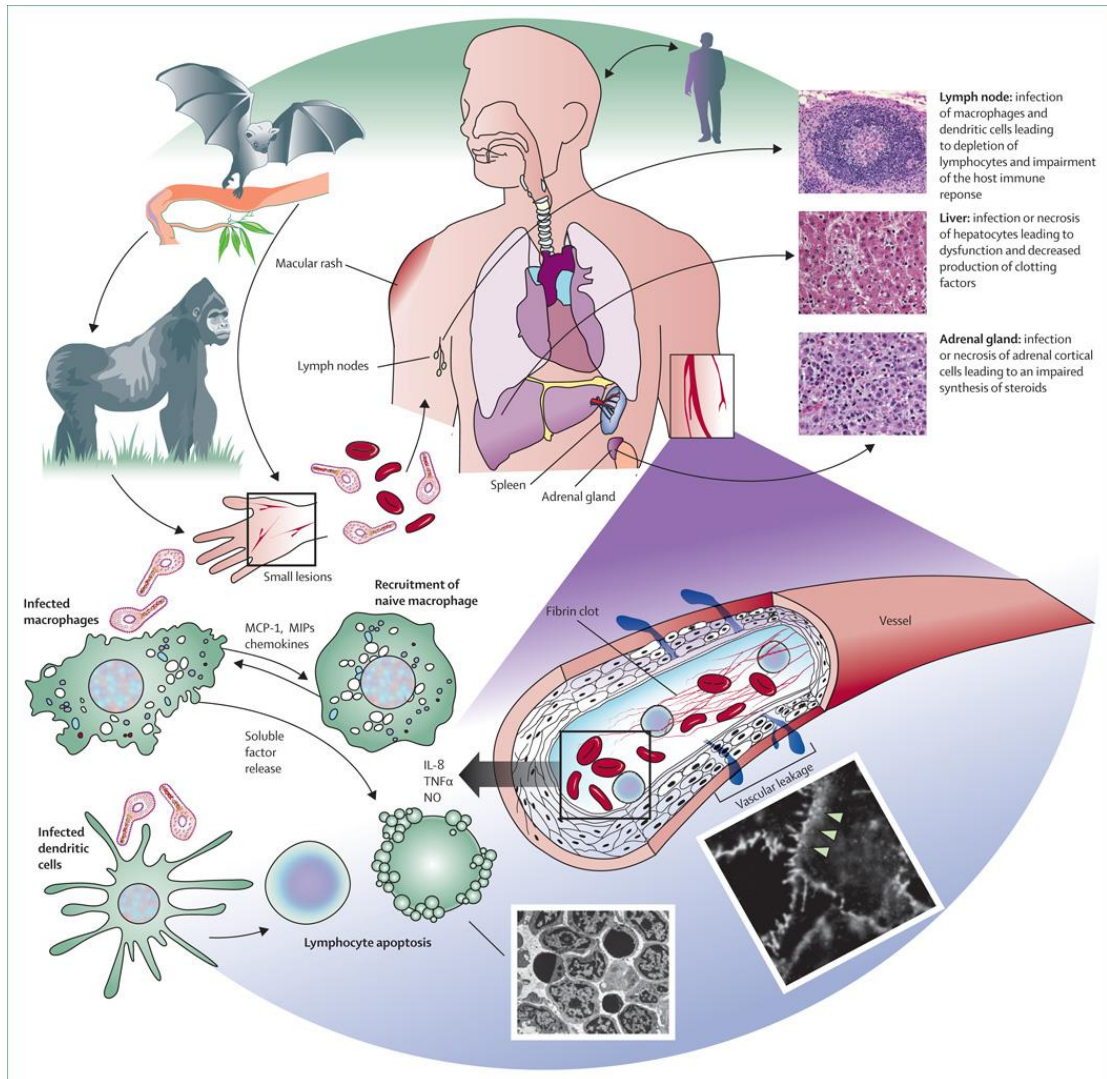
Figure 9 - Model of EBOV pathogenesis. Virus spreads from the initial infection site (small lesions) to regional lymph nodes, liver, and spleen. Although EBOV does not infect lymphocytes, a direct interaction with viral proteins cannot be excluded. Lymphocytes undergo a significant apoptosis probably resulting from a combination of factors including infection-mediated impairment of dendritic cells and release of soluble factors from monocytes and macrophages. These factors also contribute to the impairment of the vascular system leading to vascular leakage (picture box with white arrowheads). IL=interleukin. MCP-1=monocyte chemoattractant protein-1. MIPs=macrophage inflammatory proteins. NO=nitric oxide. TNFα=tumour necrosis factor α (Feldmann and Geisbert, 2011).

It is thought that infected macrophages, triggered by virus, release pro-inflammatory cytokines and chemokines, such as interleukins (IL-1β, IL-6, IL-8, IL-10), monocyte chemoattractant protein 1 (MCP1; also known as CCL2), macrophage inflammatory protein 1α (MIP1α; also known as CCL3), MIP1β (also known as CCL4) and tumour necrosis factor (TNF), as well as reactive oxygen species and nitric oxide. The release of MIP1α and MCP1attracts further macrophages to site of infection, enabling EBOV to infect more target cells. Infection of dendritic cells inhibits their maturation and thereby prevents antigen presentation to T cells (Messaoudi et al., 2015) (Figure 10).

Lymphopenia following EBOV infection is likely provoked by apoptosis of lymphocytes, occurring mainly among CD4+ T cells, CD8+ T cells and natural killer (NK) cells. However, as CD4+ T cells switch into B cell, their loss could contribute to the lack of EBOV-specific immunoglobulin M (IgM) and IgG antibodies in case fatalities (Messaoudi et al., 2015).

Researchers thought that endothelium plays an important part in the EBOV pathogenesis and that EBOV infection of endothelial cells induces structural damage, focusing on viral GP as determinant of direct vascular-cell injury which could contribute to the hemorrhage, even if no vascular lesions have been reported so far in studies (Feldmann and Geisbert, 2011). Other indirect different mechanisms have been proposed to explain hemorrhage: hepatocellular and adrenocortical infection and necrosis may result in decrease synthesis of coagulation protein and failure of homeostasis, respectively (Geisbert et al., 2003); high-level of TNF released by macrophages may increase vascular permeability (Hensley et al., 2002);
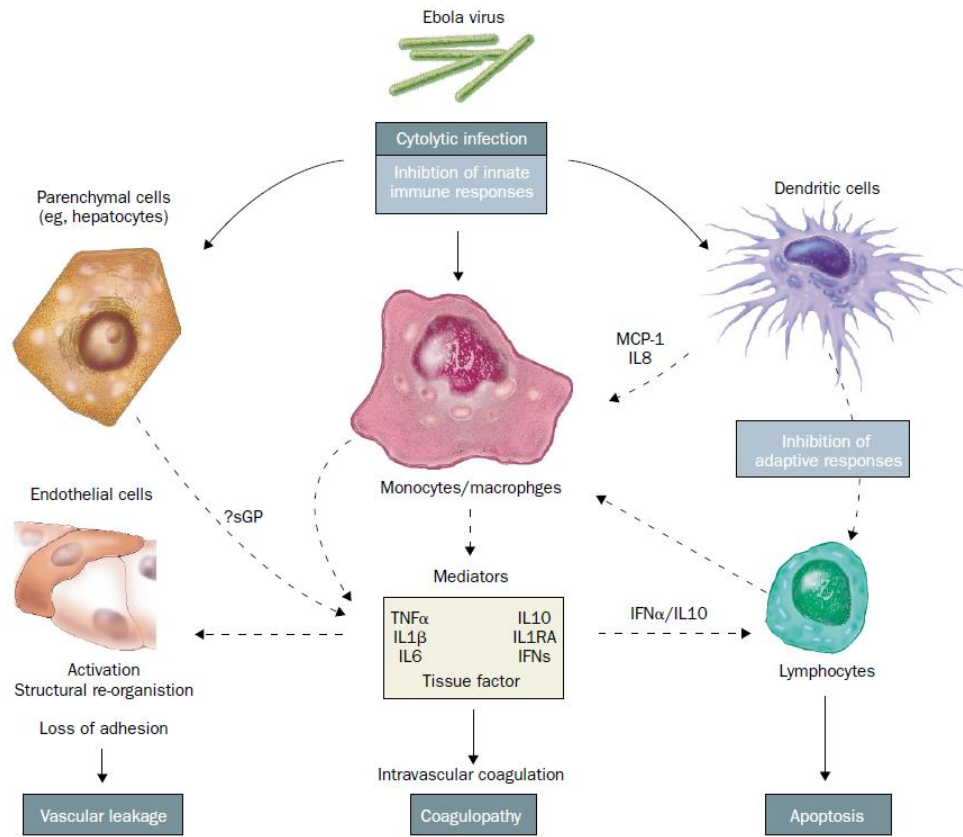
Figure 10 - The pathogenesis of Ebola virus disease. Initial entry into host leads to increased inflammation, decreased immune response, damage to vasculature, and necrosis of different cell types. EBOV infection causes lysis of monocytes/ macrophages, dendritic cells, and hepatocytes and suppresses innate immune responses in these cells. Direct injury to infected cells is accompanied by indirect effects that are mediated by pro-inflammatory and anti-inflammatory effector molecules, which also cause lymphocyte apoptosis. It contributes to further immunosuppression by weakening adaptive immune responses. IL1β= interleukin 1β, IL6= interleukin 6, TNF=tumor necrosis factor, IL10=interleukin 10, MCP=monocyte chemoattractant protein; IL1RA=interleukin-1 receptor antagonist

effect of nitric oxide released by macrophages on the homeostasis of vascular system (Sanchez et al., 2004).

In EBOV infected NHPs it has been reported a dramatic decrease in plasma levels of anticoagulant protein C about 2 days post-infection, followed by an increase in both the levels of tissue plasminogen activator, which is involved in dissolving blood clots, and of fibrin-degradation products. Furthermore, increased level of tissue factor released by monocytes and macrophages is likely to promote overactivation of the extrinsic pathway of coagulation and may cause disseminated intravascular coagulation. Thrombocytopenia and prolonged pro-thrombin time are also indicators of dysregulation of blood coagulation. Thrombocytopenia and prolonged pro-thrombin time are also indicators of dysregulation of blood coagulation. The combined effects of an increased level of procoagulation factors and a decreased level of anticoagulant factor protein C could plausibly explain the activation of coagulation and haemorrhagic features that are characteristic of filovirus infection (Messaoudi et al., 2015).

In addition to haemorrhage and intravascular coagulation, the lethality of filovirus infection is probably due, in part, to the excessive viral replication, allowed by the suppression of innate immune response, that activates the damaging host responses outlined above. The description of the mechanisms of suppression of the immune response by EBOV is the subject of a specific section of this thesis.

1.6   Life cycle

The first step of any virus lifecycle is the entry into host cells, by the attachment to cell surface receptors and the subsequent fusion between the viral envelope and the cellular membrane. In the case of filoviruses, the first and preferred cells infected are monocytes, macrophages and DCs (Geisbert et al., 2003), but they can infect most cell types as Kupffer cells in the liver, fibroblasts, hepatocytes, adrenal cortical cells, endothelial cells and several types of epithelial cells (Feldmann and Geisbert, 2011). All enveloped viruses penetrate into host cells using a viral membrane fusion protein. All stages of EBOV entry, binding to and internalization from the cell surface as well as trafficking to, and fusion with the limiting membrane of late endosomes, are mediated by trimeric GP spikes (Lee et al., 2008; Lee and Saphire, 2009).

EBOV surface GP is a heavily glycosylated class I viral fusion protein that is cleaved in the Golgi during transit to the cell surface by a furin-like protease into a receptor binding subunit (GP_1) and a fusion subunit (GP_2), that remain associated through a disulfide bond. Three $GP_{1,2}$ heterodimers assemble as trimers on the virion surface, like all class I fusion proteins (Dube et al., 2009). It is to note that the furin recognition motif is highly conserved among all species of the family *Filoviridae* (Kajihara and Takada, 2015). However, in contrast to similarly organized class I fusion proteins, it has been demonstrated that in EBOV the furin cleavage that separates GP_1 and GP_2 is dispensable for entry and replication in cell culture (Neumann et al., 2002) as well as for infection and pathogenesis in vivo, even if the GP cleavage by furin or a furin-like endoprotease may be required for EBOV replication in its natural host (Neumann et al., 2007). The lack of a requirement for

endoproteolytic processing is bewildering, since the dibasic motif is highly conserved in the envelope glycoproteins of all known strains of EBOV and the closely related MARV (Wool-Lewis and Bates, 1999). Therefore, furin is likely not the only cellular enzyme responsible for the endoproteolytic processing of EBOV GP, but it is possible that required for viral replication only in certain cell types (Wool-Lewis and Bates, 1999).

GP presents a receptor binding region (RBR), located in the first one-third of the protein, and a mucin-like region (MLR), highly glycosylated with large amounts of N- and O-linked glycans, located in the middle one-third of GP. Both regions are in GP_1 subunit in EBOV, while in MARV the furin cleavage site is in the middle of MLR (Takada, 2012) (Figure 11).

Figure 11- Primary structure of EBOV and MARV GP: furin-cleavage site (arrows) and disulphide bond (-S—S-) between GP_1 and GP_2 subunits. SP signal peptide, RBR putative receptor-binding region, MLR mucin-like region, IFL internal fusion loop, TM transmembrane domain (from Takada, 2012)

Infection is initiated by interaction with attachment factors expressed on target cell surfaces. Several host cell factors have been shown to be involved in the attachment and entry of EBOV. Although DC-SIGN on DCs, L-SIGN and LSECtin on endothelial cells, hMGL on macrophages, asialoglycoprotein receptors on hepatocytes, enhance filovirus infection, none of these proteins individually are necessary and sufficient for viral entry (Elshabrawy et al., 2015; Kajihara and

Takada, 2015; Lee and Saphire, 2009). Furthermore, several cell surface proteins such as β1-integrins and Tyro-3 family receptors (Axl, Dtk and Mer) are involved in the attachment of EBOV to the host cell surface, but they do not function as physical virus receptors, namely as molecules that actively promote virus internalization or actively induce virus penetration (White and Schornberg, 2012). The reduction of Axl expression by RNAi treatment decreases EBOV entry via macropinocytosis, suggesting that Axl enhances this process (Hunt et al., 2011).

The T-cell immunoglobulin and mucin domain protein (TIM-1), a T-cell costimulatory molecule, was identified as a candidate cell surface receptor for EBOV. Actually, human TIM-1 serves as a receptor for filovirus infection of epithelial cells, including airway epithelium, and cell lines from a broad range of tissues that are known to be targets for EBOV, but not all permissive cells were found to be TIM-1 positive (Kondratowicz et al., 2011). In a recent work, it has been demonstrated that TIM-1 binds phosphatidylserine (PtdSer) on the virus envelope, acting as a GP-independent attachment factor for filovirus entry (Moller-Tank et al., 2013) (Figure 12).
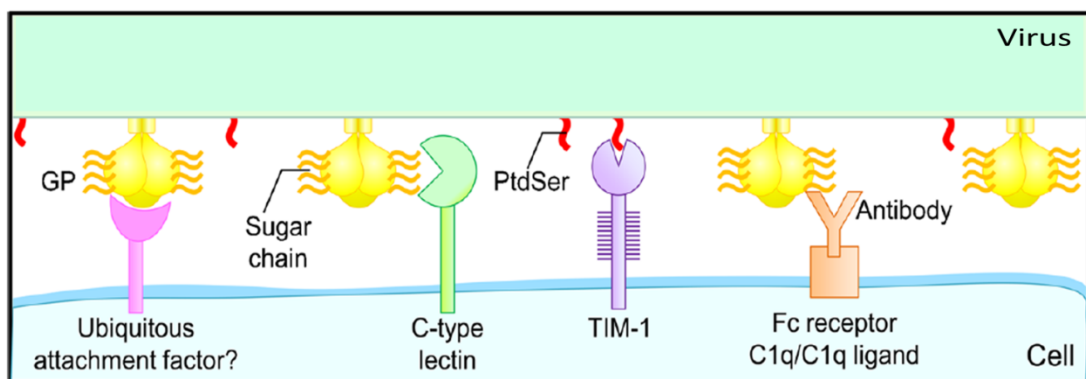

Figure 12 - Viral and host factors involved in filovirus attachment (Kajihara and Takada, 2015)

As macrophages and DCs are thought to be major targets of filoviruses, but do not express TIM-1, receptors involved in filovirus infection of these cells are other than TIM-1, the related mechanisms are still unknown and additional functional receptors for filoviruses remain to be identified (Elshabrawy et al., 2015; Kajihara and Takada, 2015; Moller-Tank et al., 2013).

Moreover, it has been shown that cultured and primary human lymphocytes in suspension contain an intracellular pool of RBR binding partners and that they could translocate from trans-Golgi network to the cell surface. Furthermore, it has been demonstrated that two adherent primate lymphocytic cell lines bind RBR at their surface and, strikingly, support GP-mediated entry and infection, suggesting that a membrane-trafficking event that translocates an RBR binding partner to the cell surface may be important in cells involved in EVD pathogenesis (Dube et al., 2010). However, based on evidence from different studies, EBOV may use different pathways to gain entry into host cells depending on the cell type (Elshabrawy et al., 2015).

Because they are surrounded by a membrane, filoviruses penetrate into the cytoplasm by membrane fusion with the limiting membrane of a late endosome. Following binding to the cell surface, filoviruses are internalized by a macropinocytosis-like process and trafficked to a late endocytic compartment, where viral envelope and late endosome limiting membrane fuse together (White and Schornberg, 2012) (Figure 13).
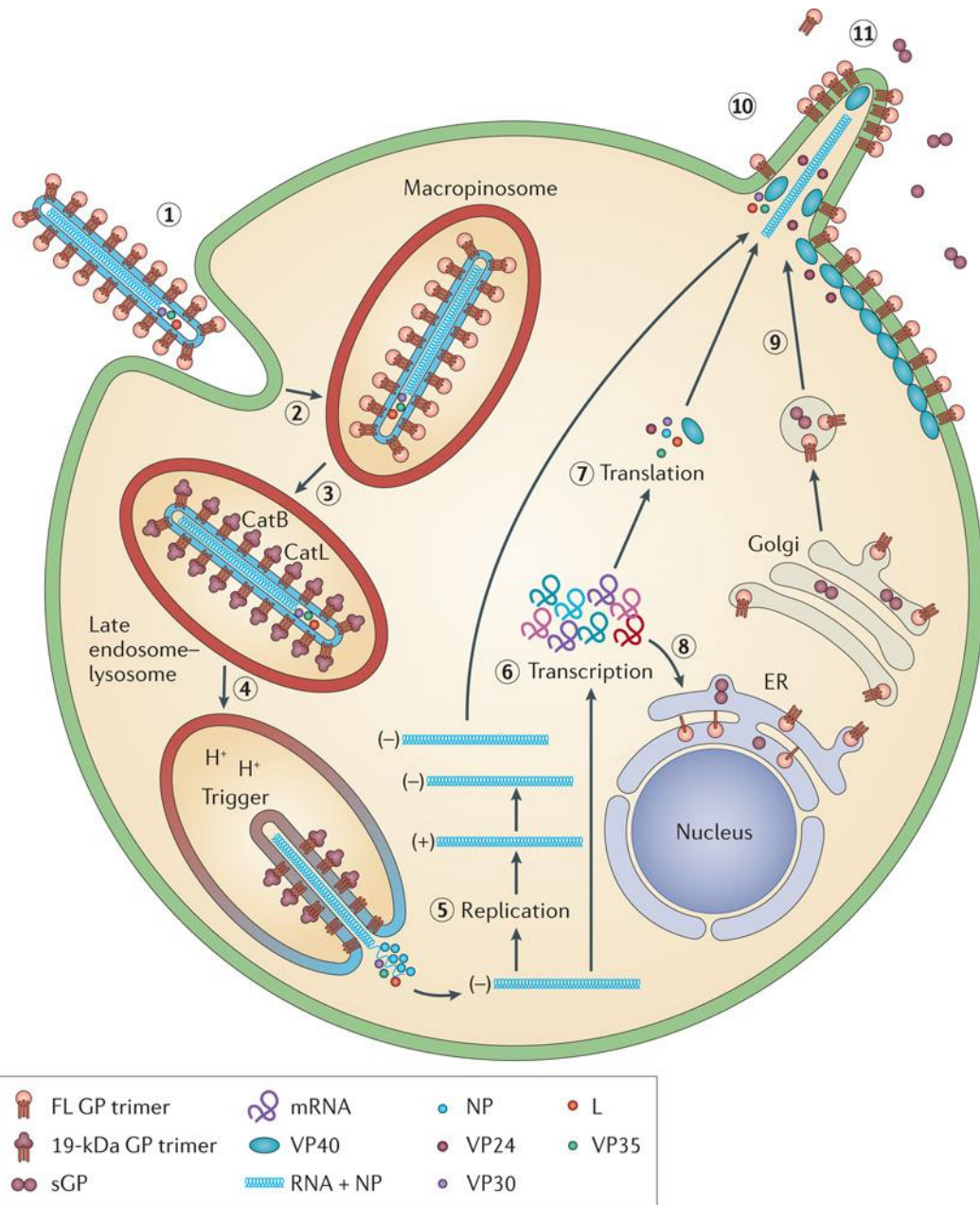
Figure 13 - Lifecycle of EBOV – The virus binds to attachment factors and receptors on the cell surface (1). Subsequently it is internalized into a macropinosome (2) and trafficked to an endosomal compartment containing the Cys proteases cathepsin B and cathepsin L(3). Cleavage of GP triggers the fusion between the viral and endosome membrane and the viral nucleocapsid is released into the cytoplasm (4), where the genome is replicated (5) and transcribed (6). mRNAs are translated by the cellular translation machinery (7). In the ER GP is synthesized, modified with N-linked sugars and trimerized (8). GP is further modified in the Golgi and delivered to the plasma membrane in secretory vesicles (9). At the plasma membrane the RNP complex and the other viral proteins assemble and the virions bud from the cell surface (10). Non-structural forms of GP (sGP) are also secreted (11) (White and Schornberg, 2012)

The furin-like cleavage that separates GP_1 and GP_2 during biosynthesis is not sufficient to prime GP for the membrane fusion process; actually, only after viral particles have been formed, bound, internalized and trafficked to a late endosome of a host cell, the priming can be completed. Host Cys proteases, cathepsin B and cathepsin L, are activated in acidic environment of late endosomes and cut the GP1 subunit (Schornberg et al., 2006), removing the C-terminus end including MLR. Priming seems to proceed in two steps: at first cathepsin L cuts and reduces GP_1 to a 20 kDa protein that it is subsequently further cleaved by cathepsin B to 19 kDa protein (
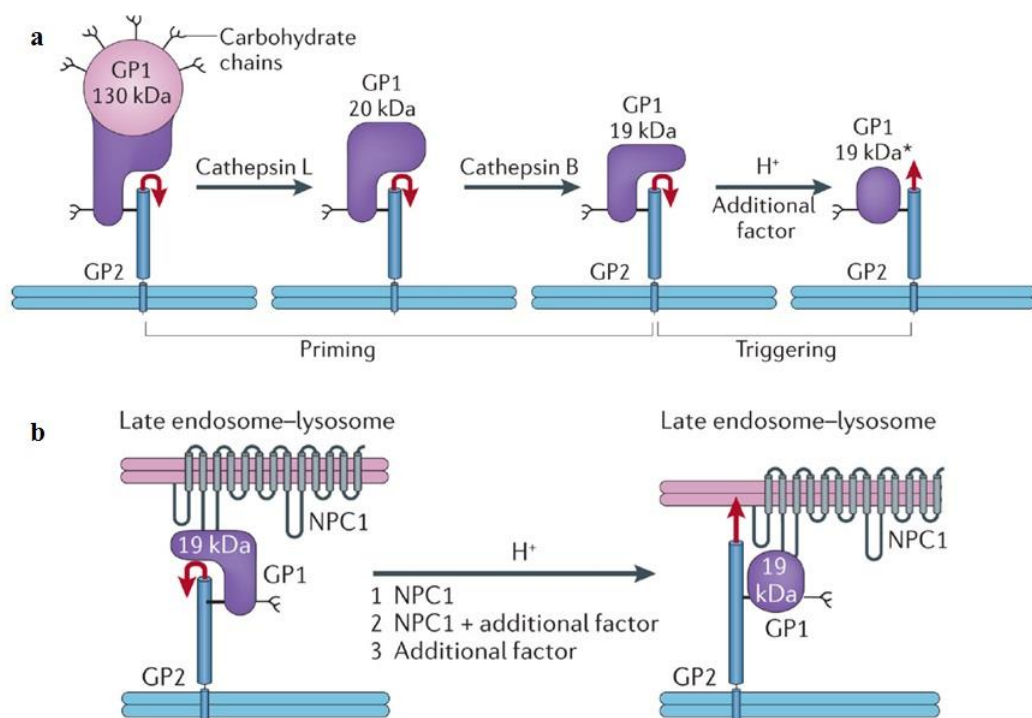
Figure 14a). The current thoughts are that the proteolytic cathepsins cleavage may expose the putative RBR on GP_1 subunit for the binding to a endosomal receptor or that priming may potentiate GP for fusion triggering (White and Schornberg, 2012). GP cleavage by furin into GP_1 and GP_2 is not a prerequisite for cathepsin digestion.

Whether proteolytic processing by other proteases in endosomes is required prior to cathepsin digestion remains unknown (Neumann et al., 2007).

The membrane fusion mediated by filovirus glycoproteins and viral exit from the endosome requires the cholesterol transporter Niemann-Pick C1 protein (NPC1), a protein primarily located in late endosome-lysosome, in independent manner from its function in cholesterol transport (Carette et al., 2011). The role of NPC1 in EBOV entry has been demonstrate by Cote et al.: NPC1 binds to primed GP in RBR of GP_1, rendered accessible by the cathepsin priming (Cote et al., 2011; Miller et al., 2012) (

Figure 14b).

After entry, the viral genome is replicated and transcribed, new viral proteins are synthesized, and new virions assemble and bud from the cell surface. Although the replication and transcription mode it is similar for all viruses belonging to the order
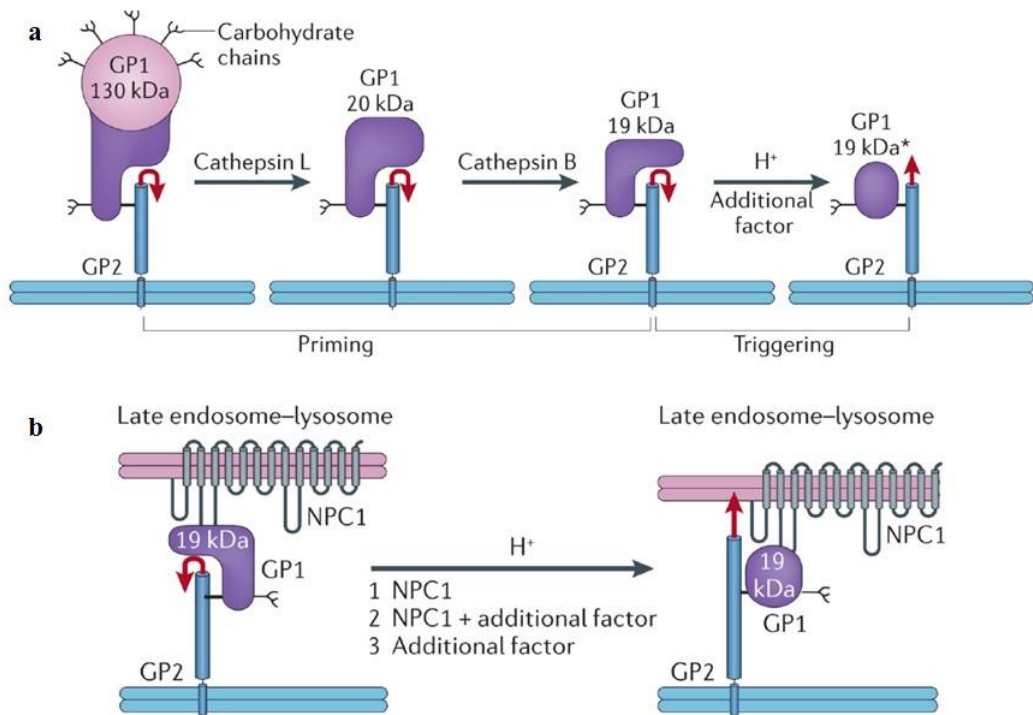
Figure 14 – EBOV GP priming and triggering: possible roles of NPC1. a) Cathepsin L and cathepsin B cleave EBOV GP_1, removing the gly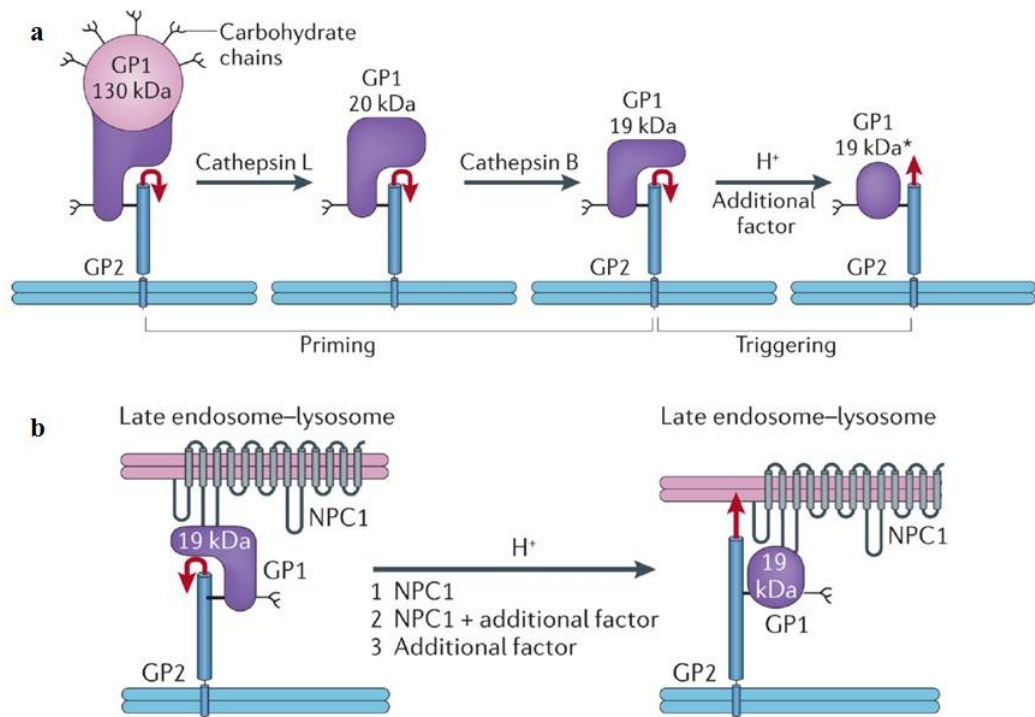can cap and mucin-like domain (pink), thereby generating a 20 kDa and then a 19 kDa form of the glycoprotein. Primed 19 kDa GP requires low pH and the activity of an additional factor to trigger rearrangements that liberate and relocate the fusion loop (red arrow), and thereby initiate the fusion cascade. b) Possible roles for NPC1 in triggering EBOV fusion. Following delivery to a late endosome–lysosome and priming by cathepsins, primed GP binds to NPC1. Three possible models are hypnotized: 1) NPC1 is the additional factor depicted in part a that, together with low endosomal pH, triggers the conformational changes that liberate and relocate the fusion loop (red arrow), leading to fusion and therefore penetration of the genome into the cytoplasm to initiate replication; 2) NPC1 binding to primed GP is necessary, but not sufficient, to trigger GP, and one or more additional factors are still required; 3) NPC1 binds to primed GP, linking the virus to the endosomal membrane, but does not induce conformational changes in GP; in this case an additional factor triggers fusion (White and Schornberg, 2012).

Mononegavirales, being the genome employed as template for both replication and transcription, filoviruses present peculiar structural and functional properties.

Moreover, there are differences in mechanism of replication and transcription between EBOV and MARV, which are related to the NC formation, to the structure of the genomic replication promoter, to the protein requirement for transcription and to the use of mRNA editing (Mühlberger, 2007).

The ebolavirus NCs are the principal units of transcription and replication of the viral genome. The NCs of all nonsegmented negative-sense (NNS) RNA viruses carry a viral RNA-dependent RNA polymerase (L), a phosphoprotein polymerase cofactor (P or VP35) and a nucleoprotein (N or NP), which encapsidate the viral genome. In the *Mononegavirales* order of viruses, L and NP interact through the phosphoprotein to carry out viral RNA synthesis. Filoviruses are unusual among mononegaviruses since they encode an additional NC component, VP30 (Kirchdoerfer et al., 2016). Furthermore, recently it has been shown that also VP24 is a component of the NC rather as a minor matrix protein as previously suggested, both in MARV (Bharat et al., 2011) and in EBOV (Bharat et al., 2012), consistently with previous results showing that EBOV VP24 plays a role in formation of a functional NC (Hoenen et al., 2006).

Replication and transcription of Filoviruses genome take place in the cytoplasm of infected cells. The enzyme utilized for these processes is the RNA-dependent RNA polymerase, coded by the viruses and present in NC. The newly entered genome is first sequentially entirely transcribed by the NC proteins associated with the intruding virus (primary transcription) and then mRNAs are translated into viral proteins. With the increase of viral protein concentration and host cell factor regulation, the

polymerase complex switches to replication mode to generate anti-genomes and new genomes (Biedenkopf et al., 2016). The transcription of negative-strand RNA genome is regulated by conserved transcription start and stop signals at the viral gene borders and produces seven monocistronic 5'-capped and 3'-polyadenylated mRNA species (Mühlberger et al., 1999). The enzymatically active part of the viral polymerase L is bound to the nucleocapsid by interaction with the polymerase cofactor VP35; L and VP35 form the active polymerase complex. The hexameric zinc-finger protein VP30 is an EBOV-specific viral transcription factor (Biedenkopf et al., 2016). In contrast to EBOV viral transcription, VP30 is not required for MARV transcription and for viral replication in both two viruses, but it works as modulator of these processes: actually it has been shown that VP30 phosphorylation inhibits viral transcription while viral replication is increased, switching from secondary VP30-dependent transcription to VP30-free replication (Biedenkopf et al., 2013). After transcription, EBOV mRNA is then translated by the cellular translation machinery, and newly formed viral proteins accumulate in inclusion bodies. Inclusion bodies are complex and dynamic structures where viral RNA replication takes place, whereas viral transcription occurs prior to inclusion bodies formation (Hoenen et al., 2012).

Replication of genome begins with the synthesis of a positive-sense replicative intermediate, the antigenome, quickly enwrapped by the nucleocapsid proteins, that serves as template for the production of new genome, which is concomitantly encapsidated by newly synthesized NP molecules (Biedenkopf et al., 2013; Olejnik et al., 2011). Three NC proteins are necessary and sufficient to allow replication: NP, L and VP35. The promoter for replication is located on the 3' termini of genome and antigenome (Mühlberger, 2007).

The driving force for NC formation is NP. It has been proposed for EBOV that NP forms helical structures which interact with VP35 and VP24, resulting in the formation of nucleocapsid-like structures (Olejnik et al., 2011). Consistently, expression of NP alone in the cytoplasm shows the formation of helical tubes whose diameter is almost the same as that of a central portion of the NCs and possessing a central channel (Noda et al., 2006).

The matrix protein VP40 is critical for transport of NCs to the cell surface and for the incorporation of NCs into virions; the interaction between NP and VP40 is likely essential for these processes (Noda et al., 2006).

In EBOV infection, newly synthesized viral proteins and genomic RNA in the form of NCs are transported to the budding site where the viral components assemble to form virions. The process of budding for EBOV occurs from the cytosolic leaflet of the plasma membrane and is driven by the matrix protein VP40 (Stahelin, 2014). VP40 has been shown to be important for EBOV budding as well as for virus structure and stability. The N-terminal domain is responsible for oligomerization of VP40, while the C-terminal domain is required for membrane binding (Baz-Martínez et al., 2016). VP40 dimers mediate the association with the interface of the plasma membrane, interacting with PtdSer and perhaps other lipids such as PIPs. This induces a conformational change of VP40, rearranging the dimers into a hexamer. The hexamers can bind with each other to form long VP40 filaments. VP40 oligomers are able to induce a negative membrane curvature generation of a filamentous particle that will be released (Stahelin, 2014). Unique among all viruses to our knowledge, EBOV particles containing NCs mainly emerge horizontally from the cell surface, whereas the other viruses bud vertically (Noda et al., 2006).

1.7 Therapy, management and prevention

At the beginning of the recent outbreak in West Africa no approved drugs were available and prior to it, there was no EBOV therapeutic in clinical trials. Although tremendous efforts have been done to advance in the discovery of therapeutics and to conduct clinical trials in an outbreak setting, there are no licensed treatments for EVD yet (Cardile et al., 2016). Nevertheless, besides some clinical trials attempted during epidemic, a few not approved drugs have been administrated to patients on the basis of a compassionate use. In fact, when such a big number of people are threatened by so dangerous diseases and no specific therapies or preventive measures exist, it can be ethically acceptable to assume greater risks and offer patients unproven interventions. It has been highlighted that experimental drug or vaccine research differs from compassionate use of experimental therapies and many debates were sparked about the ethics use of compassionate use of non-approved therapeutics and what rules should be followed in this case mainly about the selection of study population (Folayan et al., 2016; Rid and Emanuel, 2014).

A non-exhaustive list of some therapeutic candidates that underwent clinical trials during the West Africa outbreak are shown in Table 2. They may be grouped according to the mechanism of action in: nucleic-acid based inhibitors, nucleoside/nucleotide viral polymerase inhibitors and immunotherapeutics and, furthermore, vaccine candidates as ChAd3-ZEBOV (de La Vega et al., 2015) and rVSV-EBOV (Henao-Restrepo et al., 2015).

Among nucleic-acid based inhibitors there are antisense phosphorodiamidate morpholino oligomers (PMOs) and small-interfering RNAs (siRNAs).

Table 2- Treatment approaches evaluated for efficacy against Ebola virus disease in mammals (Trad et al., 2017).

Approach	Target/mechanism of action	Demonstrated Efficacy			Comments
		Rodent	NHP	Human	
Vaccines					
Plasmid DNA based vaccine VRC-EBODNA023-00-VP	DNA immunisation with boosting adenoviral vector	–	Y	Phase I (Uganda)	Process takes 6 months to provide protection in NHP
Accelerated vaccine of plasmid DNA based vaccine: ChAd-EBOV, Ad5-EBOV, cAd3-EBOV (GSK) andAd26 and MVA-EBOV (J&J)	Adenoviral vector delivers DNA encoding Ebola GPMVA used as a second dose booster	Y–	YY	Phase I (UK, US, China, Mali, Uganda, Switzerland) Phase II/III*: LiberiaPhase I*: UK, II/III* US	Process takes 28 days to provide pre-exposure protection in NHP. Potential for outbreaks. Booster induces longer term protective immunity*NCT02509494*NCT02240875, NCT02598388
rGP nanoparticle (Novavax)	Recombinant Ebola GP administered with a saponin based adjuvant (Matrix-M)	–	–	Phase I: Australia	Requires 2 injections
rVSV-EBOV (Merck), rVSVΔG-EBOV	VSV delivers Antigen	–	Y	Phase I (Kenya, U.S, Switzerland)STRIVE: Phase II/III Randomized trial in HCWs (Sierra Leone), PREVAIL: Phase II (Liberia). Ca Suffit: Phase III (Guinea)	Up to thirty minutes post infection (protection against Ebola –50%, Marburg 100%) 33% protection after 48 h, in NHP Geneva phase I trial halted for safety concerns. Less side effects with the newer strains. Potentially could provide protection after 6 days of vaccinations in humans. No booster required. Duration of protective antibodies unknown
Antibody based therapies					
IgG/IgM from convalescent patients	Virus neutralisation	–	–	Case series, INTERCEPT Phase I and Phase II/III (Guinea, Sierra Leone, Liberia)	Widely used during 2014-15 outbreak. No significant mortality benefit in 99 transfused patients. Two consecutive transfusions of 200–250 ml plasma from separate convalescent donors
Purified IgG	As above	–	Y	Y	48 h protection post infection (100%) in NPH
Cocktail of 3 x mouse monoclonal antibodies-ZMab	Targets GP to neutralize the virus (m1H3, m2G4, m4G7)	–	Y	Cases	100% effective at 24 h 50% @ 48 h
Cocktail combined with adenovirus vectored interferon-alpha	As above	–	Y	–	72 h post infection 75–100%
Cocktail of 3 x humanised monoclonal antibodies (MB-003) ZMapp and MIL-77 (China)	(c13C6, h13F9, c6D8)A combination of chimeric mAB c13C6 from MB-003 and 2 chimeric mABs (c2G4 and c4G7) from ZMab. MIL-77 is produced by CHO cells rather than tobacco plants	——	YY	Cases, Phase I/II trial (multi-centre) Liberia, Sierra Leone, U.S Phase I*	Protection 100% at 1 h, 67% at 24/48 h. 43% survival at 120 h post infection and development of viraemia and fever in NHP.50 mg/Kg/day for 3 days*NCT02389192
Drugs or small molecules					
TKM-Ebola Tekmira	Small interfering RNA cocktail against VP24, VP35, and L protein. Encapsulated in stable nucleic acid lipid particles (SNALP)	–	Y	Phase I-suspended (partial lift by FDA). Phase II: Sierra Leone Cases	IV preparation 100% protection 30 mins post exposure in NHP. Phase II trial halted in Sierra Leone. 7 daily infusions: Day1: 0.3 mg/Kg, Day2: 0.4 mg/Kg, then Days3-7: 0.5 mg/Kg
PMOs (AVI-6002)	Blocks mRNA transcription	–	Y	Phase I PEP	62.5% protection within 30 mins in NHP
Favipiravir	Pyrazine carboxamide derivative. Selective inhibition of viral RNA dependent RNA polymerase.	Y	–	Cases Phase III (U.S) Licensed in Japan for flu. JIKI Phase II trial in Guinea	Rapid viral clearance, used up to day 6 post infection- mice. Received by most European cases. Preliminary results from JIKI trial indicate effectiveness in cases with low viral load. Day0: 6000 mg then Days1-9: 2400 mg. Activity being studied in semen NCT02739477
Brincidofovir (CMX001)	Nucleotide analogue. Broad spectrum antiviral.	–	–	Cases Phase II (halted in January 2015)	Developed for CMV, BK viruses. Trial in Liberia halted due to reduction in new cases. Loading dose: 200 mg then 100 mg twice weekly for total of 5 doses
BCX4430	Adenosine analogue (PO/IM). Incorporation into viral RNA causing chain termination	–	Y	–	100% protection of NHP at 48 h post infection (Marburg virus), also thought to have anti-EVD activity.

PO: oral route, IM: Intramuscular route, NHP: Non-human primates, GP: Glycoprotein, VP: Viral protein, VSV: Vesicular stomatitis virus, CHO: Chinese Hamster Ovarian cells mAB: monoclonal antibodies PMOs: Phosphorodiamidate morpholino oligomers, PEP: Post-exposure prophylaxis, FDA: Food and drug agency, MVA: Modified Vaccinia Ankara, GSK: GlaxoSmithKline, J&J: Johnson & Johnson, *Ongoing trials as per http://clinicaltrials.gov (at the time of writing)
Note: Military vaccines (Russia, U.S.A and China) were not included in the table given unavailability of publications in scientific journals.

A key concern with these products is that they are sequence specific and may be ineffective for new outbreak variants. AVI-6002, a combination of two PMOs targeting EBOV VP24 (AV-7537) and VP35 (AV-7539) demonstrated efficacy in NHP studies, and safety in phase 1 studies, but some adverse events non dose-dependent and it has been withdrawn. A clinical trial on 14 patients that receive TKM-130803, an anti-EBOV siRNA that demonstrated efficacy against EBOV-Makona, the EBOV variant that caused the recent outbreak in West Africa, in non-clinical NHP studies, was terminated when the pre-specified futility boundary was reached, indicating a probability of survival to day $14 \leq 0.55$.

Nucleoside and nucleotide antivirals have thus far been the most successful class of antivirals given their success in treating HIV and herpes viruses. BCX4430, brincidofovir, favipiravir, and GS-5734 have been tested as anti-EBOV therapeutic candidates. BCX4430 is an adenosine nucleoside analogue that inhibits RNA synthesis by adding a highly selective monophosphate nucleotide to the nascent RNA chain, interrupting elongation, with which are being conducted Phase 1 clinical trials (Cardile et al., 2016). Brincidofovir, was originally studied as a treatment for double-stranded DNA viruses, but, because brincidofovir was in advanced trials for other viral indications, it was thought it could be an effective EBOV therapeutic. Trial began in Liberia in January 2015 and in the same months it was ceased due to low enrollment (World Health Organization, 2015). It was administered to three patients in the United States, who recovered, but the drug's relationship to their survival is not easily established due to other interventions conducted during the care of these patients (Florescu et al., 2015) and the product sponsor has withdrawn its support of brincidofovir for an EBOV indication (World Health Organization, 2015). Favipiravir

is a nucleotide analogue that acts as a pseudopurine, had completed advanced clinical trials for influenza and demonstrated efficacy in mouse models of EBOV infection. For such reasons it was considered an attractive candidate for EBOV therapy. Clinical trial during EVD outbreak began in December 2014 in Guinea and 180 have been enrolled, but no conclusions on efficacy are available (World Health Organization, 2015). GS-5734 is the newest polymerase inhibitor being evaluated as a therapeutic for EBOV. It is a small-molecule monophosphoramidate prodrug of an adenosine analogue that, in animal-model, it is rapidly converted to its pharmacologically active triphosphate form. In NHPs administration beginning 3 days after EBOV challenge resulted in 100% survival. Having been found that GS-5734 distributes into the testes, epididymis, eyes, and brain, it may also be of efficacy in post-Ebola syndrome and eradication of persistent viral replication in the genital tract. Furthermore, there are also evidences of its rapid distribution (24 h) within one of the initial target cell types for EBOV infection, the mononuclear line, hence it may also be valuable for post-exposure prophylaxis of high-risk exposures (Cardile et al., 2016). Another drug used during last epidemic was Favipiravir, a small molecule that interferes with the RNA-dependent RNA polymerase of a variety of viruses including EBOV.

Three immunotherapeutics were tested in clinical trials during the West Africa EBOV outbreak: ZMapp, convalescent plasma, and INF-β (Cardile et al., 2016). The first therapeutic used in the West African outbreak was ZMapp, a cocktail of three monoclonal antibodies developed at the Public Health Agency of Canada in collaboration with Defyrus, the United States Army Medical Research Institute of Infectious Diseases (USAMRIID), Kentucky BioProcessing, and Mapp Biopharmaceutical. ZMapp has been shown to be the most effective postexposure

intervention to date in the NHP model, with 100% protection up to five days after the challenge with EBOV (Qiu et al., 2014), but after phase 1 no conclusion on efficacy is available (World Health Organization, 2015). Other therapeutics used on the field include MIL-77, an antibody-based cocktail closely related to ZMapp, convalescent whole blood, and convalescent plasma (de La Vega et al., 2015).

In addition to the above therapies numerous other drugs were also considered during the recent EBOV outbreak such as amodiaquine, amiodarone, lamivudine, atorvastatin, irbesartan, and sertraline (Cardile et al., 2016).

Clinical trials for two vaccine candidates, the chimpanzee-adenovirus ChAd3-Zaire Ebola virus (ChAd3-ZEBOV) vaccine and the recombinant vesicular stomatitis virus-Zaire Ebola virus (rVSV-EBOV) vaccine, have also been accelerated with the support of the World Health Organization. Both the ChAd3-ZEBOV and the rVSV-EBOV vaccines began Phase III clinical trials at the beginning of 2015 (de La Vega et al., 2015). Final results from the vaccination trial with rVSV-EBOV conducted in Guinea showed a vaccine efficacy of 100% (Henao-Restrepo et al., 2015).

Final results from the vaccination trial with rVSV-EBOV may bring quickly to have an approved vaccine against EBOV. Nevertheless it is important preventing infection by EBOV, applying simple but rigorously-observed methods of protection, rapid monitoring for signs of ill and to avoid the contact with any potential source of infection. WHO gives some simple indication to minimize the risk of infection and the spread of outbreaks. These recommendations are briefly summarized in the following alerts: to be alert for symptoms that include fever, headache, joint and muscle aches, weakness, diarrhea, vomiting, stomach pain, lack of appetite and in some cases bleeding; to avoid contact with body fluids, because EBOV can be spread

though mucus, semen, saliva, vomit, stool or blood but is not considered transmissible through airborne droplets; most people who become infected with EBOV are those who live with and care for EVD patients, then caregivers in contact with EVD patients must wear a long-sleeved gown, mask, goggles and gloves, and should pay extreme attention in the handling of needles, syringes or any other cutting object; people that recover from EVD should consider to be still infectious at least for two months, but unprotected sexual intercourse with a male survivor within 12 months of the survivor's EVD recovery whose semen has not been tested must be avoid and breastfeeding by survivor woman should be consider as exposure for the baby; to be careful during funeral preparations and burial ceremonies for the high infectivity of corps of dead; and finally, to avoid bush meat, even if well cooked meat is considered virus free (World Health Organization, 2016b).

Furthermore, as pigs are the only domestic animals that have been confirmed as having an association with EVD outbreaks, they should be considered as potential amplifier hosts until proven otherwise. Precautionary measures are needed in pig farms in Africa to avoid pigs becoming infected through contact with fruit bats (Formenty, 2014).

Despite the importance of prevention and research for some people, the "adoption of containment measures with a view to strengthen health systems and infrastructure is the most effective way to curb this epidemic and prevent future ones" (Rid and Emanuel, 2014).

1.8   Antiviral innate immune response and its suppression

1.8.1   The interferon system

The severe disease provoked by filoviruses infection is characterized by massive systemic virus replication. Likely, the resulting very high blood titers induce damaging host responses, as excessive cytokine production, release of tissue factor and other mediators that contribute to a severe disease featuring liver damage, vascular leakage and bleeding (Feldmann and Geisbert, 2011). The excessive replication reflects the ability of EBOV to counteract host antiviral defenses, particularly IFN responses (Bray and Geisbert, 2005). The IFN system constitutes a major innate defense against infections by viruses and other pathogens.

IFNs are a group of signaling proteins belonging to the large class of proteins known as cytokines and are produced and released by host cells in response to the presence of several pathogens. They are divided into three classes called type I, II and III IFNs. Type I IFNs (IFN-α and -β) are produced mainly by fibroblasts (IFN-β) and leukocytes (IFN-α) as a reaction to infection and show potent antiviral activity (Parkin and Cohen, 2001). In humans, type I IFNs comprise at least 13 functional non allelic genes encoding IFN-α, one gene encoding IFN-β and the less extensively studied genes encoding other genes, such as IFN-ω, -ε, -τ, -δ and –κ (Randall and Goodbourn, 2008). Almost all cell types are capable of producing IFN-α/β; however, plasmacytoid dendritic cells (pDC) are considered as the major source for IFN-α production during the course of an infection (Siegal et al., 1999). Both α and β IFN (IFN-α/β) bind to the same heterodimeric receptor, the IFN-α/β receptor on the cell surface (Basler, 2015) and protect uninfected cells by inducing the intracellular

production of molecules that inhibit or interfere with viral RNA and DNA production. IFN-γ, the only type II IFN, also called immune IFN, is generated only by cells of the immune system (activated T cells and natural killer (NK) cells), uses a separate receptor to that of the type 1 IFNs and performs different functions: it acts directly on the immune system to activate macrophage and neutrophil intracellular killing, to stimulate NK cell function and to enhance antigen presentation by increasing MHC class II expression on antigen presenting cells (Parkin and Cohen, 2001). Type III IFN family consists in three newly identified IFN-λ1, -λ2 and –λ3 proteins, also termed IL-29, IL-28A and IL-28, respectively (Randall and Goodbourn, 2008).

When expressed, IFN–α/β are secreted from producing cells and bind the IFN-α/β receptor in an autocrine or paracrine manner, triggering a JAK-STAT signaling cascade that upregulates hundreds of genes that cumulatively render cells resistant to virus infection (Basler, 2015).

Induction of IFN-α/β gene expression is activated by several pattern recognition receptor (PRRs), that are able to detect chemical patterns or structures highly conserved in virus and microbes, so called pathogen-associated molecular patterns (PAMPs). PRRs can be classified into five families, based on their protein domain homology: Toll-like receptors (TLRs), C-type lectin receptors (CLRs), nucleotide-binding domain, leucine-rich repeat (LRR)-containing (or NOD-like) receptors (NLRs), RIG-I-like receptors (RLRs), and the AIM2-like receptors (ALRs), grouped in two main classes, membrane-bound receptor (TLRs and CLRs), and unbound intracellular receptors (NLRs, RLRs and ALRs) (Brubaker et al., 2015; Reikine et al., 2014). PRRs that induce IFN-α/β production are RLRs, TLRs and STINGs (stimulators of IFN genes). STING, a transmembrane protein predominantly located

in endoplasmic reticulum, activates TANK-binding kinase 1 (TBK1)- and IFN regulatory factor 3 (IRF-3)-mediated IFN production, contributing to the defense against viral and intracellular bacterial pathogen DNAs (Brubaker et al., 2015). RLRs, located in the cytoplasm, consist of three DExH/D box helicases: retinoic acid-inducible gene-I (RIG-I), melanoma differentiation gene 5 (MDA5), and laboratory of genetics and physiology 2 (LGP2). TLRs are a family of single-transmembrane proteins expressed predominantly in immune cells, such as macrophages and DCs (Kawai and Akira, 2007).

1.8.1.1 RIG-I-like receptors-dependent pathways

Many viruses deliver an RNA genome or generate viral RNA as product of replication or transcription into the cytoplasm. The presence of these viruses is primarily detected by RIG-I and MDA5. RIG-I recognizes 5'-triphosphate (5'-ppp) blunt ends of viral genomic dsRNA, whereas MDA5 binds internally to long dsRNA (more than 2 Kb) with no end specificity. RIG-I and MDA5 contain a tandem N-terminal caspase recruitment domains (CARDs), a DExD/H-box helicase and a C-terminal domain (CTD). In the absence of dsRNA, RIG-I has a closed inactive conformation, whereas when it binds RNA through the helicase and CTD domains it undergoes a conformational change, releasing the CARDs from an auto-repressed state. Four RIG-I molecules come together and their CARDs assemble into an oligomer stabilized by unanchored K63-linked polyubiquitin chains. The RIG-I CARDs serve as a scaffold for IFN-β promoter stimulator (IPS)–1 (Kawai et al., 2005), now called mitochondrial antiviral signaling protein (MAVS) (Seth et al., 2005), but formerly also known as IFN-β inducing CARD adaptor (CARDIF) (Meylan et al., 2005) or virus-induced signaling adaptor (VISA) (Xu et al., 2005), an

adaptor molecule possessing an N-terminal CARD, which forms a filament that is tethered on the mitochondrial or peroxisomal membrane (Figure 15).

The activation and signaling of MDA5 shows some differences. For instance, CARDs are not sequestered in the MDA5 resting form, and its activation results in the cooperative assembly of MDA5 protomers onto dsRNA helical filaments. LGP2, the third RLR, has similar helicase and CTD domains as RIG-I and MDA5, but it lacks the tandem CARDs. Its ability to recognize dsRNA allows it to act as a positive or negative regulator of RIG-I– and MDA5-mediated viral recognition (Reikine et al., 2014; Satoh et al., 2010; Venkataraman et al., 2007). MDA5 seems to require LGP2 for efficient recruitment of viral dsRNA to facilitate the initiation of signaling, and LGP2 appears to be more important for MDA5 than for RIG-I, possibly because of differences in their affinities for dsRNA (Satoh et al., 2010).

Once activated, MAVS undergoes CARD-dependent self-polymerization, creating prion-like aggregates that are important for signal transmission (Brubaker et al., 2015). MAVS polymerization recruits a set of ubiquitin ligases, tumor necrosis factor (TNF) receptor-associated factors (TRAFs), required for the activation of TRAF family member associated NFKB activator (TANK)-binding kinase 1 (TBK-1) and the inducible IkB kinase epsilon (IKK-ε) complex. The two kinases TBK-1 and IKK-ε carry out the phosphorylation of latent IFN regulatory factors 3 and 7 (IRF-3/7), leading to their dimerization and nuclear translocation (Fitzgerald et al., 2003). Once in the nucleus, IRF-3 and 7 homo- or hetero-dimers associate into an enhanceosome with other transcription factors to drive the transcription of IFN-α/β genes (Panne et al., 2007) (Figure 15).
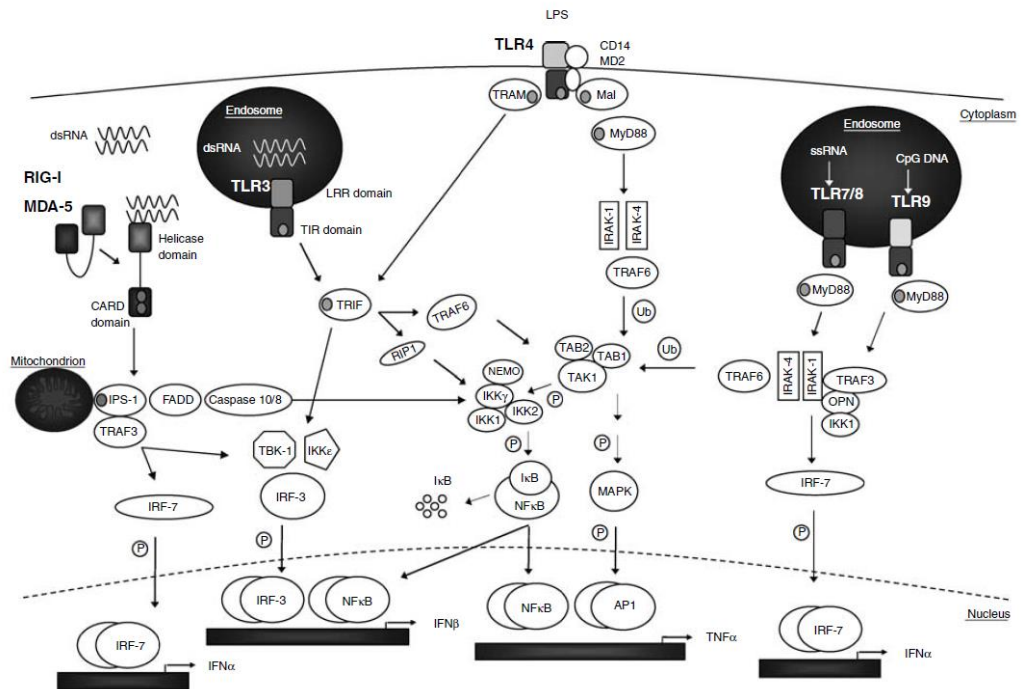
Figure 15 TLR-dependent and RLR-dependent pathways operate to detect viral infection. Recognition of dsRNA by TLR3 in the endosomal membrane recruits TRIF to the receptor, which induces proinflammatory cytokines and type I IFNs via the RIP1/TRAF6-NF-kB pathway and the TBK1/IKK-i-IRF-3/IRF-7 pathway, respectively. In contrast, detection of dsRNA in the cytoplasm by RIG-I activates TBK1/IKK-i through IPS-1, which is localized on the mitochondrial membrane. In pDCs, TLR7 and TLR9 recognize viral ssRNA and DNA, respectively. Stimulation with TLRs recruits a complex of MyD88, IRAK-4, IRAK-1, TRAF6, and IRF-7. Phosphorylated IRF-7 translocates into the nucleus and upregulates the expression of type I IFN genes (Thompson and Locarnini, 2007)

1.8.1.2 Toll-like receptors-dependent pathways

TLRs are type I integral membrane glycoproteins characterized by the extracellular domains containing variable numbers of leucine-rich-repeat (LRR) motifs and a cytoplasmic signaling domain homologous to that of the interleukin 1 receptor (IL-1R) known as the Toll/interleukin-1 receptor (TIR) domain. (Bowie and O'Neill, 2000). Although the extracellular recognition domains differ, dictating ligand specificity, TLRs share considerable homology of the TIR domain (Thompson and Locarnini, 2007).

Based on their primary sequences, TLRs can be further divided into several subfamilies, each of which recognizes related PAMPs: for instance, the subfamily of TLR1, TLR2, and TLR6 recognizes lipids, whereas the highly related TLR7, TLR8, and TLR9 recognize nucleic acids (Akira et al., 2006). TLRs are expressed on various immune cells, including macrophages, DCs, B cells, specific types of T cells, and even on nonimmune cells such as fibroblasts and epithelial cells. TLRs may be expressed extra- or intracellularly: while certain TLRs (TLRs 1, 2, 4, 5, and 6) are expressed on the cell surface and may recognize extracellular virions, typically by interaction with envelope glycoproteins, others (TLRs 3, 7, 8, and 9) are found almost exclusively in intracellular compartments such as endosomes, and their ligands, mainly nucleic acids, require internalization to the endosome before signaling is possible (Akira et al., 2006; Thompson and Iwasaki, 2008; Thompson and Locarnini, 2007). This appears to be a well-suited strategy as most viruses, or viral components, localize to the endosome either during entry and uncoating, or during assembly and budding. Double stranded RNA intermediates are produced during the replication cycle of most viruses, including viruses with DNA genomes and these RNA

secondary structures are thought to be recognized by TLR3. TLR7 and TLR8 recognize single stranded RNA (ssRNA) and induce innate immune responses to ssRNA-viruses. TLR9 is also located in the endosome and likewise mediates recognition of viral nucleic acids, in this case, precisely DNA (Thompson and Iwasaki, 2008). These TLRs are synthesized in an inactive state and must be proteolytically cleaved to become active. TLR cleavage requires multiple endosomal proteases, ensuring that endosomal TLRs function only within an endocytic compartment. It is thought that this compartmentalization may have evolved to limit the contact with host nucleic acids, which are not normally found in the endosome and might trigger inappropriate immune responses if recognized by TLRs (Brubaker et al., 2015; Thompson and Locarnini, 2007).

The engagement of TLRs by microbial components triggers the activation of signaling cascades, leading to the induction of genes involved in antimicrobial host defense. Stimulation with TLR3, TLR4, TLR7/8 and TLR9 ligands, but not the TLR2 ligand, induces type I IFN production in addition to proinflammatory signals and, furthermore, leads to DC maturation and expression of costimulatory molecules (Kaisho and Akira, 2001). After ligand binding, TLRs dimerize and undergo conformational changes required for the recruitment of TIR-domain-containing adaptor molecules to the TIR domain of the TLR. There are four adaptor molecules: MyD88, TIR-associated protein (TIRAP) or MyD88-adaptor-like (MAL), TIR-domain-containing adaptor protein-inducing IFN-b (TRIF) or TIR-domain-containing molecule 1 (TICAM1) and TRIF-related adaptor molecule (TRAM). The differential responses mediated by distinct TLR ligands can be explained in part by the selective usage of these adaptor molecules (Thompson and Locarnini, 2007).

MyD88 and TRIF adaptors are responsible for the activation of distinct signaling pathways that lead to the production of proinflammatory cytokines and type I IFNs, respectively. MyD88 is critical for the signaling from all TLRs except TLR3. Recruitment of MyD88 leads to the activation of MAP kinases (MAPKs) (ERK, JNK, p38) and the transcription factor NF-κB to control the expression of inflammatory cytokine genes. TLR7/8- and TLR9 in response to CpG DNA recruit MyD88 that forms a complex with IRF7, IRAK1, IRAK4 and TRAF6. IRF7 is phosphorylated and translocates into the nucleus inducing type I IFN induction (Kawai and Akira, 2007). IRAK1 is most likely a kinase that phosphorylates IRF7, but also IKK has been reported to have a similar role to IRAK1, having the ability to bind and phosphorylate IRF7 (Hoshino et al., 2006) (Figure 15).

TRIF is recruited to TLR3 and TLR4, and activates an alternative pathway (TRIF-dependent pathway) that culminates in the activation of NF-κB, MAPKs and the transcription factor IRF3. TRIF recruits and activate TBK1 and IKKε, which phosphorylate serine/threonine clusters present in the C-terminal region of IRF3. The receptor-interacting protein 1 (RIP1) participates in TRIF-dependent NF-κB activation. TRAF3 is required for TBK1/IKKε-dependent IRF3 activation in TLR3 and RIG-I/Mda5-signaling. Phosphorylated IRF3 forms a dimer, which translocates from cytoplasm to the nucleus to induce expression of target genes including IFN-β (Kawai and Akira, 2007).

Phosphorylated IRF-3 and IRF-7 form homodimers, translocate into the nucleus, and bind to the specific DNA regulatory elements known as IFN-stimulated response elements (ISREs), resulting in the expression of a set of IFN-inducible genes. Among nine IRF family members, IRF-3 and IRF-7 are essential for the induction of type I

IFN production. Thus, although RLRs and TLRs signal through different pathways, both appear to be able to activate the production of type I IFNs and inflammatory cytokines (McCartney and Colonna, 2009).

1.8.1.3 JAK/STAT pathway

IFNs induce a large number of genes through activating the janus tyrosine kinase (JAK)–signal transducers and activators of transcription proteins (STAT) pathway, and the binding of transcription factors to upstream regions of the inducible genes (IFN-stimulated gene, ISG) at specific DNA regulatory elements known as IFN-stimulated response element (ISRE) and gamma-activated sequence (GAS). The produced type I IFNs alert the surrounding cells by triggering signaling cascades that lead to phosphorylation and nuclear translocation of STAT1 (Satoh et al., 2010).

The type I IFN receptor (IFNAR) is composed by two distinct subunits: IFNAR1 and IFNAR2. The binding of type I IFNs to the IFNAR actives two receptor-associated tyrosine kinases, JAK1 and Tyk2; this is followed by tyrosine phosphorylation of the STAT1 and STAT2 proteins. Phosphorylated STAT1 and STAT2 combine with IRF-9 to form the trimeric ISGF-3 complex, which, upon translocation to the nucleus, binds to the ISRE, which is present in most IFN-α and IFN-β–responsive genes. In contrast, binding of IFN-γ to its receptor leads to tyrosine phosphorylation of the JAK1 and JAK2 tyrosine kinases, resulting in the phosphorylation of STAT1 but not STAT2. Phosphorylated STAT1 homodimerizes to form the GAF-AAF complex, which translocates to the nucleus and binds to the GAS present in most IFN-γ–inducible genes. Like IFN-γ, IFN-α/β signaling can also lead to the formation of the GAF-AAF complex and its binding to the GAS regulatory element. The three newly identified IFNs-λ bind to a heterodimeric

receptor. Both STAT1 and STAT2 are activated and the downstream signaling pathways activated by IFN-λ appear to be indistinguishable from those activated by IFN-α and IFN-β (Vilcek, 2003). (Figure 16)

The signaling cascade, triggered by the binding of IFNs to IFNs-receptors leads to the induction of more than 300 IFN-stimulated genes (ISGs). Many of the gene products encode pattern-recognition receptors (PRRs) that detect viral molecules and modulate signaling pathways, or transcription factors that form an amplification loop resulting in increased IFN production and protection from virus. However, some products of ISGs have a direct antiviral activity. These include proteins that catalyze cytoskeletal remodeling, induce apoptosis, regulate post-transcriptional events and proteins that are involved in subsequent post-translational modification.

Among the IFN-induced proteins implicated in the antiviral actions of IFNs in virus-infected cells are protein kinase R (PKR), IFN-stimulated protein of 15 kDa (ISG15), the 2',5'-oligoadenylate synthetase (OAS), ribonuclease L (RNaseL), and the Mx protein GTPases. However, although these four proteins are known to be important in the antiviral response, they do not represent the complete repertoire of antiviral effectors (Sadler and Williams, 2008).

ISG15 is a ubiquitin homologue that regulates many aspects of the innate immune response (for example, the activation of NF-κB) and functions of the adaptive immune system.

Mx GTPases, belonging to the guanine hydrolyzing proteins family, are strictly depending on type I and III IFNs for their expression and play an antiviral role against several viruses like orthomyxomaviruses, paramyxoviruses, rhabdoviruses,
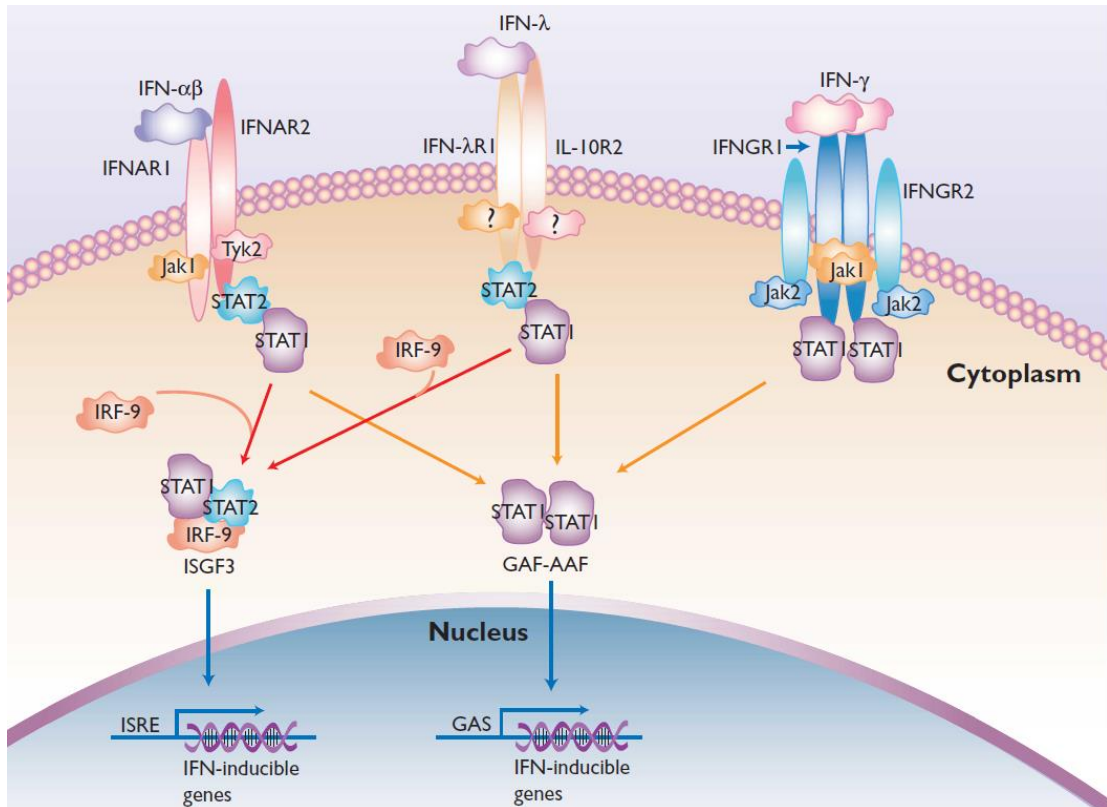
Figure 16 - Comparison of signaling pathways activated by IFN-α/β, IFN-γ and IFN-λ.
The action of the IFNs is mediated through three receptor complexes: a heterodimer of IFNα receptor 1 (IFNAR1) and IFNAR2 binds type I IFNs; the interleukin-10 receptor 2 (IL-10R2) associates with IFNλR1 (IFNλ receptor 1) to bind the three IFNλ subtypes; and a tetramer consisting of two IFNGR2 (IFNγ receptor 2) chains and two IFNGR1 chains binds dimers of the type II IFNγ. Following binding by type I IFNs, signal transduction is initiated by pre-associated tyrosine kinases Jak1 and Tyk2, which phosphorylate IFNAR1 and leads to the recruitment and phosphorylation of the signal transducers and activators of transcription (STATs). STAT1 and STAT2 heterodimer associate with IFN-regulatory factor 9 (IRF9) to form IFN-stimulated gene factor 3 (ISGF3), or STAT homodimers to form the IFNγ activation factor (GAF). These complexes translocate to the nucleus to induce IFN-stimulated genes from IFN-stimulated response elements (ISREs) or GAS promoter elements, for type I and type III, or type II IFN responses, respectively. (Vilcek, 2003).

togaviruses and bunyaviruses. Mx proteins are expressed by various cell types in peripheral tissues, for example, by hepatocytes, endothelial cells and immune cells, including peripheral blood mononuclear cells, pDCs and myeloid cells and the main target seems to be viral nucleocapsid-like structures.

OAS proteins are distinguished by their capacity to synthesize 2',5'-linked phosphodiester bonds to polymerize ATP into oligomers of adenosine, that specifically activate the latent form of RNaseL. OAS proteins can act as PRRs for the detection of viral dsRNA in the cytoplasm. RNA degraded by RNaseL can activate the other cytoplasmic PRRs, such as RIG-I and MDA5, resulting in the induction of type I IFN gene expression.

PKR belongs to a small family of protein kinases that respond to environmental stresses. It accumulates in the nucleus and cytoplasm as an inactive monomer, which is activated directly by viral RNAs, and by several other ligands, such as ceramide or the protein activator of the IFN-induced protein kinase (PACT). Phosphorylated active PKR dimerize and form the active enzyme which phosphorylates EIF2α, preventing recycling of GDP, bringing to antiviral and antiproliferative effects (Sadler and Williams, 2008).

1.8.2 Suppression of innate immune response

Coexistence of viruses and their hosts has imposed an evolutionary pressure on both the virus and the host immune system. On the one hand, the hosts have developed an immune system able to attack viruses and virally infected cells, whereas on the other hand, viruses have developed an array of immune evasion mechanisms to escape by the host's immune system. The strategies of immune evasion are directed towards three divisions of the immune system: the humoral immune response, the cellular immune response and immune effector functions.

The ability of the virus to counteract early antiviral responses plays an important role in virulence of EBOV. Because the activation of the IFN system is a central component of the host response to viral infection, it is not surprising that EBOV has evolved mechanisms to evade its activation. Several studies have demonstrated the ability of EBOV infection to block cellular responses to IFN.

Many past studies were focused on possible nucleic acid inducers and found that dsRNA is a potent trigger of the IFN response. An important discovery in the field was the finding that a 5'-ppp group on an RNA molecule also served as a potent activator of the IFN response and could provide an alternative/additional trigger to dsRNA. However, the biochemical basis for its high level of activation by both the dsRNA and 5'-ppp-RNA remains unclear to date, because there are prevailing evidences that the majority of RNA viruses employ mechanisms that protect their RNA from exposure and since cells generally process the synthesized RNA by either capping mRNA, removing 5'ppp during RNA processing, folding RNA into complex secondary structures or packaging it into RNP complexes. The question of whether and when this RNA is exposed to the cell during the viral lifecycle remains to be

answered (Baum and García-Sastre, 2010). In any case, for RNA viruses preventing recognition by host PRRs of such PAMPs is of crucial importance. Therefore, most RNA viruses encode proteins that display IFN-antagonism properties aimed to circumvent the host innate immune system. Among those proteins, most have been revealed as involved in targeting the RLR pathway at several levels (Baum and Garcia-Sastre, 2011).

Filoviruses infections are associated with unsuccessful innate antiviral responses as a result of virally encoded immune antagonists, which target type I IFN responses and render the host incapable of mounting effective innate or adaptive immune responses. In EBOV, the main antagonists are the viral proteins VP35 and VP24, even if GP and sGP were also shown to be implicated in modulating immune responses (Ramanan et al., 2011).

The main mechanism by which VP24 inhibits IFN signaling is through binding to karyopherin-α, in fact, VP24 inhibits STAT1 nuclear translocation by competing with STAT1 for the STAT1 binding site on KPN-α (Reid et al., 2006). However, other mechanisms, including VP24 altering KPN-α folding or trafficking, cannot be excluded (Ramanan et al., 2011).

1.8.2.1 EBOV VP35 inhibits the innate immune system

First suggestions that EBOV VP35 could block IFN-α/β came from the observation that VP35 expression could complement the growth of a mutant influenza A virus that was unable to counteract the IFN-α/β response and prevented activation of the IFN-β promoter following infection by Sendai virus or following transfection of polyI:C, two potent IFN-α/β inducers (Basler et al., 2000).

VP35 was subsequently demonstrated to prevent phosphorylation of IRF-3 (Basler et al., 2003), to impair RIG-I signaling and this inhibition correlated with the capacity of VP35 to bind to dsRNA (Cárdenas et al., 2006; Hartman et al., 2004), to interact with either IKKε or TBK1 via their more conserved kinase domains, blocking the phosphorylation of either IRF-3 or IRF-7 (Prins et al., 2009). Furthermore, VP35 interacts with the host SUMOylation machinery, including Ubc9 and PIAS1, the SUMO E2 enzyme and E3 ligase, respectively and with IRF-3 and -7, bringing these IRFs to the SUMOylation machinery and promoting SUMOylation of IRF-3 and IRF-7. The premature SUMOylation of the IRFs abrogates their ability to activate IFN transcription causing diminished IFN production (Chang et al., 2009).

Two VP35 point mutants, K309A and R312A, were found to be greatly impaired in their dsRNA-binding activity and showed a related decreased but measurable IFN antagonist activity, but they have the same ability then wild-type to inhibit activation of the IFN-β promoter induced by overexpression of MAVS (Cárdenas et al., 2006).

Leung and coworkers reported the crystal structure of IID alone and bound to 8-bp dsRNA, showing that conserved basic residues in VP35 IID recognize the dsRNA backbone, whereas a pocket of hydrophobic residues caps the dsRNA blunt ends. They spotted the critical residues for RNA binding (R312A and K339) and demonstrated that these residues are also important for IFN inhibition in vivo, but not for viral polymerase cofactor function of VP35 (Leung et al., 2010a, 2009a; Prins et al., 2010b).

In addition, expression of VP35 mutants unable to bind to dsRNA was effective as that of wild-type to inhibit the activation of IFN-β gene transcription, when IKKε or TBK1 are over-expressed. These same mutants are severely impaired in blocking

IFN–α/β induction by Sendai virus or transfected dsRNA, indicating that there are two distinct mechanism of inhibition of IFN-α/β activation by VP35: a dsRNA binding-independent and a dsRNA binding-dependent mechanism, with the second that seems to offer the major contribution to suppression of RIG-I-dependent IFN-α/β responses. To explain this behavior two dsRNA-dependent mechanisms have been proposed: the sequestration of RLR-activating RNAs and the interaction of VP35 with cellular protein PACT, which interacts with RIG-I and facilitates its activation by dsRNA (Leung et al., 2010a; Luthra et al., 2013; Prins et al., 2010b). VP35 interacts with PACT in such a manner that PACT is unable to interact with RIG-I. Point mutations in VP35 that disrupted dsRNA binding abrogated VP35-PACT interaction and VP35 became unable to disrupt PACT-RIG-I interaction. This resulted in a loss of VP35 inhibition of PACT-facilitated activation of RIG-I. Given that PACT is also a dsRNA-binding protein, it has been hypothesized that dsRNA acts as a bridge between VP35 and PACT. However, in vitro binding studies using purified components in the absence or presence of RNAses showed a direct protein-protein interaction, suggesting that the same VP35 amino acid residues that mediate interaction with dsRNA also contribute to direct interaction with PACT (Luthra et al., 2013). Furthermore, interaction of PACT with VP35 has a second functional consequence: it inhibits EBOV RNA polymerase activity and this impairment requires interaction with VP35, because the RNA synthesis system is affected by PACT when wild-type VP35 is used, but not when the PACT binding-defective mutants of VP35 are used in minigenome reporter gene expression (Luthra et al., 2013; Mühlberger et al., 1999). In addition to suppressing IFN-α/β production, VP35 inhibits the activation of the IFN-induced PKR, with a mechanism of inhibition

dsRNA-binding independent (Schümann et al., 2009). In addition to all discussed

functions of EBOV BP35, it has been reported to act as RNA silencing suppressor
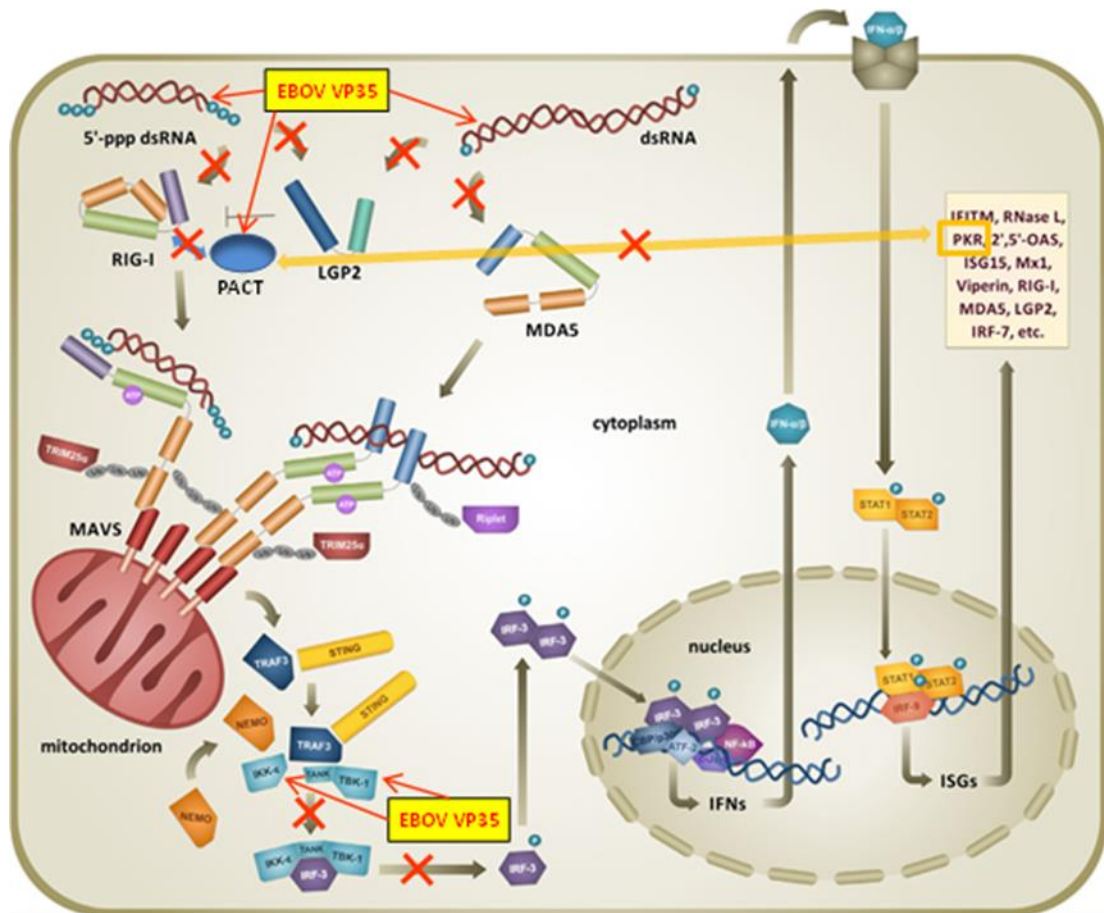
(Haasnoot et al., 2007) (Figure 17).

Figure 17 – Suppression of type I IFN antiviral response triggered by the RLRs pathway upon dsRNA detection by EBOV VP35. Viral short 5'-ppp dsRNA and long dsRNA are preferentially recognized by the CTD of RIG-I (violet) and of MDA5 (azure) respectively, with LGP2 modulating the activity of RIG-I helicase. VP35 sequesters dsRNA to RIG-I and MDA5 recognition and binds to PACT impairing its interaction with RIG-I and with PKR. Downstream VP35 interacts with the IRF-3 kinases IKK-ε and TBK-1, preventing phosphorylation of IRF-3 and its translocation to the nucleus and inhibiting in this way the expression of IFN-α/β (Zinzula and Tramontano, 2013).

1.9   Aim of the research

The knowledge gained to date on the strategies that the EBOV uses to evade the innate immune response of the host and on the biological mechanisms underlying these strategies, lets us say that the VP35 protein is a key factor for the evasion of the host defenses by the virus and therefore for the high pathogenicity of the virus. EBOV VP35 is undoubtedly a significant target for the pharmacological research, and one of the possible pharmacological targets against VP35 may be actually identified into its binding to the dsRNA.

In this contest, the present research work was aimed to develop a biochemical assay for the screening of small molecules able to inhibit the binding between VP35 to dsRNA in order to find compound that may become in the future drugs against EBOV.

The research work is divided in three main topics. The first, presented in chapter 3, explains the development of a new method for the purification of the recombinant EBOV VP35 protein in a bacterial system and the establishing of a robust biochemical fluorescence-based assay for the above mentioned screening. The second part of the research is focused on the effect of three point mutations in the coiled-coil region of the VP35 N-terminal domain on the binding to dsRNA and on the ability to inhibit the IFN pathways in a cellular assay and it is presented in the chapter 4. In the chapter 5, it has been shown then the results of the screenings of plants extract and related compounds, performed with the biochemical fluorescence-based assay.

2 MATERIALS AND METHODS

2.1 Cell Line and viral infection

A549 cells were grown in DMEM (Gibco™) supplemented with 10% Fetal Bovine Serum (E.U.-approved, South America Origin, Gibco™) and 1% penicillin/streptomycin (Euroclone®). Cells were incubated at 37 °C in humidified atmosphere of 5% CO_2 and 95% air. For production of viral RNA (vRNA), A549 cells were infected with Influenza virus A/Puerto-Rico/8/34 (H1N1) strain (IAV/PR/8/34) with a multiplicity of infection of 5. Five hours after infection, total RNA was isolated using the RNeasy Kit (Qiagen).

2.2 Plasmid construction and cloning

Cloning of the EBOV VP35 gene in pET45b(+) vector (Novagen) and production of pET45b-EBOV-VP35 plasmid for the expression of recombinant N-terminal His6-tag-VP35 protein (rVP35) was performed as previously described (Zinzula et al., 2009). Cloning of the EBOV VP35 gene in pcDNA3 plasmid (Invitrogen) and production of pcDNA3-EBOV-VP35 plasmid for the transfection of rVP35 was performed as previously described (Cannas et al., 2015).

2.2.1 Construction of EBOV VP35TM procariotic expression plasmid

To introduce three point mutations (leucine 90 to alanine, leucine 93 to alanine and leucine 107 to alanine) into the pET45b-EBOV-VP35 plasmid, a series of three consecutive site-directed mutagenesis was performed using the QuickChange Lightning Site-Directed Mutagenesis kit (Agilent technologies), following indication of producer. Obtained plasmid encodes for the triple mutant EBOV-VP35-L90A/L93A/L107A recombinant protein , here briefly named rVP35TM. Sequences of primers utilized for the mutagenesis were the following:

— **L90A:**   Forward primer
5'-GAGGAGGTAGTACAAACAGCGGCTTCATTGGCTACTGTTGTGC-3'
— **L90A:**   Reverse primer
5'-GCACAACAGTAGCCAATGAAGCCGCTGTTTGTACTACCTCCTC-3'

— **L107A**:   Forward primer
5'-CCATCGCATCAGAATCAGCAGAACAACGCATTACGAGTCTTGAG-3'
— **L107A**:   Reverse primer
5'-CTCAAGACTCGTAATGCGTTGTTCTGCTGATTCTGATGCGATGG-3'

— **L93A**:   Forward primer
5'-GTACAAACAGCGGCTTCAGCGGCTACTGTTGTGCAACAACAAACC-3'
— **L93A**:   Reverse primer
5'-GGTTTGTTGTTGCACAACAGTAGCCGCTGAAGCCGCTGTTTGTAC-3'

PCR reaction was carried out in a mixture containing: pET45b-EBOV-VP35 plasmid (100 ng), each primer (125 ng) and other components provided within the kit. The PCR mixtures were filled with nuclease-free water to a final volume of 50 µL and the PCR cycle consisted of: an initial denaturation at 95 °C for 2', 18 cycles of denaturation at 94 °C for 20", annealing at 60 °C for 10", extension at 68 °C for 3'30", and a final extension at 68 °C for 5'. XL10-Gold® Ultracompetent Cells were transformed with PCR products following suggested heat shock protocol – 30' on ice,

30" at 42 °C, 2' on ice – and cultured. Plasmids was extracted and sequenced step by step for control.

2.2.2   Construction of EBOV VP35TM mammalian expression plasmid

Starting from pcDNA3-EBOV-VP35 plasmid, a site-direct mutagenesis was performed using Q5® Site-Directed Mutagenesis Kit in order to obtain new insert that express the triple mutant EBOV-VP35TM recombinant protein in a mammalian cellular system.

Sequences of primers utilized for the mutagenesis were the following:

⸻ **L90A/L93A/L107A**:   Forward primer
5'-ACCATCGCATCAGAATCAGCAGAACAACGCATTACGAGTCTTGAGAATG-3'
⸻ **L90A/L93A/L107A**:   Reverse primer
5'-GTTGTTGCACAACAGTAGCCGCTGAAGCCGCTGTTTGTACTACCTCCTC-3'

PCR reaction was carried out in a mixture containing: pcDNA3-EBOV-VP35 plasmid (25 ng), each primer (0.5 μM) and Q5 Hot Start High-Fidelity 2X Master Mix (12.5 μl) provided within the kit. The PCR mixtures were filled with nuclease-free water to a final volume of 25 μL and the PCR cycle consisted of: an initial denaturation at 98 °C for 30", 25 cycles of denaturation at 98 °C for 10", annealing at 59 °C for 30", extension at 72 °C for 2'30", and a final extension at 72 °C for 2'.

After PCR, following steps were performed: the kinase, ligase and Dpn-I (KLD) treatment, that allows phosphorylation, circularization and template removal in a single 5' step and the subsequent transformation of 50 μl of NEB-5α competent cells with 5 μl of KLD products, following suggested heat shock protocol – 30' on ice, 30" at 42 °C, 5' on ice – and cultured. Plasmid was extracted and sequenced step by step for control.

2.3 Protein expression

BL21AI Escherichia coli cells competent for transformation (Invitrogen), were prepared and transformed with pET45b-EBOV-VP35 and pET45b-EBOV-VP35TM plasmids. Transformants were selected on Luria-Bertani (LB) medium (10 g Tryptone, 10 g NaCl, 5 g Yeast extract per liter of H_2O) agar plates containing 150 µg/ml of ampicillin. A transformed bacterial colony was inoculated in 50 ml of LB medium with the same quantity of antibiotic and left to grow overnight (ON) at 200 rpm at 37 °C. Bacterial culture was transferred in 4 liters of LB medium containing 150 µg/ml of ampicillin and 0.1% (w/v) glucose and incubated at 37°C with shaking (200 rpm) until OD_{600} reaches 0.6. Protein expression was inducted adding 0.4 % (w/v) arabinose and 0.65 mM IPTG and culture was incubated ON at 200 rpm at 18 °C. After incubation, the cell culture was centrifuged at 4500xg at 4 °C for 20 min and bacterial pellets were collected and then frozen at -80 °C.

2.4 Protein purification: denaturation and refolding

The bacterial pellet was re-suspended in lysis buffer 5 ml (100 mM sodium phosphate pH 8.0, 500 Mm NaCl, 1 mM 2-mercaptoethanol, 10 % glycerol, 20 mM imidazole, 6 M urea) per 1 ml of pellet. The suspension was incubated on ice for 15 min and subsequently sonicated on ice. The cell lysate was centrifuged at 32,000xg at 4 °C for 45 min. Supernatant was slowly loaded (0.5 ml/min) to an IMAC Econo Column (Biorad) prepared with 3 ml of Ni-Sepharose High Performance (GE

Healthcare) resin, pre-equilibrated in binding buffer (100 mM sodium phosphate pH 8.0, 300 mM NaCl, 1 mM 2-mercaptoethanol, 10 % glycerol, 20 mM imidazole, 6 M urea). The column was connected to the BioLogic LP Chromatographic System (Biorad) for the management and the reading of the purification.

Urea was gradually removed from the column by a decreasing gradient of concentration from 6 up to 0 M with a flow rate of 0.5 ml/min for around 130 column volumes (800 minutes). The column was washed for several bed volumes with Washing buffer with increasing concentrations of imidazole (50 mM sodium phosphate pH 8.0, 300 mM NaCl, 1 mM 2-mercaptoethanol, 10% glycerol, 70 mM - 150 mM - 250 mM imidazole). Refolded recombinant proteins were eluted using 90 ml of the same buffer having 1M imidazole and collected in fraction. Significant eluted fractions, selected on immobilized metal ion affinity chromatography (IMAC) chromatogram, were analyzed running on 12% SDS–PAGE. Fractions containing rVP35 protein were gathered and dialyzed against Dialysis buffer (50 mM sodium phosphate pH 8.0, 800 mM NaCl, 1 mM 2-mercaptoethanol, 10 % glycerol). Afterwards protein concentration was determined by Bradford assay with the Protein Quantification Kit-Rapid (Fluka – Sigma Aldrich).

2.5   Preparation of dsRNA substrates

500 bp dsRNA was produced by in vitro transcription using the T7 MEGAscript RNAi kit (Ambion) from the linearized DNA provided with the kit as template, according to manufacturer's instructions. In vitro transcribed (IVT) oligomers were

purified from transcription reaction with Quick Spin G25 columns (Roche), and quantified by spectrophotometry. In the same way we generated a 500 bp radiolabeled dsRNA by supplementing the in vitro transcription reaction with 0.15 μCi of ^{3}HGTP (35.5 Ci/mmol).

A fluorescent dsRNA oligomer of 30 bp in length and an analogue not fluorescent were prepared by annealing from three different ssRNA purchased from Metabion International AG (Germany). Sequences purchased are the following: a) 5'-ppp-cccuuuccuccuuccuuuuguuccucuccc-3', b) 5'-gggagaggaacaaaaggaaggaggaaaggg-3', c) 5'-Fluorescein-gggagaggaacaaaaggaaggaggaaaggg-3'. Annealing was been conducted in order to have each dsRNA one end with triphosphate. The integrity of DNA templates, IVT dsRNAs and synthetic dsRNA molecules was assessed by agarose-gel electrophoresis.

2.6 Magnetic pull-down assay

First phase of the magnetic pull-down assay was the conjugation between 2 μg of rVP35 and 2 mg of paramagnetic Talon Dynabeads (Invitrogen) in a volume of 700 μl of binding/washing buffer (50 mM Sodium Phosphate pH 7.5, 150 mM NaCl, 0.03% Tween-20) for 30 minutes at 4 °C under gentle rotating agitation (20 rpm). Applying a magnetic field, we removed supernatant with unconjugated rVP35 and we further washed beads twice with binding/washing buffer. Pellets with conjugated rVP35 were re-suspended in a reaction mixture having 50 mM Sodium Phosphate pH 7.5, 100 mM NaCl, 20 mM MgCl2, 0.03% Tween-20, transferred in a 96-multiwells

plate in conjunction with labeled, and eventually not labeled, dsRNA (depending on the type of experiment to be carried out) up to a final volume of 100 μl and incubated for 60 min at 37 °C (200 rpm). After the incubation, supernatant with unbound dsRNA was removed under the application of magnetic field, followed by two washing with 200 μl of buffer to remove it entirely. After 10 minutes incubation at room temperature with 200 μl of elution buffer (50 mM Sodium Phosphate pH 7.5, 300 mM NaCl, 1 M imidazole, 0.03% Tween-20), supernatant containing the complex rVP35-dsRNA was recovered and transferred into a black 96-multiwells plate to determine the fluorescence signal with Multilabel counter plate reader Victor 3 (Perkin Elmer model 1420-051) equipped with filters for fluorescein fluorophore 490/528 nm.

2.7 Nickel-coated plates assay

In a Pierce® Nickel Coated Plate, (Thermo Fisher), 700 ng of VP35 were added in each well in a volume of 200 μl of coating buffer (Final concentration 50 mM Sodium Phosphate pH 7.5, 150 mM NaCl) and incubated for 30 minutes at 4 °C under rotating agitation (120 rpm), then washed twice with 200 μl of washing buffer (50 mM SP pH 7.5, NaCl 150 mM, 0.03% Tween-20). After removing supernatant, a volume pair to 100 μl was added with 7.5 nM of 30 bp 5'-fluorescein-dsRNA and, where needed, the compound to screen, in a reaction mixture having 50 mM Sodium Phosphate pH 7.5, 100 mM NaCl, 20 mM $MgCl_2$, 0.03% Tween-20 and plate was incubated for 60 min at 37 °C (200 rpm). After the incubation, unbound dsRNA was

removed by two washing with 200 μl of reaction mixture and then, adding 200 of μl of the same buffer, fluorescence signal of samples were read with the mentioned plate reader (Victor 3 -Perkin-Elmer).

2.8   SDS-PAGE and Western blot analysis

Samples of the rVP35 protein from aliquots of the IMAC collected fractions were loaded and run on a SDS–Nu–polyacrylamide gel (PAG) 12% Bis–Tris gel, using a XCell SureLock Mini-Cell (Invitrogen) apparatus, following manufacturer's instructions. Samples were visualized by staining with the SimplyBlue Safe Stain kit. Presence of the full length rVP35 was confirmed by Western blotting analysis, running same samples on a SDS–Nu–PAGE 12% Bis–Tris gel and transferring the proteins onto a PVDF Invitrolon membrane, using Nu-PAGE Transfer Buffer 1X (Life Technologies) with a Trans-Blot Electrophoretic Transfer Cell (Biorad), under a 400 mAh current for 1 h at 4 °C. At the end of the transfer, membrane was incubated in Tris-buffered saline with Tween 20 (TBST) buffer (50 mM Tris, 150 mM NaCl, 0.05% Tween-20) pH 7.6 + 5 % Milk at room temperature for 30 minutes at 50 rpm, followed by four washing with TBST buffer for 5 minutes each one. After, membrane was incubated ON at 4 °C with a mouse anti-His6-tag monoclonal primary antibody (1:5,000 dilution) and 5 % of BSA in TBST buffer. After incubation, it was washed four times for 5 minutes in PBST and then was probed for 1 h at 4 °C with a rabbit anti-mouse IgG peroxidase-conjugated secondary antibody (1:50,000 dilution). Four further washings of 5 minutes in TBST buffer were performed before 3 minutes incubation in 10 ml ECL Plus Western Blotting Substrate A + B (40:1 ratio) (Thermo

Scientific). The specific protein bands were visualized by an enhanced chemiluminescent (ECL) detection system with the Chemidoc™ MP System instrument (Biorad).

2.9 Determination of kinetics parameters (Kd and Bmax)

Using two different approaches we determined the equilibrium dissociation constant (K_d) and maximum binding capacity (B_{max}) for the binding between rVP35 and 30 bp dsRNA. Both methods were performed using magnetic pull-down and Nickel-coated plate assays described above. The first method consists in performing two parallel saturation experiments, one with 30 bp dsRNA with a molecule of fluorescein at one of the 5'-ends as labeled ligand and the second one with same concentration of fluorescent ligand in presence of a fixed concentration of the not fluorescent ligand. The concentration of fluorescent ligand ranged from 200 to 1.5 nM, while the one of non-fluorescent ligand was 2 μM. Values obtained were analyzed both by Scatchard-plot analysis and by a non-linear regression, in order to calculate K_d and B_{max} (Bylund and Murrin, 2000).

The second method consisted in a homologous competition (competition between labeled and corresponding unlabeled ligand) assays that have been used to measure binding parameters for many years: a fixed concentration of fluorescent ligand (7.5 nM) and multiple concentration of non-fluorescent ligand (from 0.02 nM to 2000 nM) competed for binding to the VP35 RBD. Kd and Bmax values were calculate starting from the values of IC_{50} and B_0 (where B_0 is the difference between the concentration

of the higher plateau minus that of the lower plateau), following the equations $K_d =$ $IC_{50} - L$ and $B_{max} = B_0 \, IC_{50} / L$ (DeBlasi et al., 1989).

The saturation analysis and the homologous competitive binding experiment have also been done using the Nickel-coated plates assay. First analysis with this method was performed using concentrations of fluorescent ligand ranged from 0.125 to 32 nM, while that one of non-fluorescent ligand was 200 nM. In the homologous competitive binding experiment, a fixed concentration of fluorescent ligand (7.5 nM) competed for binding to VP35 RBD with multiple concentration of non-fluorescent ligand (from 0.15 nM to 500 nM) . For the calculation of the kinetic parameters through non-linear regression model it was used the SigmaPlot 11.0 software (Systat).

2.10 In silico model of homo-oligomerization of VP35 coiled-coil domain.

Residues 83 to 119 of the N-terminal domain of VP35 were chosen for the modelling of the 3D structure of oligomers and to investigate the extent of coiled-coil formation.

The model based on the crystal structure of the Nipah virus 4N5B phosphoprotein tetramerization domain (Bruhn et al., 2014). Template was chosen between four templates analyzed using Modeller 9.13, a program used for homology or comparative modeling of protein three-dimensional structures (Sali and Blundell, 1993), to study self-assembly and dimerization.

A model, in which two monomer helices were placed parallel at a distance of at least 15 Å from each other, was created to study dimerization. The system was firstly

converted from an atomic description to a coarse-grained (CG) model using the Martini22 (de Jong et al., 2013) force field to describe interactions among beads. The Martini force field uses a four-to-one mapping in which four atoms (on average) and their associated hydrogens are represented by one CG bead. The software DSSP 2.0.4 (Kabsch and Sander, 1983) was used to assign secondary structure to each protein fragment.

CG simulations were performed with the GROMACS (Abraham et al., 2016) simulation package as follows: first, each monomer underwent 10000 steps of structural relaxation *in-vacuo*; then two of them were aligned as described above and solvated using the *genbox* command. Martini treats explicit water using the same coarse-graining scheme as for other macromolecules, hence four water molecules are combined into a single CG bead. An adequate number of counter-ions were added to neutralize the net charge of the systems.

Each couple of monomers was subjected to structural relaxation, followed by a 500 ps long equilibration with position restraints on protein backbone in order to relax the side chains and their interaction with the solvent; finally, MD simulations of 200 ns in length were performed. Every independent replica was initialized with different random velocities. All the CG simulations were performed at 300 K using a 20 fs integration time step with the other simulation parameters set to the recommended values for coarse-grained simulation of proteins. The pressure was controlled at 1 atm and the temperature was retained at 300 K using Parrinello-Rahman Barostat (Parrinello and Rahman, 1981) and V-rescale thermostat (Bussi et al., 2007) respectively.

2.11 Luciferase reporter gene assay for measuring IFN-β induction

The luciferase reporter gene assay was performed as previous described (Cannas et al., 2015). A549 cells (5×10^4 per well) were transfected with T-Pro P-Fect Transfection Reagent (T-Pro Biotechnology, Twin Helix) and with the construct pGL IFN-β luc. Twenty-four hours after transfection, cells were additionally transfected with Influenza virus A/PR/8/34 (H_1N_1) and incubated for further 6 hours at 37 °C with 5% CO2 in presence or absence of the extract. Next, cells were harvested with Luciferase Assay Buffer (50 mM Na-MES pH 7.8, 50 mM TrisHCl pH 7.8, 1 mM dithiothreitol, 0.2% Triton X-100).

The crude cell lysates were clarified by centrifugation and 50 µL of cleared lysates were added to 50 µL of luciferase assay buffer (125 mM Na-MES pH 7.8, 125 mM Tris-HCl pH 7.8, 25 mM magnesium acetate, 2.5 mg/mL ATP) in a white 96-well plate (OptiPlate, PerkinElmer). Immediately after addition of 50 µL of 1 mM D-luciferin into each well, the luminescent signal was measured in Victor3 luminometer (Perkin Elmer).

The relative light units measured (RLU) were normalized as the fold activity of the unstimulated control. Each assay was carried out in triplicate.

2.12 EBOV VP35 luciferase reporter gene inhibition assay

The above described luciferase reporter gene assay was also performed for evaluating the IFN-β induction prevention mediated by EBOV VP35 protein. When the pcDNA3-ZEBOV-VP35 was used as control, was co-transfected with the pGL IFN-β luc plasmid. The relative light units measured (RLU) were normalized as the fold activity of the unstimulated VP35 control. Each assay was carried out in triplicate.

2.13 Plant extracts preparation

The collected plants were dried in a ventilated stove, then their aerial parts were macerated in ethanol for the raw extract preparation, while for the process of extraction of the various fractions other solvents were also employed. For extraction, the crushed aerial parts were placed in a container and let stand in the dark for a period of 2-8 days, which is necessary to dissolve the soluble material.

After filtering, solvent was removed by rotary dryer (rotavapor) and the obtained crude extract was subsequently dissolved in dimethyl sulfoxide (DMSO) for storage at -20 °C. Fractions obtained by chromatographic separation from the crude extract by the use of different solvents, such as water, ethyl acetate, ethanol and n-butanol in various percentages. The separation was monitored by thin layer chromatography (TLC). The compounds isolated from the fractions are identified through the use of spectroscopic methods, mainly the nuclear magnetic resonance spectroscopy (NMR).

3 PROTEIN PURIFICATION AND FLUORESCENCE-BASED ASSAY

3.1 Introduction

As described above, VP35 protein has been proposed to be a key determinant for EBOVs virulence. During infection VP35 is able to cap dsRNA to prevent detection of the virus by cellular PRRs and, hence, it may contribute to block the innate immune response, antagonizing the IFN-α/β production pathway (Cárdenas et al., 2006; Hartman et al., 2006, 2004). In fact, EBOVs bearing mutations in the VP35 dsRNA RBD, which reduce or suppress VP35–dsRNA binding, display greatly attenuate viral growth rate or are non-virulent in animal models (Hartman et al., 2008; Prins et al., 2010b), demonstrating the importance of the VP35 binding to dsRNA for virus pathogenicity and revealing that this protein function is an attractive pharmacological target.

To explore VP35 as drug target, a binding assay was established to determine VP35-dsRNA binding activity (Zinzula et al., 2012), using full-length EBOV VP35 His-tagged VP35 purified in bacterial system (Zinzula et al., 2009). The assay was based on the use of paramagnetic beads specifically binding the His-tagged recombinant proteins that, in turn, bind to dsRNA while unbound dsRNA substrates can be washed out. In fact, in this assay, rVP35 beads conjugated was incubated with a 500 bp IVT ^{3}H-dsRNA, the undound ^{3}H-dsRNA washed out and the rVP35–^{3}H-dsRNA complex was then eluted with imidazole and quantified by radioactivity measurement (Zinzula et al., 2012). These protocols highlighted two limits: firstly, since, after the expression of rVP35, most of the protein was aggregated in inclusion

bodies, the quantity of rVP35 available for IMAC was very limited, forcing to grow high volumes of bacterial cultures to produce sufficient amount of protein; secondly, the use of radioactive labeled dsRNA, that is obviously hazardous and expensive.

Hence we focused our attention firstly to obtain higher rVP35 yields solubilizing the inclusion bodies in urea buffer and properly refolding the protein. Secondly, we developed a new 96-well plate biochemical assay to quantify VP35-dsRNA binding activity using a 5'-fluorescein-dsRNA as substrate. We measured the equilibrium dissociation constant for rVP35-dsRNA binding, showing that binding parameters calculated with this assay are similar to those reported in previous studies and validating the assay to screen EBOV VP35 inhibitors.

3.2   Purification of EBOV rVP35 under denaturing conditions

In order to improve the yield of protein purification, rVP35 expressed in *E. coli* was denatured with high urea concentrations as already done with success with several other small proteins (Swietnicki, 2006). The pellet of BL21AI *E. coli* cells in which rVP35 was expressed was re-suspended in 6M urea buffer, sonicated, centrifuged and the supernatant was loaded to an IMAC column as described in details in material and methods. Denatured rVP35 was then refolded on-column, while they are still bound to the Ni-Sepharose® resin, by gradually removing the denaturant agent with a slow inverse gradient. Then, after imidazole elution, fractions were collected and analyzed by SDS-PAGE that showed a main band of recombinant protein corresponding to a molecular weight of ~40 kDa and one fainter around 80

kDa, in addition to some other bands lower than 40 kDa that have been interpreted as degradation fragments of the expected recombinant protein (Figure 18). The main band was expected at ~40 kDa, since the presence of 10 additional amino acids in rVP35 sequence brings the theoretical molecular weight to be near to 38.6 kDa, while the band close to 80 kDa was interpreted as dimeric form of recombinant protein. In order to confirm that all bands observed in SDS-PAGE came from rVP35 a Western blot analysis was performed using anti-His6-tag monoclonal primary antibody. The assay confirmed this hypothesis showing that all bands in SDS-PAGE were indeed EBOV rVP35 (data not shown). Of note, as compared to the previous metholdolgy (Zinzula et al 2009), the rVP35 yield was considerably increased, rising from about 150 μg per liter of bacterial broth obtained under non-denaturing conditions (Figure 19) to approximately 2-2.5 mg per liter, obtained under denaturing conditions, with a 13-15 fold increase in protein yield.

3.3   Validation of dsRNA binding of EBOV rVP35 purified under denaturing conditions

After having obtained a high yield purified EBOV rVP35, it was then needed to verify whether the refolded protein still had the ability of binding dsRNA or if, conversely, it lost it. Hence, we used the previously described magnetic pull-down assay (Zinzula et al., 2012), using as dsRNA substrate a labeled 500 bp [3]HGTP-dsRNA, to test the ability of rVP35 proteins obtained under both denaturing and non-denaturing conditions to bind dsRNA. Results clearly showed that both proteins were

able to bind dsRNA (Figure 20), demonstrating that the rVP35 obtained under denaturing conditions and consequently refolded still retain full ability of dsRNA binding.

3.4 Determination of kinetics parameters (Kd and Bmax) of refolded rVP35 with the magnetic pull-down assay

Once verified that ZEBOV rVP35 purified under denaturing conditions was indeed able to bind dsRNA, it was required to establish a new biochemical assays using a fluorescence substrate to measure the VP35–dsRNA binding and to characterize this interaction. Hence 30 bp long dsRNA with a triphosphate in a 5' end and a fluorescein molecule in the other 5' end was designed, since it is known that EBOV VP35 is able to bind dsRNA > 8 bp (Bale et al., 2013; Cárdenas et al., 2006; Kimberlin et al., 2010; Leung et al., 2010a, 2010b, 2009b).

The ability of the refolded rVP35 to bind the newly designed fluorescent dsRNA substrate was firstly assessed using the above described magnetic beads assay. After rVP35 conjugation to the beads, fluorescent dsRNA binding, washing of unbound fluorescent dsRNA, the complex rVP35-fluorescent dsRNA was eluted and fluorescence was measured. Once demonstrated that the binding of the refolded rVP35 to the newly designed fluorescent dsRNA could effectively be measured, in order to further verify that the refolded rVP35 could really be comparable to the native rVP35, the biochemical parameters of the refolded rVP35 were determined
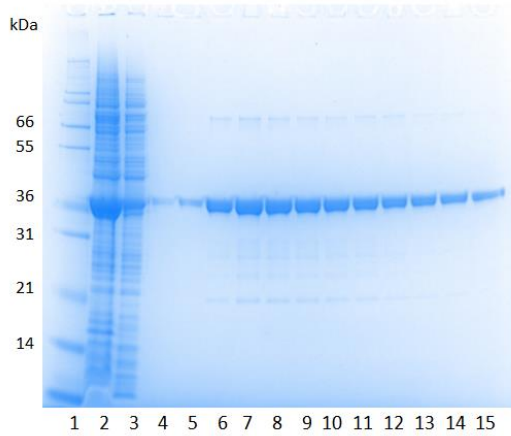
Figure 18 - Coomassie Blue-stained SDS-polyacrylamide gels of purification under denaturing conditions of EBOV rVP35. Lanes 1 and 16, molecular weight marker; lane 2, crude extract cell lysate; lane 3, flow through; lane 4, washing fraction; Lines 5-15 and 17-30; elution fractions.
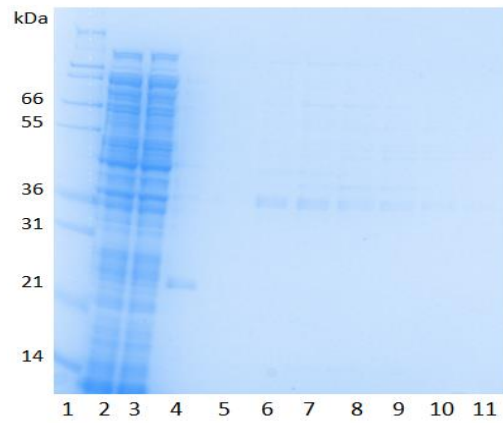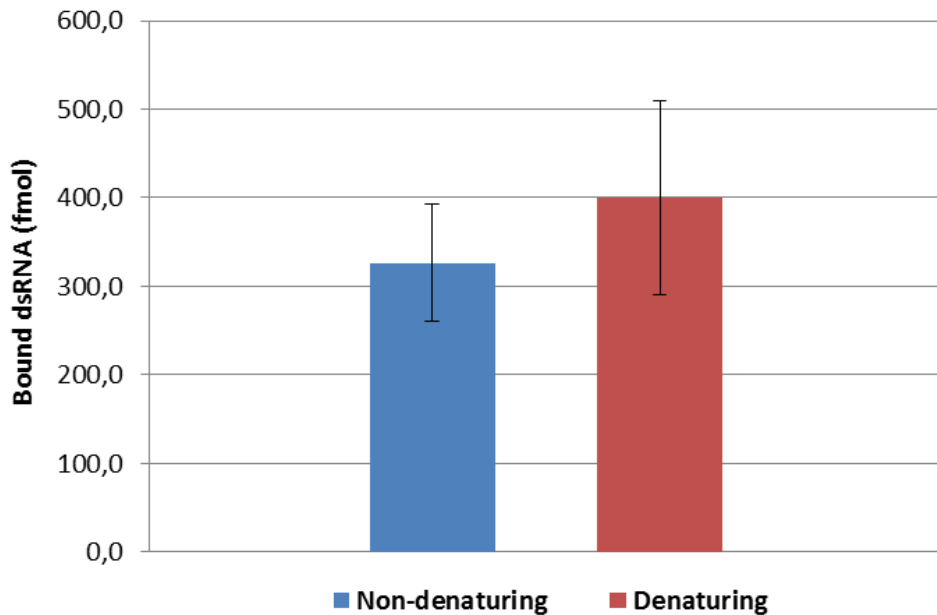
Figure 19 - Coomassie Blue-stained SDS-polyacrylamide gel of purification under non-denaturing conditions of EBOV rVP35. Lanes 1, molecular weight marker; lane 2, crude extract cell lysate; lane 3, flow through; lane 4, washing fraction; Lines 6-11, fractions correspondent to elution peak.

Figure 20 - Comparison between the binding activity of EBOV rVP35 purified without and with denaturation and refolding. The amount of 500 bp ^{3}H-dsRNA able to bind rVP35 was measured by performing the magnetic pull down assay as described.

and compared to the ones of the native rVP35.

The biochemical parameters were determined firstly by a series of saturation experiments that allowed to calculate the equilibrium dissociation constant (Kd) and maximum binding capacity (Bmax). Of course, because the measurement of fluorescent signal included both specific and non-specific binding signals, and it was not possible to measure specific binding directly, we calculated the rVP35 dsRNA specific binding as the difference between total dsRNA binding minus non-specific dsRNA binding (Yamamura, 1974). To this end, a series of parallel saturation experiments were performed, a first one with fluorescent dsRNA only and the second one with the same fluorescent dsRNA in the presence of high concentration non-fluorescent dsRNA. The excess of non-fluorescent RNA led to a shift of fluorescent dsRNA from the unspecific binding site, so that the measured signal could come only from non-specific binding. In this way, the specific binding was calculated indirectly as it is shown in the saturation curve plot. Results were analyzed Scatchard-plot analysis, in order to calculate the equilibrium dissociation constant (K_d) and maximum binding capacity (B_{max}). The K_d value obtained were respectively 3.9 ± 0.3 nM and 29.5 ± 3.7 nM (Figure 21).

Next a homologous competition study was performed, in which the refolded rVP35 was incubated with the fluorescent ligand at the fixed concentration of 7.5 nM competed by the non-fluorescent ligand in multiple concentration (from 0.01 nM to 2000 nM) (Figure 22). K_d and B_{max} values calculated from the obtained values of IC_{50} and B_0, were $K_d = 11.4 \pm 5.2$ nM and $B_{max} = 15.3$ nM.

Overall the K_d value obtained for the folded rVP35 to dsRNA (3,9 nM) was comparable to the Kd value (3.2 nM) previously reported for the native rVP35

measured with a longer (50 bp) radioactive-labeled dsRNA substrate (Zinzula et al 2012), further demonstrating that indeed the rVP35 protein obtained with urea-denaturation and in column refolding has the same biochemical properties of the native rVP35.

3.5 Establishment of 96-well nickel-coated plates assays to measure refolded rVP35 binding to fluorescent dsRNA.

Since it was needed to establish a robust 96-well assay for rVP35 binding to fluorescent dsRNA, an assay with the same rVP35 protein and the same fluorescent 30 mer dsRNA was performed using Nickel-coated 96-well plates that are able to bind the his-tagged rVP35.

At first different amount of folded rVP35 (from 100 ng to 900 ng, step 100 ng) were bound to the Nickel-coated plate wells and bound to an saturating amount of 5'-fluorescein-dsRNA (250 nM). Signal plateau was reached around 700 ng (Figure 23), hence this rVP35 amount was used for the successive assays.
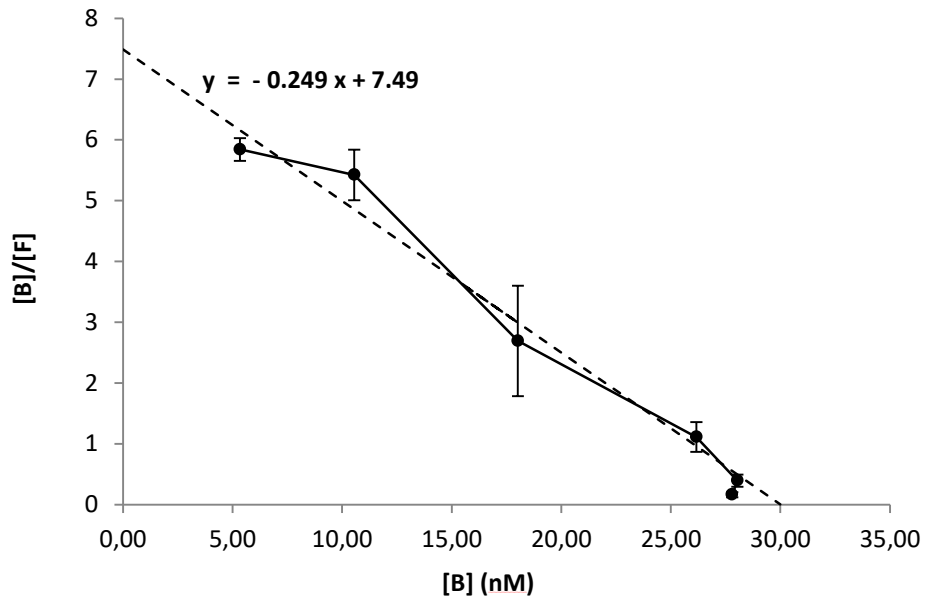
Figure 21 - Scatchard-plot analysis. Values of bound [B] and free [F] obtained with the experiment of saturation analysis were used in the Scatchard-plot analysis, obtaining that K_d = 3.9 ± 0.3 nM and B_{max} = 29.5 ± 3.7 nM.
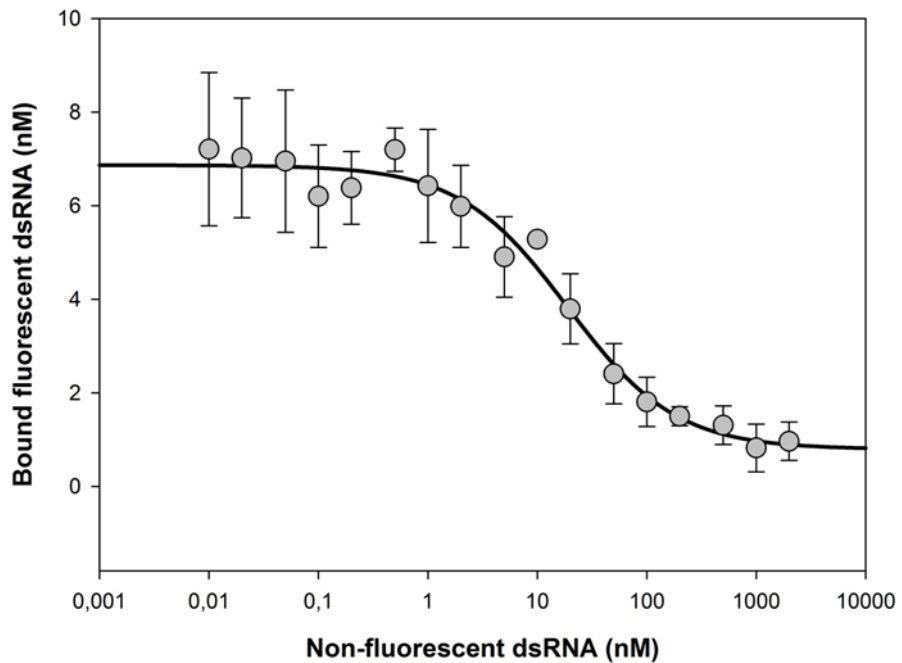
Figure 22 - Homologous competition performed with magnetic pull down assay. Increasing concentrations of unlabeled 30 bp dsRNA from 0.01 to 2000 nM competed with a fixed concentration of fluorescent 30 bp dsRNA. K_d and B_{max} obtained with this method were 11.4 ± 5.2 nM and B_{max} = 15.3 nM.

Then we asked which dsRNA concentration was needed in the assay, and then performed a saturation curve of dsRNA with a fixed amount (700 ng) of rVP35 (Figure 24). Results allowed to calculate by a non-linear regression the K_d value (6.1 ± 1.2 nM) and the dsRNA concentration of 7.5 nM was chosen for subsequent experiments.

Subsequently, we performed the saturation analysis with the Nickel-coated plate assay, also calculating indirectly the specific binding as described above (Figure 25) and calculated by non-linear regression a K_d value of 5.9 ± 0.5 nM and a B_{max} value of 10.1 ± 0.3 nM, while K_d and B_{max} obtained with the Scatchard-plot analysis were respectively 1.6 ± 0.2 nM and 8.0 ± 1.5 nM. Of note, kinetic parameters obtained in the were Nickel-coated plate assay were comparable to the ones obtained in the magnetic beads assays, showing that the Nickel-coated plate assay was reliable.

Finally, we performed the homologous competition assay using fixed concentration of fluorescent dsRNA (7.5 nM) competed by increasing concentrations the unlabeled dsRNA (from 0.5 nM to 500 nM) (Figure 26). Using the simplification of the equation of Cheng and Prussof presented by De Blasi et al. (DeBlasi et al., 1989), we then again calculated the refolded EBOV rVP35 kinetics parameters values K_d (5.8 ± 0.4 nM) and B_{max} (4.5 nM), that were comparable to the ones previously calculated.
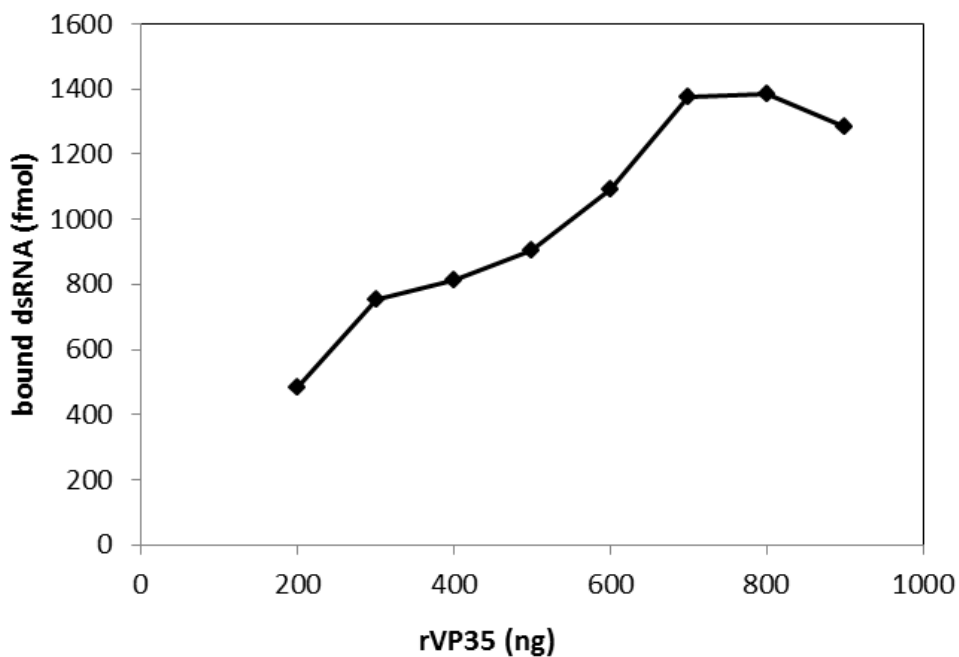
Figure 23 – Refolded Evaluation of the best amount of rVP35 linear dsRNA binding curve in the Nickel-coated plates assay. Figure shows that the optimal quantity of protein for the assay is 700 ng
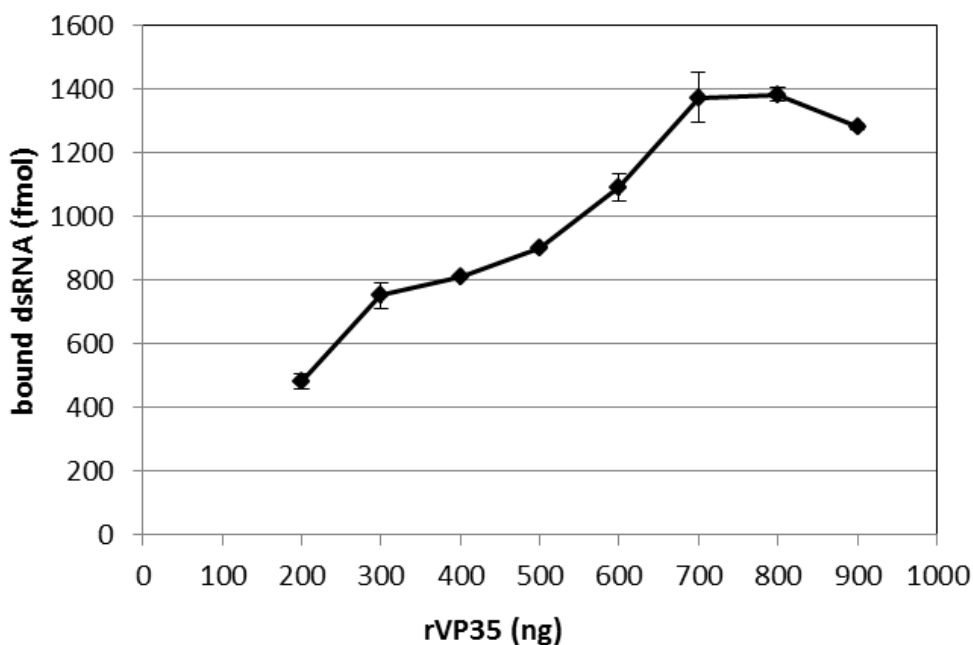

Figure 24 – Fluorescent dsRNA saturation curve in the Nickel-coated plates assay. K_d value obtained with the data of this experiment through a non-linear regression was 6.1 ± 1.2 nM.
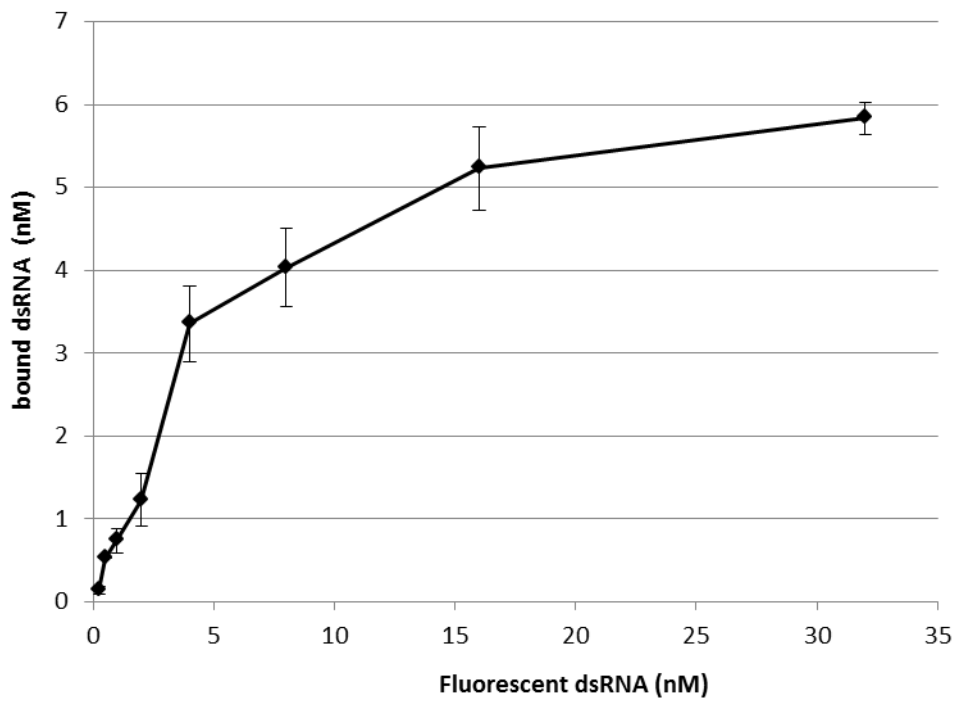
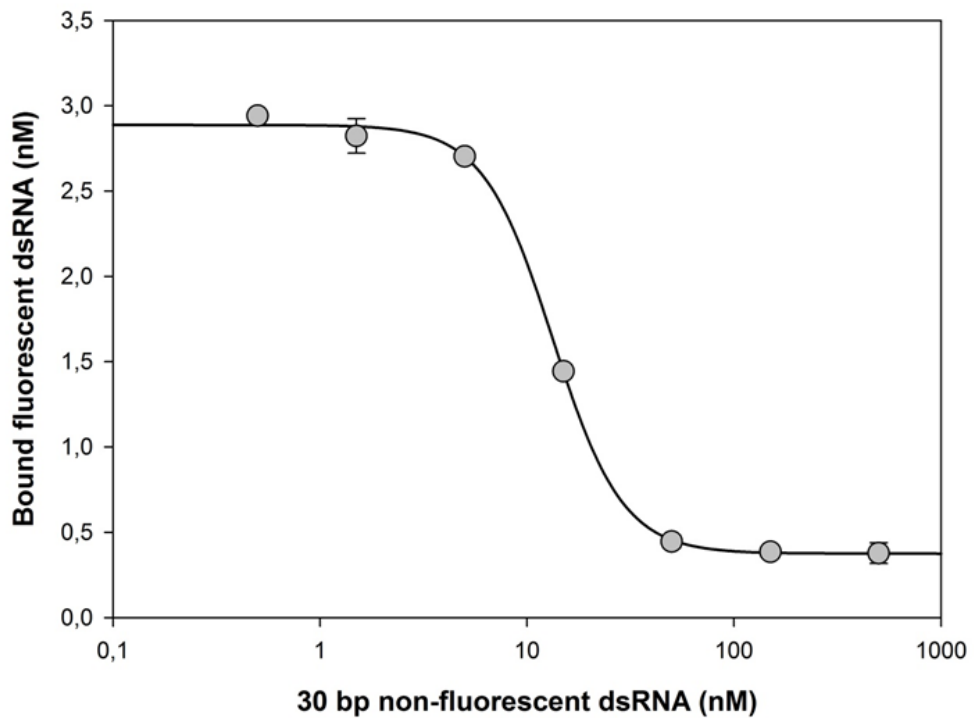Figure 25 - Saturation analysis of dsRNA specific binding performed with Nickel-coated plates assay.

Figure 26 - Homologous competition performed with Nickel-coated plates assay. Increasing concentrations of unlabeled 30 bp dsRNA from 0.5 nM to 500 nM competed with a fixed concentration of fluorescent 30 bp dsRNA.

3.6 Validation of rVP35 binding assays using fluorescent dsRNA ligand for drug screening

Since we wanted to use the nickel-coated plates assays to measure the ability of small molecules to inhibit rVP35 binding to dsRNA, we wanted to validate both magnetic pull-down and Nickel-coated plates assays as screening assays. Since it has been previously shown that the rVP35 bidnign to dsRNA is dependent on the presence of 5'-ppp but does not change significantly increasing the dsRNA length (Leung et al., 2010a; Zinzula et al., 2012), we used a 500 bp IVT dsRNA as competitor in a heterologous competition assay performing two analogous series of assays using the two methods described above. Results showed that that in both the magnetic pull-down assay (IVT dsRNA concentration range from 0.1 up to 300 nM) (Figure 27) and Nickel-coated plate assay (IVT dsRNA concentration range from 0.15 up to 500 nM) (Figure 28) the 500 bp dsRNA was able to compete with the fluorescent 30 bp dsRNA for the binding to rVP35. The competing IC_{50} values were 11.1 ± 3.3 nM and 5.0 ± 0.4 nM, in the magnetic pull-down assay and in the Nickel-coated plate assay, respectively, confirming what previously observed for native rVP35 (Zinzula et al 2012). Furthermore, for a further validation of the assay the Z'-factor was calculated, obtaining a value equal to 0.69, which is indicative of a robust assay (Zhang et al., 1999).
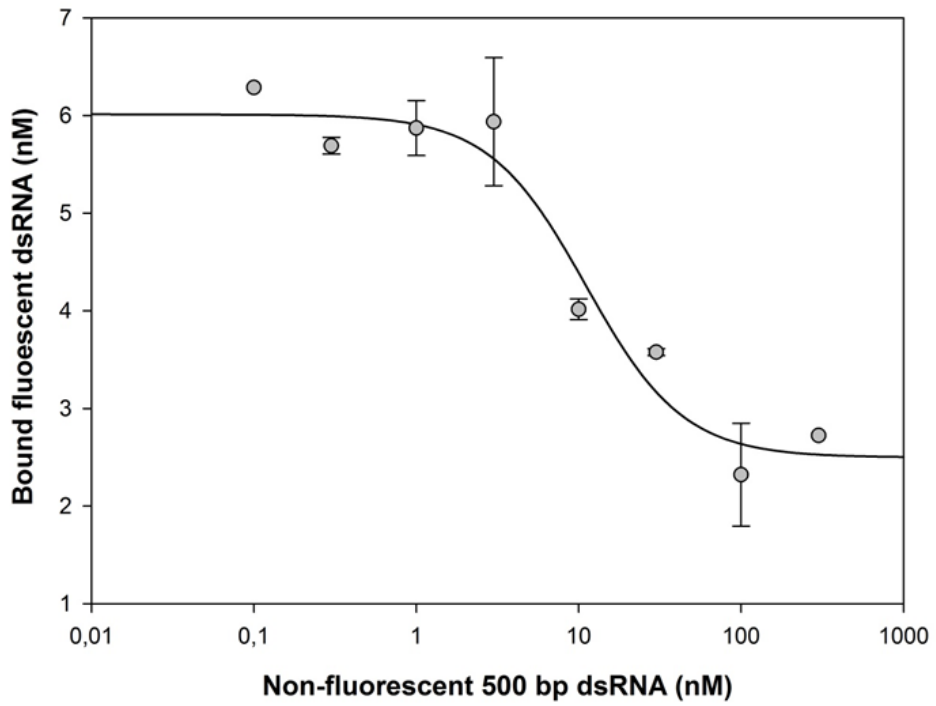
Figure 27 - Heterologous competition performed with magnetic pull down assay. Increasing concentrations of unlabeled 500 bp dsRNA from 0.1 up to 300 nM competed with a fixed concentration of fluorescent 30 bp dsRNA.
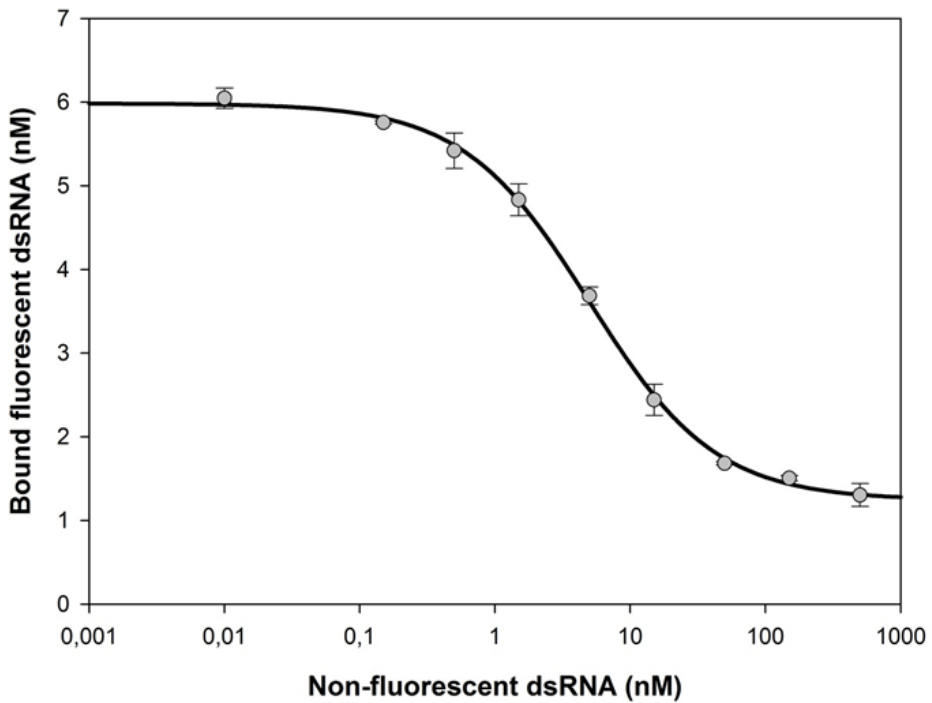

Figure 28 - Heterologous competition performed with Nickel-coated plates assay. Increasing concentrations of unlabeled 500 bp dsRNA from 0.15 up to 500 nM competed with a fixed concentration of fluorescent 30 bp dsRNA.

3.7 Discussion

The ability to bind viral dsRNA to prevent the detection by cytoplasmic PRRs has been indicated as one of key points for drug discovery. Any molecule able to bind VP35 and to inhibit its binding to the viral dsRNA, could be an interesting molecule for drug development.

Despite this, until now the only information on the binding between rVP35 and dsRNA obtained with the full-length viral protein came from a single previous study (Zinzula et al., 2012), while all other studies used only the RBD portion (Bale et al., 2013; Cárdenas et al., 2006; Kimberlin et al., 2010; Leung et al., 2010b, 2010c; Leung et al., 2009b). Recently, a new assay has been establish to screen compounds able to inhibit the VP35-RNA binding, based on electrophoretic mobility shift assays; however, also in this case it has been used only the VP35 RBD (Glanzer et al., 2016)

The current study overcomes the drawbacks observed in the biochemical assay based on a radiolabeled ligand and in the related method of protein purification (Zinzula et al., 2009). To improve the yield of purification we developed the described protocol based on the recovery of rVP35 from inclusion bodies by denaturation in 6M urea buffer. As reported, the conversion of aggregated proteins into soluble and biologically active proteins could be done in different methods; however the on-column refolding during the chromatography gives better quality proteins and higher yield (Swietnicki, 2006). The results obtained have demonstrated that the refolded protein has maintained the capacity to bind dsRNA, allowing us to use it for biochemical studies. Furthermore, in the SDS-PAGE we observed two main bands: the larger, expected, corresponding to a molecular weight of ~40 kDa, and one

fainter around 80 kDa. The same bands were detected in the electrophoresis gel of the full-length rVP35 purified without denaturation and subsequent refolding (Zinzula et al., 2009) and in the Western blot performed in this work using anti-His6-tag monoclonal primary antibody. Then we can speculate that with high probability these 80 kDa bands are rVP35 homodimers and that the homodimerization binding is strong enough to resist to the denaturation of a SDS-PAGE, as it has been observed for other different proteins (Grigorian et al., 2005). Since the presence of SDS in the polyacrylamide gel should have had disrupted subunit hydrophobic interactions, their persistence even in a small percentage suggests that this binding is very stable, so it would be interesting investigate its nature. Overall, we observed that both denatured and refolded and native EBOV rVP35s have the same behavior in SDS-PAGE. Of note, when the when the nickel-coated plates assays was optimized, we observed that the plateau was reached at 700 ng of protein, corresponding at 18 pmol of rVP35, exactly the double of the value indicated for the binding capacity by the manufacturer (Thermo Fisher Scientific Inc, 2011), strongly suggesting the homo-dimeric structure of the rVP35 that could bind to the his-tagged wells.

We demonstrated that rVP35 purified by on-column refolding is suitable to be used for subsequent assays, and determined the best experimental conditions. Furthermore, the denaturation of the recombinant protein expressed in E. coli rVP35 offers the additional advantage of ensuring that rVP35 is purified without the presence of any bacterial RNA linked to it, that might interfere in the type of essays subject of this work in which the ligand is precisely the dsRNA.

We determined the values of K_d and B_{max} in different way and for both kinds of assay: we use the saturation binding data to calculate the kinetics parameters both

with non-linear regression and Scatchard-plot analysis, while the data coming from competitive binding experiments have been analyzed only by non-linear regression. We observed that the trend of points for nonspecific binding related to the ligand concentration is linear, as usually expected, and its value is negligible respect of the total binding, particularly at low concentrations of fluorescent dsRNA (data not shown).

K_d values obtained with homologous competition binding experiments were substantially similar in two different assays, being equal to 11.4 nM and 5.8 nM for pull-down assay and Nickel-coated plate assay, respectively. This last value is very close to the K_d value obtained with the Scatchard-plot analysis for the Nickel-coated plate assay (5.9 nM). The observed differences in the values of B_{max} between two different assays were expected, since B_{max} is the total number of binding sites that is different in the pull-down and in the Nickel-coated plate assay. Analysis of binding between VP35 and dsRNA reported in previous publications gave analogous values of K_d. Zinzula et al., working with full-length VP35, obtained values of K_d, 2.8 ± 0.1 nM, 2.4 ± 0.3 nM and 3.2 ± 0.5 nM, respectively for 500, 150, 50 bp IVT dsRNA, while using a 8 bp 5'-phosphate dsRNA the K_d value was 64 ± 9 nM (Zinzula et al., 2012). Isothermal titration calorimetry experiments showed a value of K_d equal to 30 nM for the binding between VP35 IID (215-340) and a IVT 8 bp dsRNA containing 5′-ppp (Leung et al., 2010b).

Since competitive binding experiments are used to determine whether a drug binds to the receptor (Motulsky and Neubig, 2010), we used heterologous binding experiment conducted with IVT 500 bp dsRNA to confirm the validity of the assays. The IC_{50} value obtained with the magnetic pull-down assay was 11.1 ± 3.3 nM,

while the IC_{50} value in the Nickel-coated plate was 6.0 ± 0.4 nM. In all the competitive binding experiments, the downhill from the maximum to the minimum plateau happened in two logarithmic unit of concentration meaning that labeled and unlabeled ligands compete for a single binding site (Motulsky and Neubig, 2010).

Overall, a novel methodologies to obtain high yield dsRNA binding competent rVP35 and measure its binding to a fluorescent 30bp dsRNA were validated.for further drug development studies. These methodologies could be also adapted and used with other viral proteins whose mechanism of inhibition of the innate immunity involves the dsRNA binding.

4 SCREENING OF PLANT EXTRACTS

4.1 Introduction

Plants are used for medicinal purposes since ancient times: for instance, the therapeutic usage of plants is described as early as 3000 BC. The best known Egyptian document, recording over 700 drugs mostly of plant origin, dated from 1500 BC, even if Egyptian medicine dates from about 2900 BC, whilst the first Chinese and Indian Ayurvedic documents, in which herbal therapies were used, are dated around 1000 BC (Cragg and Newman, 2013).

Even in Mediterranean area, including Sardinia, it exists an ancient tradition for the use of plants and their parts as the primary source of remedies to health disorders and human and livestock diseases (Atzei, 2009).

In the early 19th century, with the development of the chemical analysis, active molecules began to be extracted from plants, up to directly synthetizing the isolated molecules identified as plant metabolites in the most recent decades. Over time, the use of herbal medicines declined in favor of drugs, until the past decades, when pharmaceutical industry focused mainly on libraries of synthetic compounds as drug discovery source, for the easiness of their production and resupply, coinciding, however, at the same time with a declining trend in the number of new produced drugs (Atanasov et al., 2015). Despite this, the impact of natural products for drug discovery is still very high: more than the half of the new chemical small molecules that had been approved between 1981 and 2010 were derived or inspired from nature (Newman and Cragg, 2012).

Medicinal plants have historically demonstrated to have a great therapeutic potential, and nowadays they still represent an important pool for the identification of novel drug leads (Atanasov et al., 2015). In fact, with approximately 500,000 worldwide plant species, of which only 1% has been phyto-chemically studied, the nature continues to be the major producer of compounds, offering a huge source from which it is possible to lay for the discovery of novel bioactive compounds. In fact, recent research trends clearly indicate that natural products will be among the most important sources of new drugs also in the future (Cragg and Newman, 2013; Palombo, 2011).

In the present study, to identify new molecules that may be used as antiviral agents to subvert EBOV VP35 effects or as lead compounds for further drug development, we tested several herbal extracts coming from plants of the Sardinian flora and plants commonly utilized in Indian Ayurvedic traditional medicine, utilizing the Nickel-coated biochemical assay presented in chapter 3 and the luciferase reporter gene assay previously developed (Cannas et al., 2015).

This study has been developed in cooperation with the research teams of Prof. Mauro Ballero and Dr. Cinzia Sanna of the University of Cagliari and Prof. Poli of the "*Alma Mater Studiorum*" University of Bologna that kindly provided the plant extracts, fractions and the identified single small molecules.

4.2 Evaluation of the effect of plant extracts on VP35 binding to dsRNA in biochemical assay

Dry plant extracts were resuspended in DMSO at concentration of 2.5 mg/ml. In order to evaluate their effects on the VP35 binding to dsRNA, the extracts were all tested at the concentration of 100 µg/ml (Table 3). A short dsRNA oligomer was used as positive control for the inhibition.

Out of the fifteen plant extracts screened, one was discarded because it emitted a fluorescence signal that interfered with the assay, while four of them were not able to interfere on the VP35-dsRNA binding, namely *Asparagus racemosus, Calamintha nepeta, Mentha pulegium* and *Solanum sodomaeum* (Table 3).

The other ten extracts showed some inhibition effect on the VP35 dsRNA binding at concentration of 100 µg/ml and were tested via dose-response curves and allowed to determine the IC_{50} values (Table 3). In particular, the most interesting extracts were from *Berberis aetnensis*, *Centaurea calcitropa*, *Daphne oleoides*, *Emblica officinalis*, *Hypericum hircunum*, *Hypericum scruglii*, *Limonium morisianum* and *Onopordum illyricum*.

Based on their potency of inhibition of the VP35 binding to dsRNA and the possibility to further fractionate the extracts, seven plants were selected to continue the investigations: *B .aetnensis*, *D. oleoides*, *E. officinalis*, *H .hircunum*, *H. scruglii*, *L. morisianum* and *O .illyricum*.

Table 3 - Inhibition of EBOV VP35 binding to dsRNA by screened plants extracts

Plant extracts	[a]IC$_{50}$ (μg/ml)
Asparagus racemosus	> 100 (63%)[b]
Berberis aetnensis	26.2 ± 2.5
Calamintha nepeta	> 100 (85%)
Centaurea calcitropa	43 ± 21
Daphne oleoides	27.5 ± 1.7
Emblica officinalis	10.8 ± 1.1
Euphorbia paganorum	69 ± 3.0
Hemidesmus indicus	69 ± 16
Hypericum hircinum	23.5 ± 2.5
Hypericum scruglii	20.3 ± 3.8
Limonium morisianum	19.2 ± 6.7
Mentha pulegium	> 100 (61%)
Onopordum illyricum	26.9 ± 3.3
Solanum sodomaeum	> 100 (87%)
dsRNA 30 bp	35.9 ± 11.4[c]

[a]Extract/compound concentration (mean ± standard deviation) required to inhibit VP35 binding to dsRNA by 50%.
[b]Percentage of control binding of VP35 to dsRNA in the presence of 100 μg/ml extract concentration.
[c]Concentration expressed in nM.

For the purpose of the present thesis, only the results related to four of these plants, namely *H. hircunum*, *H. scruglii*, *L. morisianum* and *O. illyricum*, will be shown since the evaluation of the components of the other extracts is still under completion.

4.2.1 Hypericum hircinum L.

The genus *Hypericum* of the *Guttiferae* family comprises mostly herbs and also several shrubs producing large and showy flowers, that are widely used in traditional medicine in various parts of the world. Several phytochemical investigations on this genus have led to the isolation of antimicrobial, antifungal and cytotoxic compounds (Pistelli et al., 2000). The species *Hypericum hircinum* is distributed in the Mediterranean region, in damp and shady places.

In Sardinia the plant is used for curative purposes such as i) balsamic anticatarrhal-lung and anti-asthmatics (drinking the infusion of the dried plant); ii) wound healing, especially in burns; iii) analgesic in rheumatic pains, sciatica and sprains and dislocations; iv) analgesic stomach and intestinal pains in the form of infusion; and finally v) healing wounds agent (Atzei, 2009). In south of Italy (Basilicata) it is also reported that the plant is still used as traditional cure for sore throats and colds, and as an antitussive, from which it take is common name of "*the cough herb*" (Quassinti et al., 2013).
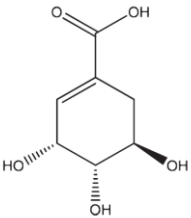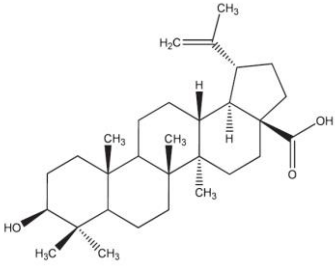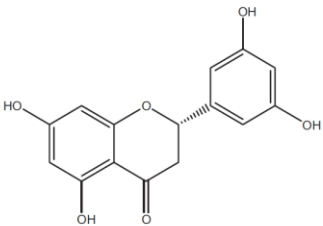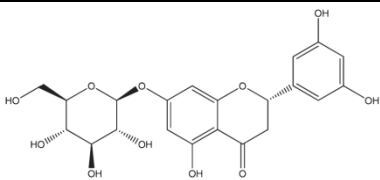
The extract of *H. hircinum* and its isolated compounds were studied in the past. In recent works, it has been demonstrated that quercetin, a component of its methanol extract, is active as inhibitory of monoamine oxidase A activity (Chimenti et al., 2006), its essential oil was reported to have antimicrobial, antioxidant and
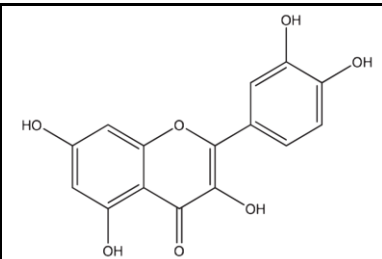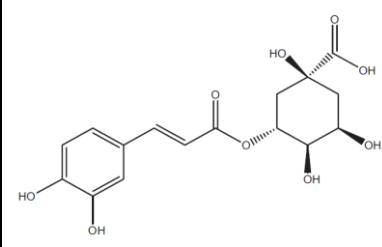
antiproliferative activities (Pistelli et al., 2000; Quassinti et al., 2013; Sagratini et al., 2008), while and other components of its ethanol extracts such as betulinic acid and 5,7,3,5'-tetrahydroxy-flavanone-7-O-glucoside have been shown to affect both HIV-1 reverse transcriptase (RT)-associated activities, DNA polymerase and ribonuclease H (Esposito et al., 2013).

Given the effect of the whole extract on VP35 binding to dsRNA, the extract was fractioned as previous described (Esposito et al., 2013), and fractions were firstly tested at concentration of 100 μg/ml (Table 4). Fraction I and IIa and IIc showed some inhibition of VP35-dsRNA binding, even if the general trend of the inhibition ability was quite similar for all the fractions (Table 4).

As previously described (Esposito et al., 2013), six compounds are present in these fractions, namely shikimic acid, betulinic acid, 5,7,3',5'- tetrahydroxyflavonone, 5,7,3',5'-tetrahydroxyflavonone-7-O-glucoside , quercitin and clorogenic acid. Hence, all these compounds were tested in biochemical assay. Results showed that only shikimic acid has a moderate ability to inhibit the VP35-dsRNA binding dose-dependently (Figure 29) with an IC_{50} value of 67.8 ± 0.6 μM (Table 4).

Table 4 - Inhibition of EBOV VP35 binding to dsRNA by *Hypericum hircinum* L.

Hypericum hircinum	Structure	[a]IC$_{50}$ (µM)
Extract		23.5 ± 2.5 [b]
Fraction I		73.7 ± 3.8 [b]
Fraction IIa		100 [b] $(50.6\ \%)$ [c]
Fraction IIb		< 100 [b] $(43.3\ \%)$ [c]
Fraction IIc		85.9 ± 3.7 [b]
Fraction III		< 100 [b] $(41.8\ \%)$ [c]
Fraction IV		< 100 [b] $(39.3\ \%)$ [c]
Fraction V		< 100 [b] $(40.6\ \%)$ [c]
Shikimic acid		67.8 ± 0.6
Betulinic acid		$> 100\ (95\%)$ [c]
5,7,3',5'- tetrahydroxyflavonone		350
5,7,3',5'- tetrahydroxyflavonone - 7-O-glucoside		$> 220\ (60\%)$ [c]

Quercitin		330
Clorogenic acid		280
dsRNA 30 bp		0.036 ± 0.011

[a]Extract/compound concentration (mean ± standard deviation) required to inhibit VP35 binding to dsRNA by 50%.
[b]Concentration expressed in µg/ml.
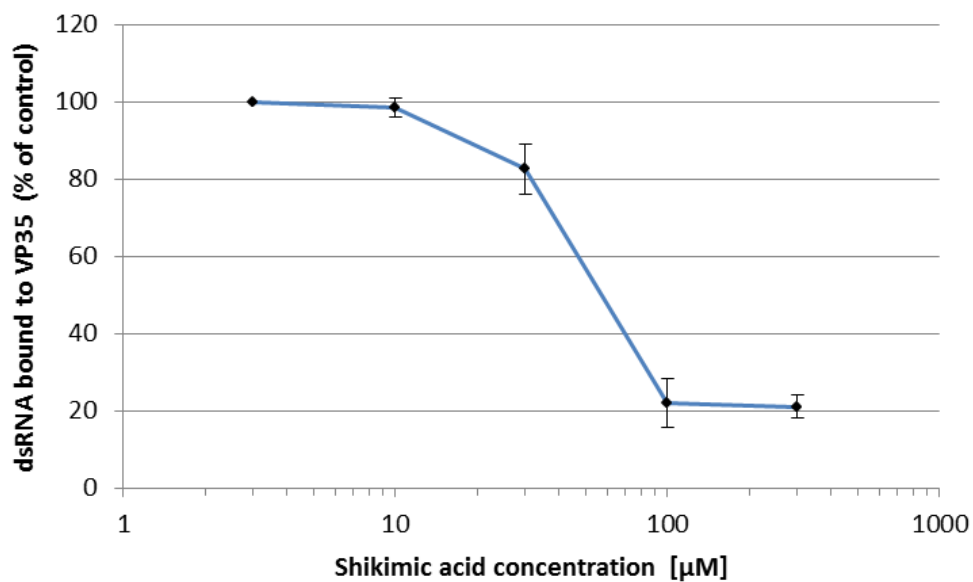[c] Percentage of control binding of VP35 to dsRNA in the presence of 100 µg/ml extract concentration.

Figure 29 –Inhibition curve of VP35 binding to dsRNA by Shikimic acid.
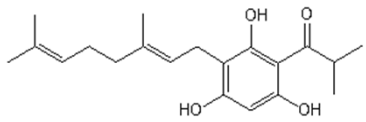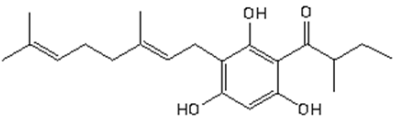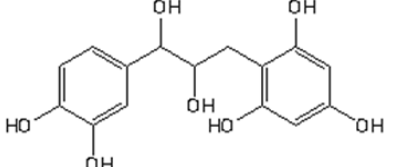
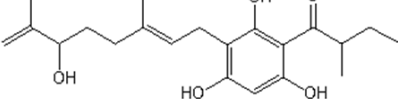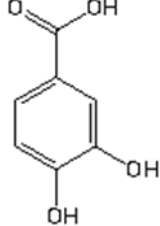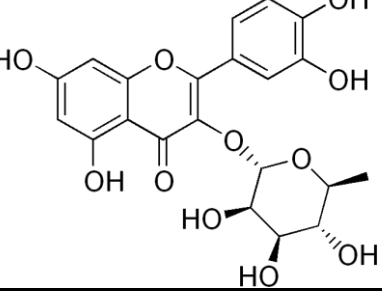*4.2.2* *Hypericum scruglii* Bacch.

H. scruglii is a Sardinian endemic plant, previously classified as *H. tomentosum* L., that differs from this last one by several morphologic characteristics. According to the authors of the new classification *H. scruglii* should be differentiated from *H. tomentosum* based on geographical isolation (Bacchetta et al., 2010).

Despite the great scientific interest, the high potential therapeutic uses and the high economic value of many species of the genus *Hypericum,* particularly *H. perforatum*, better known as "Saint John's wort", and *H. hircinum*, no research has been made nowadays on therapeutic effects of *H. scruglii* and *H. tomentosum*.

From the ethyl acetate fraction of *H. scruglii* extract fourteen compounds belonging to different classes have been isolated and characterized. Among them twelve fluoroglucinolic derivatives have been isolated, compounds typically described in the genus *Hypericum.* In addition, other two compound were isolated: the quercitrin and a compound identified for the first time in this study, the 3-(13-hydroxygeranyl)-1-(2'-methylbutanoyl)-phloroglucinol (personal communication by Dr. Cinzia Sanna - unpublished work).

Among the fourteen compounds, the six most abundant were tested in biochemical assay at the initial concentration of 100 µg/ml (Table 5). The IC_{50} values calculated for most of the compounds were >100 µg/ml. Quercitrin showed to be the most potent in inhibiting the VP35 binding to dsRNA with an IC_{50} value of 72.3 µg/ml, corresponding to 161.3 µM (Table 5).

Table 5 - Inhibition of EBOV VP35 binding to dsRNA by *Hypericum scruglii* Bacch.

Hypericum scruglii	Structure	[a]IC$_{50}$ (uM)
Extract		20.3 ± 3.8[b]
3-Geranyl-1-(2'-methyl butanoyl)phloroglucinol		> 315 (73.8 %)[c]
3-Geranyl-1-(2'-methyl propanoyl)phloroglucinol		> 300 (77.5 %)[c]
Filiferol		325
3-(13-hydroxylgeranyl)-1-(2'-methylpropanoyl)phloroglucinol		> 287 (100.0 %)[c]
Protocatechuic acid		> 650 (74.0 %)[c]
Quercitrin		161.3 ± 29.0
dsRNA 30 bp		0.036 ± 0.011

[a]Compound concentration (mean ± standard deviation) required to inhibit VP35 binding to dsRNA by 50%.
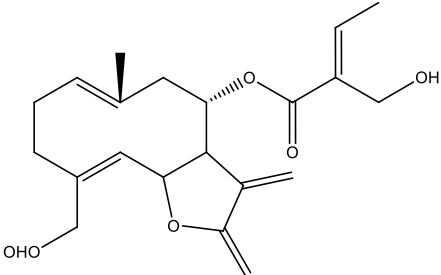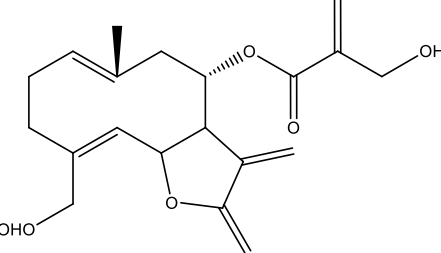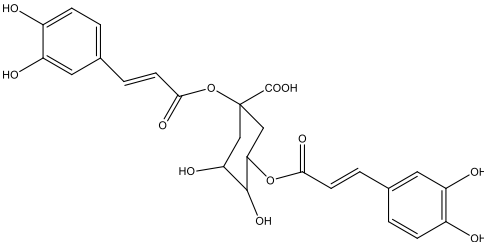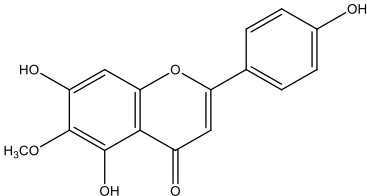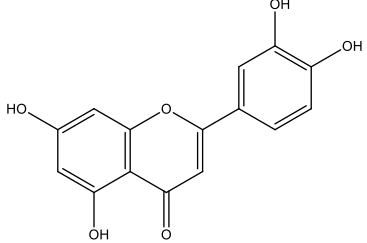[b]Extract concentration expressed in μg/mL.
[c]Percentage of control binding of VP35 to dsRNA in the presence of 100 μM compound concentration.
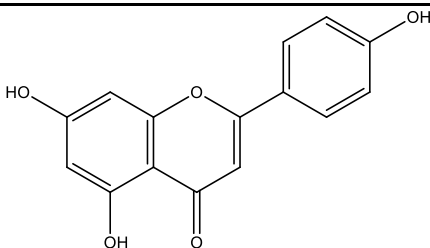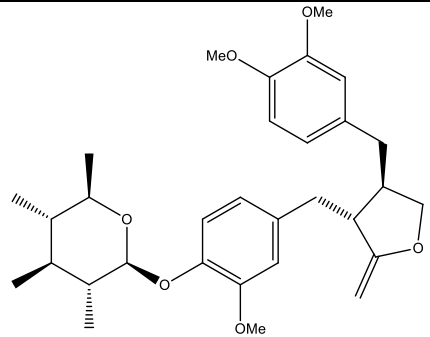
108

4.2.3   *Onopordum illyricum* L

Onopordum illyricum is widely distributed along the Mediterranean coast of Italy, including Sardinia, where some parts are usually eaten. Its therapeutic use as traditional natural drug is common. In the Mediterranean area it is used for the treatment of respiratory and urinary inflammations, to treat skin ulcers and exanthemas, and as antipyretic. The decoction is used as a digestive, cough sedative and in biliary disease (Formisano et al., 2017).

We tested in the biochemical assay four fractions obtained starting from ethanolic extract by separation in chromatographic column with different eluents: ethyl acetate, n-hexane, butanol and water (Table 6). The calculated IC_{50} values were substantially similar for all fractions, with the butanolic fraction showing a slightly lower IC_{50} value (Table 6). For the reason, we tested the seven compounds isolated from the butanolic extract, namely deoxyonopordopicrin, onopordopicrin, 1,5-dicaffeoylquinic acid, hispidulin, luteolin, apigenin and arctiin. Of note, one of them, the 1,5-dicaffeoylquinic acid, showed the lower IC_{50}value equal to 8.5 μM, while the deoxyonopordopicrin compound showed an IC50 value of 53.7 μM (Table 6 and Figure 30).

Table 6 - Inhibition of EBOV VP35 binding to dsRNA by *Onopordum illyricum* L.

Onopordum illyricum	Structure	[a]IC$_{50}$ (µM)
Extract		26.9 ± 3.3[b]
Fraction 1 - O.I. AcoEt		36.9 ± 14.7[b]
Fraction 2 - O.I. n-esano		34.1 ± 8.2[b]
Fraction 3 - O.I. BuOH		27.6 ± 3.2[b]
Fraction 4 - O.I. aqueous solution		32.0 ± 15.4[b]
Deoxyonopordopicrin		53.7 ± 24.2
Onopordopicrin		110 ± 20
1,5-dicaffeoylquinic acid		8.5 ± 0.6
Hispidulin		> 100 (93.0 %)[c]
Luteolin		> 100 (65.8 %)[c]

Apigenin		> 100 (64.2 %)[c]
Arctiin		> 100 (75.5 %)[c]
dsRNA 30 bp		0.036 ± 0.011

[a]Compound concentration (mean ± standard deviation) required to inhibit VP35 binding to dsRNA by 50%.
[b]Extract concentration expressed in μg/mL.
[c]Percentage of control binding of VP35 to dsRNA in the presence of 100 μM compound concentration.
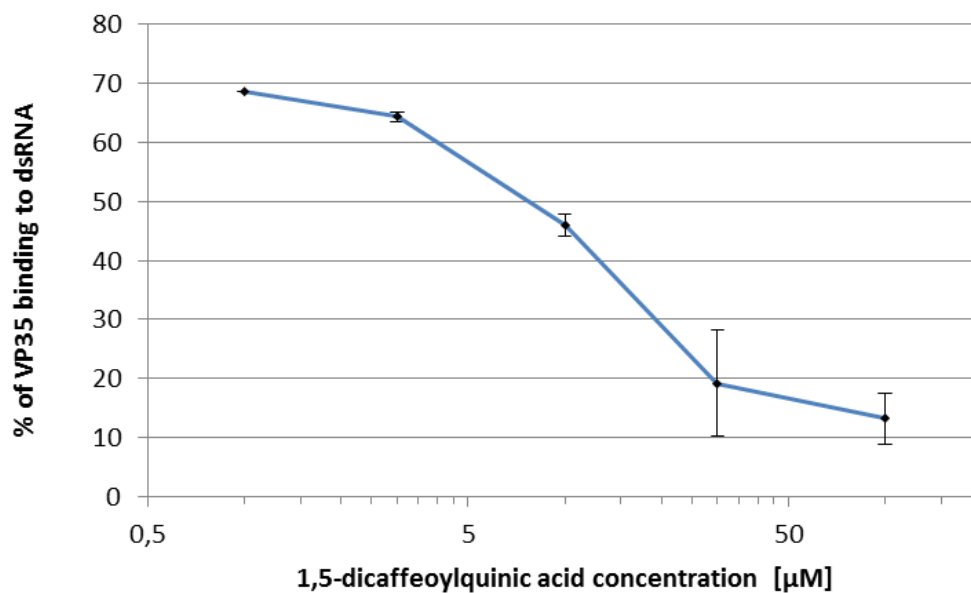

Figure 30 – Inhibition curve of VP35 binding to dsRNA by 1,5-docaffeoylquinic acid.
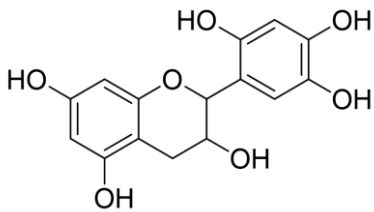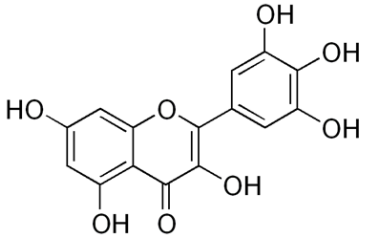
4.2.4 *Limonium morisianum* Arrigoni

L. morisianum is an endemic Sardinian species with very few available information about its folk use as medicinal plants and its biology. However, the use of some plant of the *Limonium* genus was reported. In particular, *L. densiflorum* is known as cardio-protectives, and for anti-bacterial and anti-inflammatory properties (Murray et al., 2004), *L. brasilense* is commonly used to treat hemorrhage, menstrual disorder in women and rheumatism, and *Limonium wrightii* is also used for the treatment of fever or arthritis (Aniya et al., 2002). In addition, antiviral, cytotoxic and antibacterial activity of Limonium spp has been also reported (Ksouri et al., 2011; Medini et al., 2011). However, no publication was reported on the medical properties of *L. morisianum*.

Hence, the crude extract of *L. morisianum* was fractionated firstly by methanol extraction and secondly by solubilization in ethyl acetate, butanol and water.

The effect of the ethyl acetate fractions on the VP35-dsRNA binding in biochemical assays, showed that the ethyl acetate extract and fractions 5, 8, 9 and 10 were able to inhibit the VP35-dsRNA with IC_{50} values < 20 µg/ml (Table 7). Since fractions 8 and 9, the ones with the lowest IC_{50} values were, two main compounds were identified, a derivative of the cathechin (compound 8.2) and the Myricetin, they were also tested by dose-response curve and showed IC_{50} values of 43.5 ± 4.2 e 4.2 ± 1.4 µM, respectively (Figure 31-Figure 32).

Table 7 - Inhibition of EBOV VP35 binding to dsRNA by *Limonium morisianum* Arrig.

Limonium morisianum	Structure	[a]IC$_{50}$ (μM)
Extract		$19,2 \pm 6,7$ [b]
Fraction 1		> 100 [b] (79,8 %) [c]
Fraction 2		> 100 [b] (94,9 %)
Fraction 3		> 100 [b] (74,3 %)
Fraction 4		> 100 [b] (66,1 %)
Fraction 5		13.2 [b]
Fraction 6		100 [b] (55,0 %)
Fraction 7		100 [b] (53,3 %)
Fraction 8		2,1 [b]
Fraction 9		$4,9 \pm 3,8$ [b]
Fraction 10		20,0 [b]
Compound 8.2 (cathechin)		43.5 ± 4.2
Myricetin		4.2 ± 1.4
dsRNA 30 bp		0.036 ± 0.011

[a]Compound concentration (mean ± standard deviation) required to inhibit VP35 binding to dsRNA by 50%.
[b]Extract concentration expressed in μg/mL.
[c]Percentage of control binding of VP35 to dsRNA in the presence of 100 μM compound concentration.
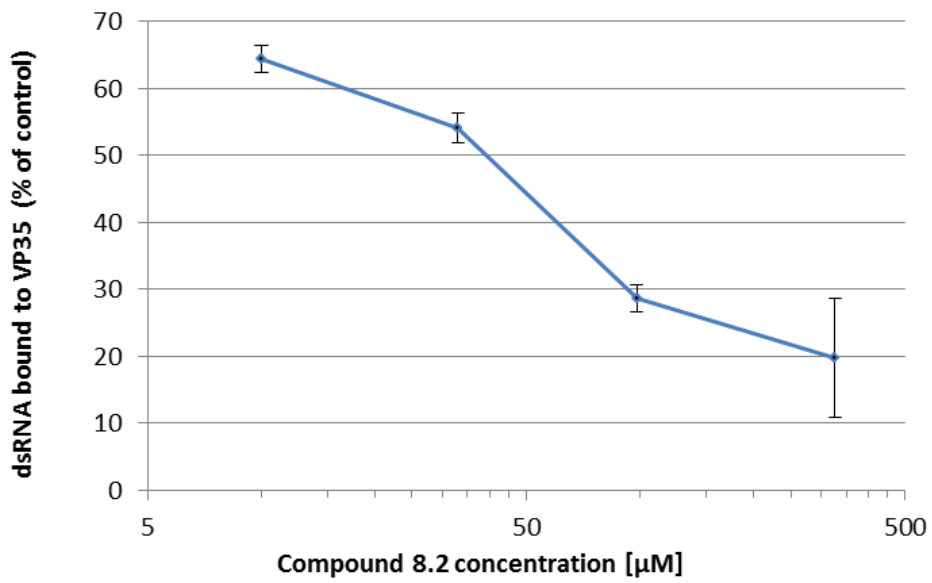
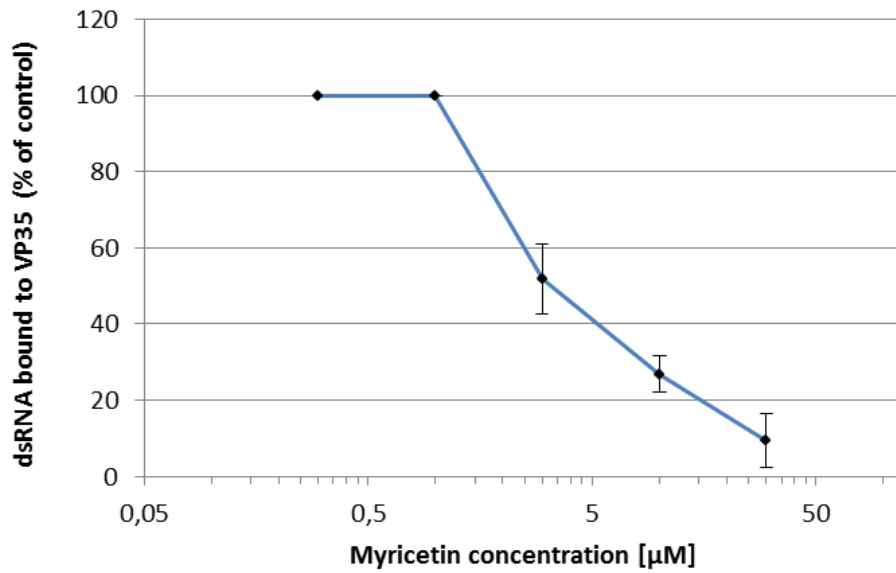Figure 31 - Inhibition curve of VP35 binding to dsRNA by compound 8.2.

Figure 32 - Inhibition curve of VP35 binding to dsRNA by myricetin.

4.3 Evaluation od the effect of plant extracts/single small molecules on VP35 binding to dsRNA in luciferase reporter gene assay

The previously described luciferase reporter gene assay (Cannas et al., 2015) allows to evaluate the inhibitory effect of EBOV VP35 on the RIG-I signaling cascade that brings to the IFN-β production after an artificial induction of innate immune response triggered by the transfection of Influenza virus A/Puerto Rico/8/1934 viral RNA (IAV PR8 vRNA) into A549 cells containing pGL IFN-β luc plasmid, which has the luciferase gene controlled by the IFN-β promoter. Luciferase expressed in cells catalyzes the oxidation of luciferin in oxyluciferin with emission of light and the light signal is detected by a plate reader. Then, the activation of RIG-I signaling cascade leads to a luminescent signal that is related to the amount of IFN-β expressed in the system. EBOV VP35 acts at different levels of the signal cascade, interacting with several host protein like TBK-1, IKK-ε, PACT as well as hiding the dsRNA to host receptor and inhibiting in this way the RIG-I pathway that brings to the IFN production.

Obviously, the system does not distinguish at what level of RIG-I pathway the cascade is inhibited, showing only the final effect of the suppression by VP35.

Hence, we tested in the luciferase reporter gene assay the same four plant extracts and some of the related fractions and compounds that showed the best inhibitory activity in the biochemical assay. A549 cells were cotransfected with 250 ng of pGL interferon β (IFN-β) luc and 250 ng of pcDNA3-VP35 as described.

4.3.1 *Hypericum hircinum* L.

The total extract of *H. hircinum* and two among the six compounds isolated from the extract, Shikimic acid and Quercetin, were tested in the luciferase reporter gene assay. The results showed that the extract was able to revert the inhibition of the IFN production induced by VP35, with significant efficacy at the concentration of 3 µg/ml (Figure 33). Conversely, the shikimic acid did not show any appreciable effect of reversion on the IFN inhibition (Figure 34), while the quercetin was able to partially revert it at the concentration of 10 µg/ml (Figure 35). These data suggest that Quercetin could be the active component of the *H. hircinum* extract.

4.3.2 *Hypericum scruglii* Bacch.

Similarly, the total extract of *H. scruglii* and the isolated compound quercitrin that was shown to have some effect in the biochemical assay were tested in the luciferase reporter gene assay. Results showed that they were unable to revert the inhibition of IFN production at any tested concentration (Figure 36-Figure 37).

4.3.3 *Onopordum illyricum* L

Subsequently, the extract from *O. Illyricum* and the isolated compound 1,5-dicaffeoylquinic acid that was shown to inhibit in the biochemical assay the rVP35 binding to dsRNA were tested in the luciferase reporter gene assay. Of note, both the extract and the 1,5-dicaffeoylquinic acid were able to revert the EBOV VP35 inhibition of the cellular IFN production. In particular, 1,5-dicaffeoylquinic acid was more potent than the extract (Figure 38-Figure 39), suggesting that it could be the active component of the *O. Illyricum* extract.

4.3.4 *Limonium morisianum* Arrigoni

Finally, the extract from the fraction 8 of *L. morisianum* and two isolated compounds, namely compound 8.2 and myricetin, that were shown to inhibit in the biochemical assay the rVP35 binding to dsRNA were tested in the luciferase reporter gene assay. Results showed that fraction 8 of *L. morisianum* has a moderate ability to revert the EBOV VP35 inhibition of the cellular IFN production, while no effects were observed when two compounds were tested (Figure 40-Figure 43).

pGL IFN-β luc	+	+	+	+	+	+
pcDNA3 EBOV-VP35 wt	-	+	+	+	+	+
vRNA	+	+	+	+	+	+
Total extract	-	-	30 ug/mL	10 ug/mL	3 ug/mL	1 ug/mL

Figure 33 – Effect of the *H. hircinum* extract on the EBOV VP35 ability to inhibit the IFN production in the luciferase reporter gene assay.

pGL IFN-β luc	+	+	+	+	+	+
pcDNA3 EBOV-VP35 wt	-	+	+	+	+	+
vRNA	+	+	+	+	+	+
Shikimic acid	-	-	30 μM	10 μM	3 μM	1 μM
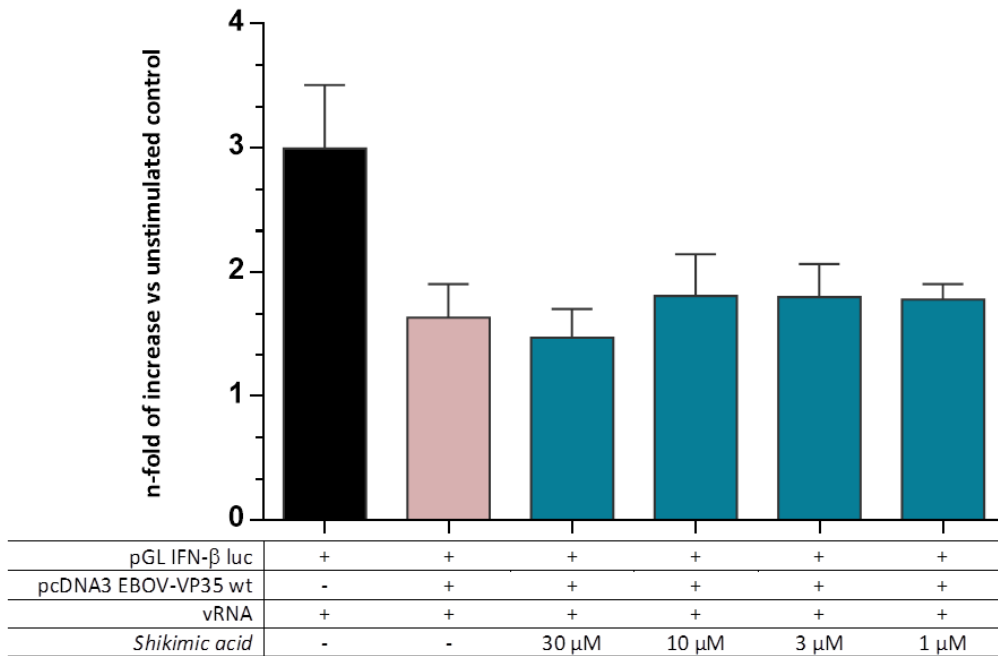
Figure 34 - Effect of shikimic acid on the EBOV VP35 ability to inhibit the IFN production in the luciferase reporter gene assay..

pGL IFN-β luc	+	+	+	+	+	+
pcDNA3 EBOV-VP35 wt	-	+	+	+	+	+
vRNA	+	+	+	+	+	+
Quercetin	-	-	99.3 μM	33.1 μM	9.93 μM	3.31 μM
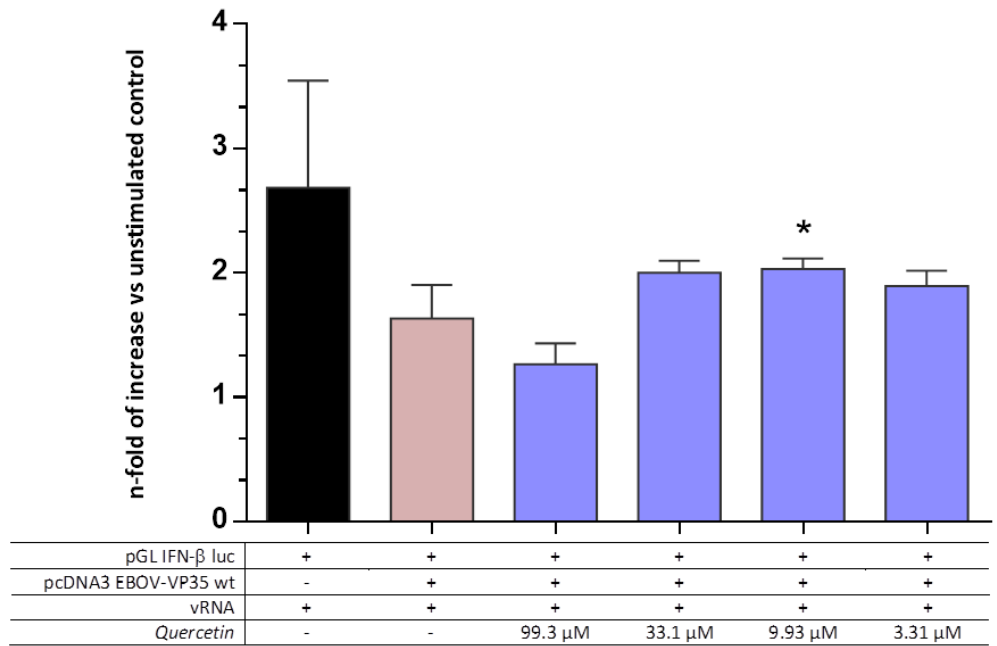
Figure 35 - Effect of quercetin on the EBOV VP35 ability to inhibit the IFN production in the luciferase reporter gene assay.

pGL IFN-β luc	+	+	+	+	+	+
pcDNA3 EBOV-VP35 wt	-	+	+	+	+	+
vRNA	+	+	+	+	+	+
Total extract	-	-	30 ug/mL	10 ug/mL	3 ug/mL	1 ug/mL

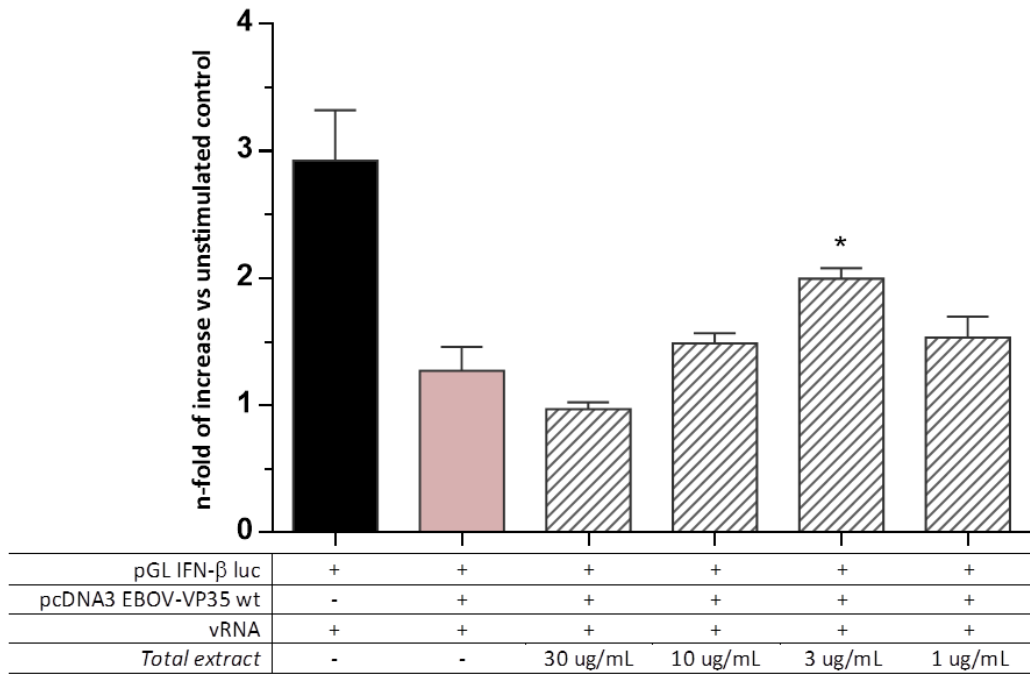Figure 36 - Effect of *H. scruglii* extract on the EBOV VP35 ability to inhibit the IFN production in the luciferase reporter gene assay.

pGL IFN-β luc	+	+	+	+	+	+
pcDNA3 EBOV-VP35 wt	-	+	+	+	+	+
vRNA	+	+	+	+	+	+
Quercitrin	-	-	66.9 μM	22.3 μM	6.69 μM	2.23 μM

Figure 37 - Effect of quercitrin on the EBOV VP35 ability to inhibit the IFN production in the luciferase reporter gene assay.


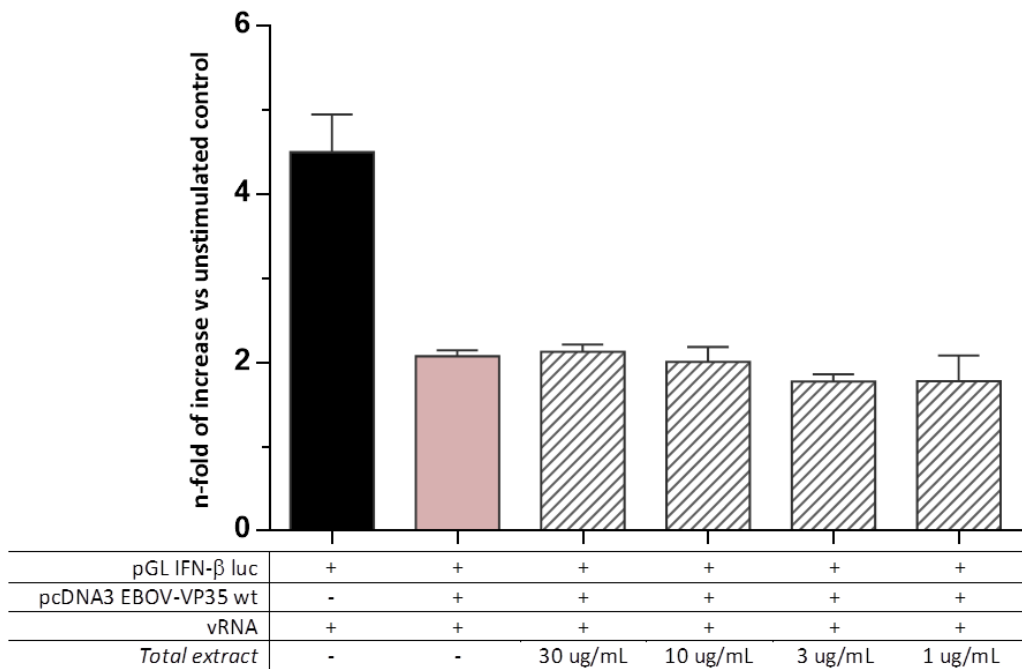|					
pGL IFN-β luc	+	+	+	+	+	+
pcDNA3 EBOV-VP35 wt	-	+	+	+	+	+
vRNA	+	+	+	+	+	+
Total extract	-	-	30 ug/mL	10 ug/mL	3 ug/mL	1 ug/mL

Figure 38- Effect of *O. Illyricum* extract on the EBOV VP35 ability to inhibit the IFN production in the luciferase reporter gene assay.

Figure 39 - Effect of 1,5-dicaffeoylquinic acid on the EBOV VP35 ability to inhibit the IFN production in the luciferase reporter gene assay.

pGL IFN-β luc	+	+	+	+	+	+
pcDNA3 EBOV-VP35 wt	-	+	+	+	+	+
vRNA	+	+	+	+	+	+
1,5-dicaffeoylquinic acid	-	-	30 μM	10 μM	3 μM	1 μM

Figure 40 - Effect of *L. morisianum* extract on the EBOV VP35 ability to inhibit the IFN production in the luciferase reporter gene assay.

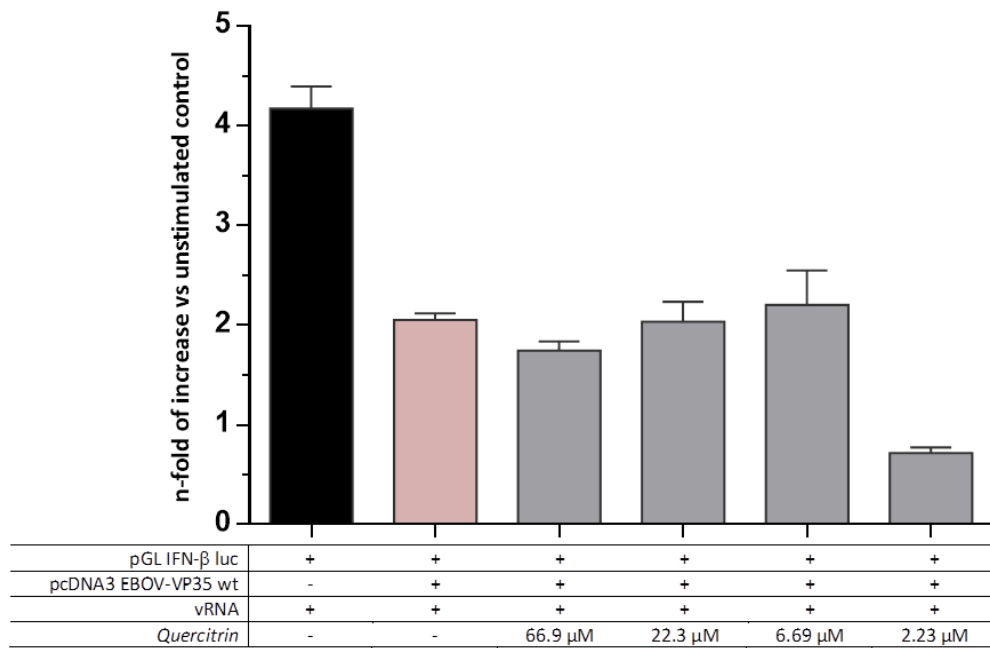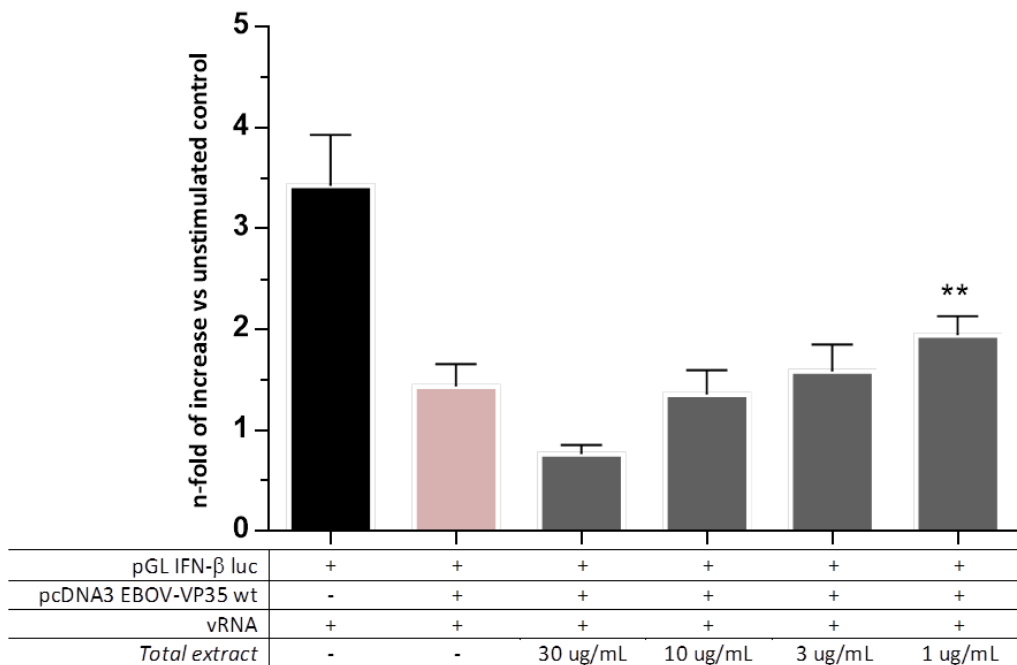|					
pGL IFN-β luc	+	+	+	+	+	+
pcDNA3 EBOV-VP35 wt	-	+	+	+	+	+
vRNA	+	+	+	+	+	+
Total extract	-	-	30 ug/mL	10 ug/mL	3 ug/mL	1 ug/mL

pGL IFN-β luc	+	+	+	+	+	+
pcDNA3 EBOV-VP35 wt	-	+	+	+	+	+
vRNA	+	+	+	+	+	+
Fraction 8	-	-	30 ug/mL	10 ug/mL	3 ug/mL	1 ug/mL

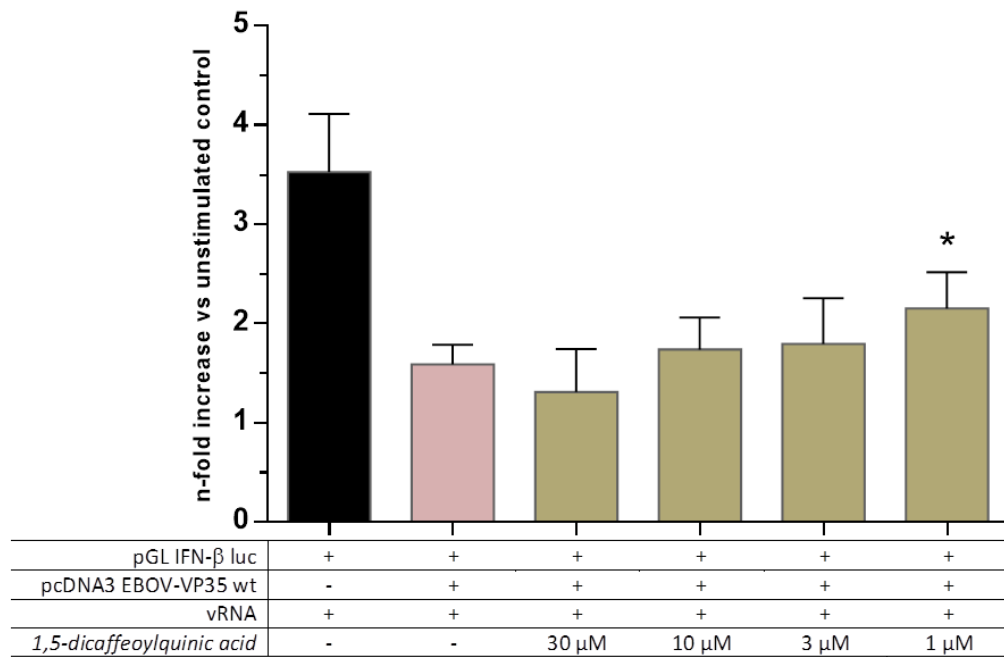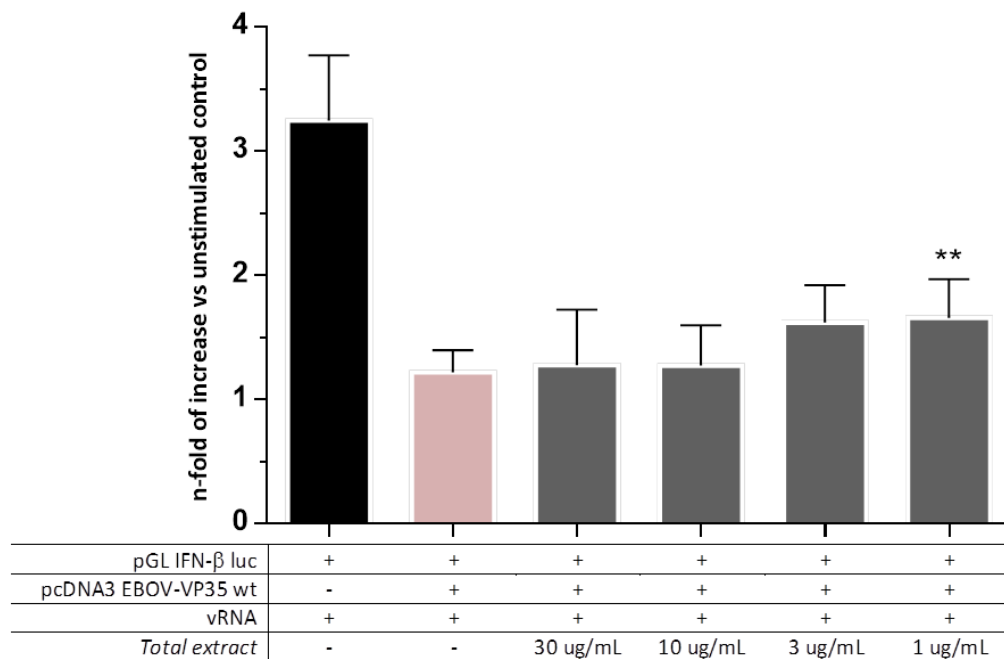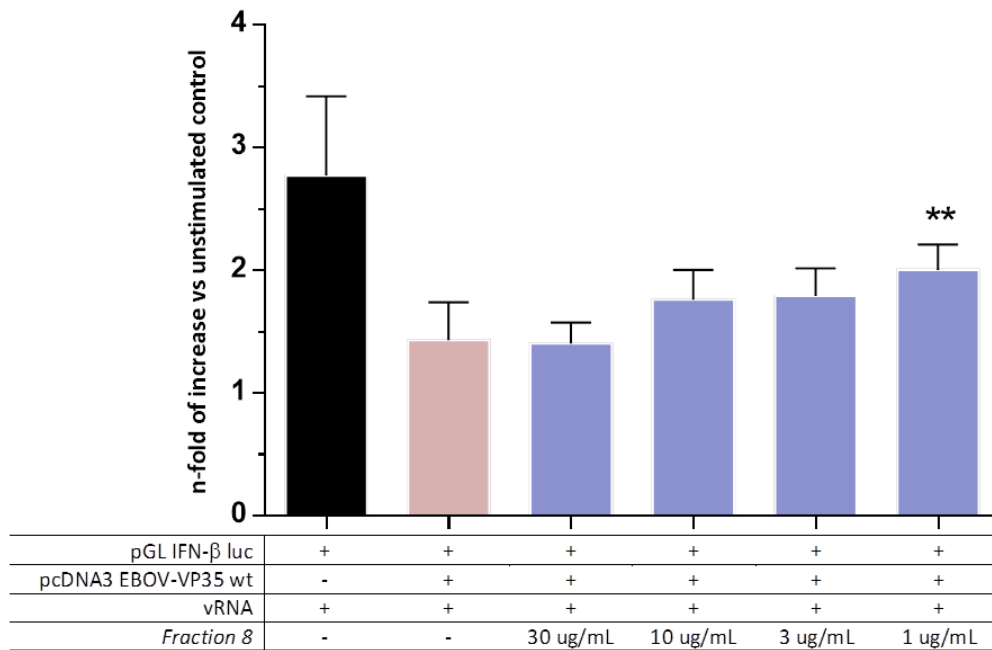Figure 41 - Effect of fraction 8 on the EBOV VP35 ability to inhibit the IFN production in the luciferase reporter gene assay.

pGL IFN-β luc	+	+	+	+	+	+
pcDNA3 EBOV-VP35 wt	-	+	+	+	+	+
vRNA	+	+	+	+	+	+
Catechin	-	-	98 μM	32.7 μM	9.8 μM	3.27 μM

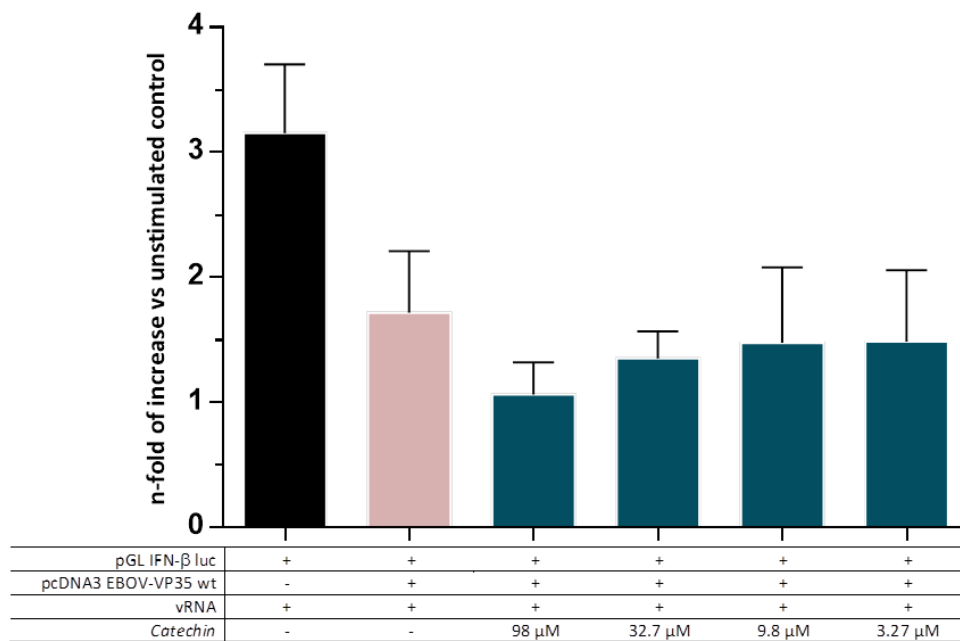Figure 42 - Effect of compound 8.2 on the EBOV VP35 ability to inhibit the IFN production in the luciferase reporter gene assay.

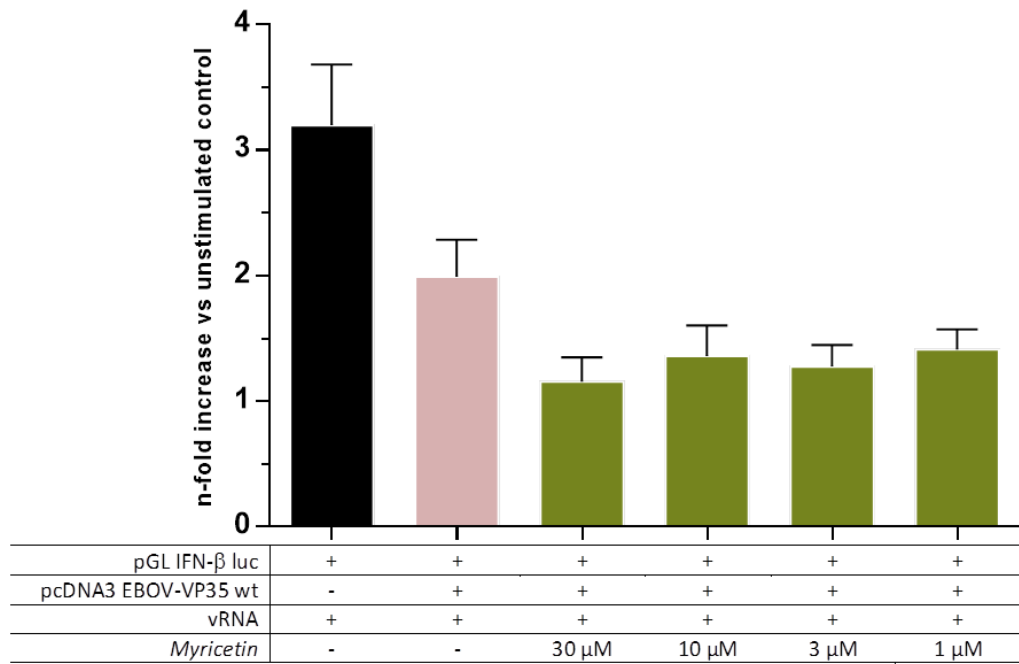|					
pGL IFN-β luc	+	+	+	+	+	+
pcDNA3 EBOV-VP35 wt	-	+	+	+	+	+
vRNA	+	+	+	+	+	+
Myricetin	-	-	30 μM	10 μM	3 μM	1 μM

Figure 43 - Effect of myricetin on the EBOV VP35 ability to inhibit the IFN production in the luciferase reporter gene assay.

4.4   Discussion

The huge variety of products of plant metabolism offers an inexhaustible source of small molecules that can be used for the research of new drugs. For this purpose, we tested in our systems the effects of four Sardinian plants extracts.

Despite the fact that the antiviral activity of the plants tested during this thesis have been previously poorly studied, a number of studies on the biological activity of many compounds isolated from these plants have been reported.

The flavonoid compound myricetin, as well as several other flavonoid, showed numerous biological effects since it has been reported i) to inhibit HIV-1 integrase (IN), nucleic acid synthesis (Cushnie and Lamb, 2005), ii) to inhibit HIV-1 reverse transcriptase (RT) (Ono and Nakane, 1990), iii) to have antioxidant and prooxidant activities that could increase damages to non-lipids components such carbohydrates and DNA, induction of DNA degradation *in vitro*, iv) to possess antiviral activities against viruses other than HIV-1 (Ong and Khoo, 1997).

Quercetin was described to have inhibitory activity against mono amino oxidase A (Chimenti et al., 2006), HIV-1 RT (Ono and Nakane, 1990) and IN, and against other viruses including herpes simplex virus (HSV), respiratory syncytial virus, poliovirus and Sindbis virus (Cushnie and Lamb, 2005). Furthermore it is shown to be a powerful inhibitor of DNA polymerase β (Ono and Nakane, 1990) and to have anti-bacterial activity, at least partially attributable to inhibition of DNA gyrase, demonstrated in *E. coli* (Cushnie and Lamb, 2005).

Interestingly, quercetin, that was found to be component of *H. hircinum*, and apigenin and luteolin, that were found to be component and *O. Illyricum*, have shown

to have immune-stimulating properties, suggesting that these natural compounds bind to the STING protein to induce expression of ISG (Khiar et al., 2015). Of note, we did not test apigenin and luteolin in the cellular assay, because they did not show appreciable effects in biochemical tests, while quercetin showed a significant ability to revert the IFN production in presence of VP35. Hence, while we showed that quercetin is able to inhibit the VP35-dsRNA binding in biochemical assay, it cannot be excluded that quercetin mechanism of action in cell-based assay could include also other targets, interacting as proposed by Khiar et al (Khiar et al., 2015), with STING, to activate TBK-1 stimulating the IFN production.

Myricetin and quercetin are flavonols, commonly found in vegetables and fruits, that differ only in number of hydroxyl groups attached to the B ring (compare Table 4 and Table 7) (Bilyk et al., 1984). Such structural difference seems to be important for the biological activities of the two compounds. In fact, in biochemical assay, myricetin showed a good ability to inhibit the VP35 binding to dsRNA, while quercetin showed to be 24 fold less potent. Conversely, in cellular gene reporter assay, myricetin did not show any ability to revert the VP35 inhibition of the IFN production, while quercetin showed to be able to revert it, suggesting that it may act through a mechanism of action different from the inhibition of the dsRNA sequestration by VP35.

Only a few information have been found in literature on shikimic acid, most often in relationship with the shikimic acid pathway, a metabolic route used by bacteria, fungi, algae, some protozoan parasites and plants for the biosynthesis of folates and aromatic amino acids (phenylalanine, tyrosine, and tryptophan) (Herrmann and Weaver, 1999), and also used by pharmaceutical industry as base

material for production of oseltamivir (Tamiflu) (Nie et al., 2009). Shikimic acid has been also tested against the HIV-1 RT-associated functions and while it was not able to inhibit the Ribonuclease H activity, it inhibited the RDDP activity at high concentrations (Esposito et al., 2013).

1,5-dicaffeoylquinic acid, known also as cynarin, is formed from esterification of two units of caffeic acid and one unit of quinic acid. It is the active principle of the artichoke, but it has been found also in other plants. It is able to inhibit taste receptors, making water (and other foods and drinks) seems to be sweet (Topal et al., 2016). It has been shown to have some pharmacological properties including hypocholesterolemic, hepatoprotective (Gebhardt, 1998; Gebhardt and Fausel, 1997), antiviral, antibacterial, and antihistamic effects, as well as antioxidant, antiradical, and anticholinergic activities (Topal et al., 2016).

It is worth to note that the comparison between the efficacy of the compounds able to inhibit the rVP35 binding to dsRNA in biochemical assays with the ones of the compounds able to reverse the VP35 inhibition of the IFN production showed that in most cases no correlation. Quercetin was not able to inhibit rVP35 function in biochemical assay, while it reverted the VP35 inhibition of the IFN production in cell assays. Of note, quercetin was previously shown to stimulate IFN production acting as STING agonist (Khiar et al., 2015). On the contrary, myricetin was able to inhibit rVP35 binding to dsRNA in biochemical assay while it was ineffective in the cellular assay. 1,5-dicaffeoylquinic acid (cynarin) was the sole compound that showed a good ability to inhibit the VP35-dsRNA binding in the biochemical assay (Table 6 and Figure 30) and, at the same time, to revert the inhibition of IFN production provoked

by VP35 in the luciferase reporter gene assay, where it showed the ability to a significant restore of the IFN production at concentration of 1 µg/ml (Figure 39).

The discrepancy observed for the biological activities of myricetin and quercetin opened the hypothesis that, on the one side, VP35 binding to dsRNA could not the driving force of the RLR pathway inhibition by VP35, as generally considered, suggesting that VP35 interactions with cytoplasmic host proteins may play a major role in its inhibition of IFN production. On the other side, the fact that 1,5-dicaffeoylquinic acid was able to inhibit VP35 function in both assays, may suggest that, even in the case the VP35 binding to dsRNA may not be the main RLR cascade step inhibited by VP35, compounds with bigger steric hindrance may still inhibit VP35, possibly due to the fact the VP35 pocket binding to dsRNA is the same that it should interact with other cellular RLR cascade components. Hence we wanted to assess the relevance of dsRNA binding in the ability of VP35 to inhibit IFN production after dsRNA induced RLR cascade activation.

5 HOMO-OLIGOMERIZATION OF VP35

5.1 Introduction

The results obtained with the screening of plants extracts showed unexpected different effects of some extracts/compounds in biochemical and in cellular assay: for instance, we observed that the compound Myricetin, extracted from *L. morisianum*, that was able to inhibit VP35 binding to dsRNA by 50% at concentrations of 4.2 µM in the biochemical assay (Table 7), showed a different behavior in the cellular assay, being not able to revert the inhibition of IFN production determined by VP35 in the cellular assay (Figure 43), whereas the extracts and the tested fraction, that showed IC50 values lower than 20 µM in the biochemical assay of the same plant (Table 7), showed a discrete ability to subvert the VP35 inhibition (Figure 40-Figure 41).

Therefore, among the several possible mechanisms that could explain these results, we wanted to verify the hypothesis that the VP35 binding to dsRNA could not be the main point of RLR pathways inhibition while VP35 could exerts its main inhibitory effect acting on another steps of IFN cascade.

In order to verify this hypothesis we considered the results by Basler and coworkers that identified a coiled-coil domain in the N-terminal half of EBOV VP35 (Reid et al., 2005). In fact, with cross-linking analyses they showed that VP35 forms oligomers, and with coimmunoprecipitation (Co-IP) experiments they confirmed that the putative coiled-coil domain is required for the oligomer formation. Different VP35 mutants were used for Co-IP against the wild type protein, a truncation mutant containing the predicted coiled-coil domain but lacking amino acids 171–340

(VP35$_{1-170}$); another mutant lacking the amino-terminal 170 amino acids (VP35$_{171-340}$), a third mutant deleted of the predicted coiled-coil domain (VP35Δ_{82-118}); and, finally, mutant in which key leucines of the predicted coiled-coil domain were substituted with alanine (VP35$_{L90/93/107A}$). Using these mutants they demonstrated that VP35$_{171-340}$ inhibited the IFN production in a cellular system, but with lower efficacy than wild type VP35, while VP35$_{1-170}$ was unable to suppress the IFN production. The full IFN-antagonist activity of VP35$_{171-340}$ was then restored when a heterologous trimerization domain derived from the bacteriophage T4 fibritin protein, the so called ''foldon'' domain, was fused to the VP35$_{171-340}$ N-terminus. Hence, they demonstrated that the VP35 oligomerization is necessary to have a full suppression of IFN production and that the mentioned N-terminal VP35 coiled-coil domain is needed for the oligomerization. However, is to notice that VP35$_{L90/93/107A}$ mutant was not tested in the cellular system.

Starting from the premise that VP35$_{L90/93/107A}$ mutant lost the ability to oligomerize (Reid et al., 2005), in collaboration with the professor Ruggerone's research team of the Department of Physics of University of Cagliari, an *in silico* model of the coiled-coil wt VP35 dimerization domain was designed. To this model, mutations L90A, L93A and L107A were introduced, to confirm if they are able to bring to a loss of dimerization of the coiled-coil domain. Having the computational model confirmed the hypothesis, we performed site-direct mutagenesis on the pET45b(+)-EBOV-VP35 plasmid in order to obtain a plasmid encoding the VP35$_{L90/93/107A}$ (VP35TM) and evaluated its ability to bind dsRNA and, subsequently, we tested its effect as INF pathway inhibitor in the luciferase reported gene assay previously described (Cannas et al., 2015).

5.2   In silico model of homo-oligomerization of VP35 coiled-coil domain.

Residues 83 to 119 of the N-terminal domain of VP35 were chosen for the modelling of the 3D structure of oligomers and to investigate the extent of coiled-coil formation.

In order to model the VP35 coiled-coil forming helix, a knowledge-based approach was employed to obtain four templates that have a coiled-coil domain as hypothesized for EBOV VP35 and also belong to the order *Mononegavirales*: the templates were the structures of phosphoproteins of Mumps virus, Measles virus, Nipah virus and Sendai virus. The selected structures are identified by Protein Data Bank identification codes 4EIJ (Cox et al., 2013), 4C5Q (Blocquel et al., 2014), 4N5B (Bruhn et al., 2014), 1EZJ (Tarbouriech et al., 2000), respectively, and were used as templates to model the EBOV VP35 coiled-coil domain using Modeller 9.13 (Sali and Blundell, 1993) as described in the methods. We found that only the model based on template 4N5B remained stable during the simulation, while the other models showed unwinding or curling (data not shown). Therefore, the model based on the 4N5B template was chosen to study self-assembly and dimerization.

Once established the VP35 coiled-coil domain model, we generated from it the *in silico* model of coiled-coil domain bearing the three mutations (leucines 90, 93 and 107 into alanines). In order to increase the statistical significance of the results, for each system, we performed 12 independent simulations of the dimerization process as described.

The results showed that VP35 presents a good propensity (~60%) to form stable coiled-coil dimers during the simulation time, whereas the mutant showed poor

ability to even properly dimerize (~17%) (Figure 44). In fact, the mutant VP35 coiled-coil domain showed only two stable configuration out of twelve, while VP35 wild type coiled-coil domain showed seven out of twelve, suggesting that indeed the presence of the L93A, L93A and L107A mutations strongly impaired the coiled-coil domain dimerization *in silico*. Overall, these results may confirm in silico the importance of the coiled-coil domain for VP35 oligomerization.
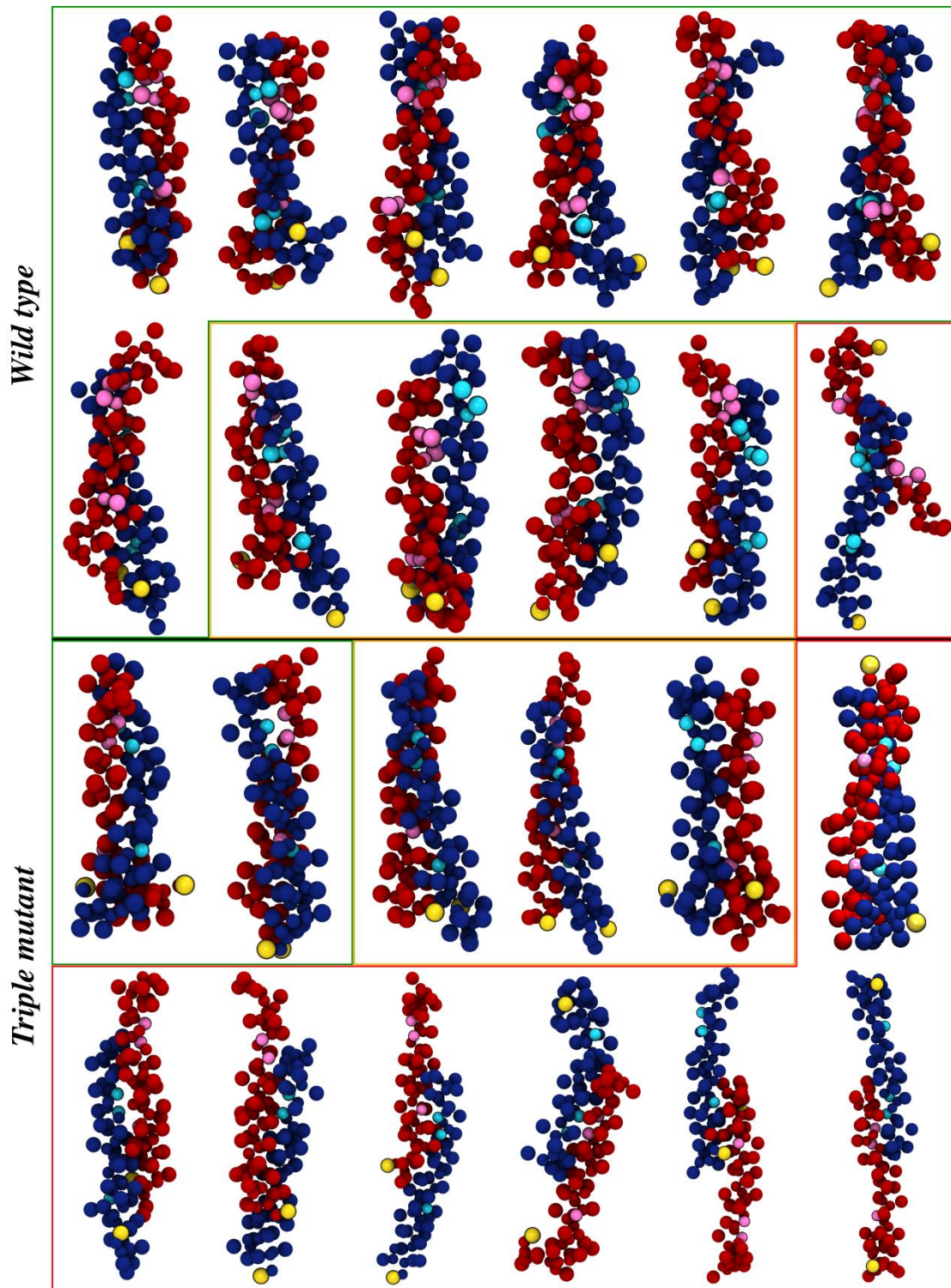
Figure 44 - Final configurations of wild type (top) and triple mutant (L90A/L93A/L107A) (bottom) VP35 coiled-coil domain from 12 independent replicas of coarse-grained simulations (200 ns). Dimers resulting in a proper coiled-coil configuration are shown in green boxes, improper coiled-coil and uncoiled dimers are in yellow boxes while disordered oligomers are in red boxes. The monomers are shown in beads colored red and blue with the mutated residues in cyan and pink, respectively; terminal prolines shown in yellow give the relative orientation (parallel/anti-parallel) of the monomers.

5.3   rVP35TM binding to dsRNA in biochemical assay

Having the *in silico* analysis confirmed that the presence of the three point mutations L90A, L93A and L107A should bring to a loss of dimerization ability of the coiled-coil domain, hypothesizing that the coiled-coil domain is the driving force for the full length VP35 dimerization, we wanted to verify if the presence of the three mutations in the full length rVP35 could influence the protein binding to dsRNA.

Similarly to what we have performed for the analysis of the rVP35-dsRNA binding, we tested rVP35TM binding to dsRNA in the assay described in chapter 3. As described in the chapter 2, the point mutations have been generated on the pET45b(+)-EBOV-VP35 plasmid for the expression of recombinant N-terminal His6-tag-VP35 protein, expressed and purified as described. Hence we performed a series of experiments to measure the ability of rVP35TM to bind dsRNA, detectable by its fluorescein signal.

Firstly, we performed three experiments of binding at fixed concentration of ligand pair to 7.5 nM, just to compare rVP35 and rVP35TM ability to bind 5'-ppp-dsRNA. The results demonstrated that rVP35TM showed a > 4-fold reduced ability to bind to dsRNA as compared to wild type VP35 (Figure 45).

Subsequently, in order to calculate the rVP35TM K_d and B_{max} parameters for the dsRNA binding, we incubate rVP35TM with increasing concentrations of dsRNA from 0.5 to 64 nM. However, the limited ability of VP35TM to bind dsRNA did not allow to obtain a well-defined saturation curve and, consequently, to calculate binding parameters (data not shown).
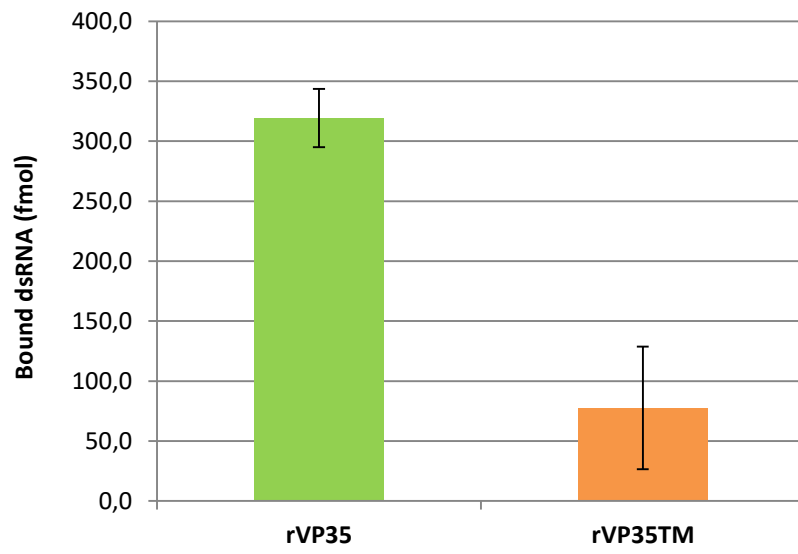
Figure 45 - Biochemical assay: comparison between wild type rVP35 and rVP35TM ability to bind to dsRNA

5.4   Effects of rVP35TM in luciferase reporter gene assay

Since rVP35TM was shown to have a reduced ability of binding to dsRNA, we wanted to verify if the mutant protein was still able to inhibit the IFN response in the in the luciferase gene reporter cellular assay. Starting from pcDNA3-EBOV-VP35 plasmid, we performed a site-direct mutagenesis to obtain an insert expressing the triple mutant EBOV-VP35TM in a mammalian cellular system.

In order to compare the IFN inhibitory ability of rVP35 and rVP35TM, cells were transfected with different amounts (100, 150, 200, 250 ng) of the mammalian expression vectors pcDNA3-EBOV-VP35 and pcDNA3-EBOV-VP35TM.

The result showed that the VP35TM still maintains the ability to inhibit the RIG-I signaling cascade but to a lower extent with respect to wild-type VP35 and this difference is higher at lower amount of transfected plasmid (Figure 46), hence at lower level of protein expressed.
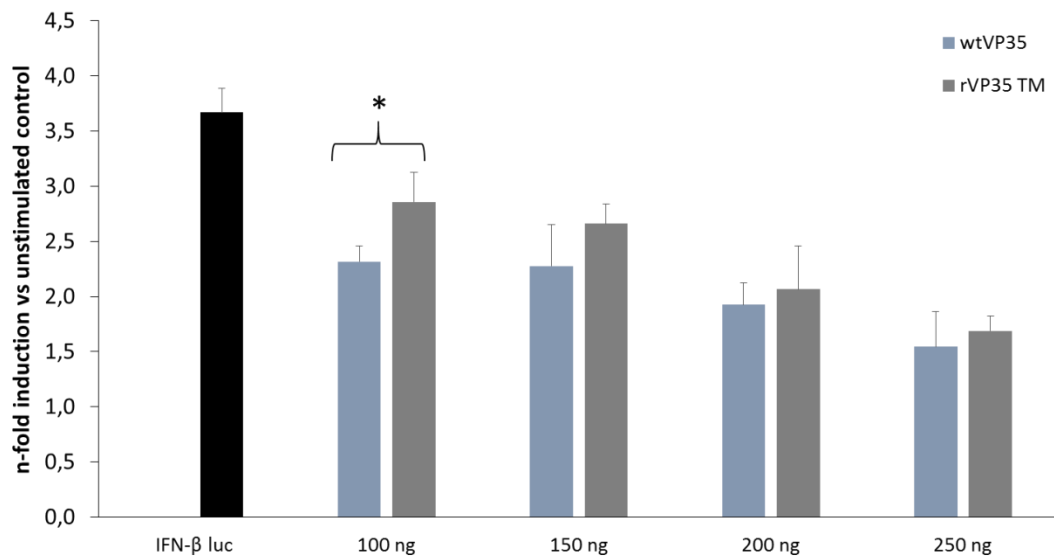
Figure 46 - Comparison of the inhibitory effect of EBOV wild-type VP35 and VP35TM in the luciferase reporter gene assay in 48-well plates. A549 cells were cotransfected with 250 ng of pGL interferon β (IFN-β) luc and various amounts (100, 150, 200, 250 ng) of pcDNA3-wtVP35 or pcDNA3-rVP35 TM. Twenty-four hours after transfection, cells were additionally transfected with 250 ng of IAV RNA. After an additional 6 hours, cells were lysed, and luciferase activity was measured. Results show the inhibition of luciferase expression indicated as the fold activity of the unstimulated control (p value < 0.05).

5.5 Discussion

Previous studies suggested that VP35 multimerizes forming homotrimers, that a putative coiled-coil domain appears to be required for efficient homo-oligomerization and that this region facilitates the ''IFN-antagonist'' function of the protein (Reid et al., 2005). Furthermore, it has been demonstrate that VP35 binds to dsRNA forming an asymmetric homodimer that is able to bind both the dsRNA phosphate backbone and blunt ends (Bale et al., 2012; Kimberlin et al., 2010; Leung et al., 2010a).

The EBOV VP35 coiled-coil domain *in silico* homo-dimerization model confirmed the importance of the presence of leucine residues 90, 93 and 107 to promote and maintain a stable and proper coiled-coil dimerization profile. Even if our study focused exclusively on dimerization, while Reid et al. in cited work suggested that VP35 forms trimers, the importance of our model derives from following studies demonstrating that VP35 binds to dsRNA forming an asymmetric homodimer (Kimberlin et al., 2010; Leung et al., 2010a). Hence, we confirmed this model, utilizing both the full-length rVP35 and rVP35TM, demonstrating that the described mutations brings to a partial loss of ability to bind the dsRNA in biochemical assays.

However, at this partial loss of rVP35TM binding ability does not correspond an equally decreased inhibition of the IFN response in the cellular system. As it is known that VP35 acts in several point of RLRs pathway, these results would seem to confirm our initial hypothesis that the VP35 binding to dsRNA might be is not so important in the IFN inhibitory function of this viral protein.

6 CONCLUSIONS

Infections caused by RNA viruses are some of the most important diseases in terms of morbidity, mortality and economic impact, being responsible for a huge spectrum of important acute, chronic and emerging human infections. RNA viruses are also frequently responsible for zoonotic diseases, viral infections of animal hosts that are spread to humans. These include the highly lethal viral hemorrhagic fever caused by filoviruses, particularly by EBOV, which causes a severe, frequently fatal hemorrhagic syndrome in humans and non-human primates. EBOV is classified by the Centers of Diseases Control and Prevention as Category A biowarfare agent, because of the high virulence and the consequent ability to induce panic. The average EVD case fatality rate in the past epidemic in West Africa caused by EBOV has been reported to be around 40%. At the moment, the treatment involves early, aggressive supportive care with rehydration, but no approved vaccine or drug is available for EVD treatments.

The EBOV VP35 protein plays an important role in the inhibition of the initial innate immune responses to EBOV infection leading to EVD development. In fact, VP35 interaction with the RLR cascade components inhibits IFN production, impeding proper host immune response. Hence, it has been shown that VP35 is a validate drug target.

EBOV VP35 contains an N-terminal coiled-coil domain and a C-terminal RBD, containing highly conserved protein patches, important for the VP35 interaction with dsRNA as well as other cellular component of the RLR cascade. Of note, any drugs that act on these domains is likely to be effective against all EBOV VP35 variants.

Importantly, when the sole VP35 RDB is expressed into cells, it is not able to suppress the type I IFN activation at the same level than the full length protein, suggesting that proper studies for drug development need to be addressed to the full-length VP35 protein.

Full-length His-tagged rVP35 has been previously expressed in prokaryotic system and used to validate a biochemical pull-down assay for the screening of small molecules targeted to the VP35-dsRNA interactions. However, low rVP35 amount of purified protein and the use of radioactive substrate for binding evaluation, strongly limited the screening system.

In the present study, a new method for high-yield rVP35 expression and purification, based on denaturation and subsequent protein refolding was established. Subsequently, the use of a fluorescent labeled 30mer dsRNA was validated, showing that the rVP35 K_d value for this substrate was comparable to the K_d value previously reported for longer ^{3}H-labeled dsRNA substrate (Zinzula et al., 2012).

Furthermore, the 30mer fluorescent oligomer was used as substrate in a novel assay based on the use of Nickel-coated plates, that was validated showing that also in this assay the rVP35 K_d value was around 4 nM and that the Z'-factor was 0.69, indicating a good assay.

In order to identify small molecules able to inhibit EBOV VP35 block of the innate immune system activation, we utilized this biochemical assay to screen the ability of plant extracts and derived compounds to inhibit the rVP35 binding to dsRNA. Active plant extracts and derived compounds were also tested in a cellular luciferase reporter gene assay to evaluate their ability to counteract the inhibitory activity of VP35 on the IFN response.

Overall, we identified a number of compounds able to inhibit the VP35 function. In particular, we identified the flavonol myricetin from the plant *L. morisianum* that was able to inhibit rVP35 binding to dsRNA in biochemical assay but it was ineffective in the luciferase reporter gene assay. Conversely, we identified another flavonol compound, quercetin, from the plant *H. hircinum*, that was unable to inhibit rVP35 binding to dsRNA in biochemical assay, while it subverted VP35 inhibition of IFN production. These results suggested that, on the one side, dsRNA masking by VP35 may not be the driving force of the VP35 inhibition of the IFN cascade. On the other side, they suggested that alternative mechanisms of action could be involved in quercetin anti-VP35 efficacy, possibly as it has been suggested for quercetin and other flavonol derivatives (Khiar et al., 2015). Of note, we identified one compound, cynarin, from the plant *O. illyricum*, that was active in both biochemical and cellular assays. Considering that the VP35 pocket binding to dsRNA has been also involved with the interaction with other cellular factors such as IKK-ε and TBK-1, these results may suggest that some small molecules may have the ability to interact with this VP35 pocket disrupting VP35 interaction with multiple targets. The assessment of cynarin ability to effectively inhibit EBOV replication in proper cell based assays will be required. Furthermore, the development of cynarin derivatives with more potent anti-VP35 activity will be needed in the effort to develop an effective anti-EVD therapy.

In order to understand the relative role of VP35-dsRNA binding in inhibiting the RLR cascade, we wanted to study the effects of the lack of VP35 dimerization, which has been proposed to be essential for VP35 binding to dsRNA. For this purpose, we introduced three single point mutations into the coiled-coil VP35 domain that were

been proposed to be essential for VP35 dimerization (Reid et al., 2005). We confirmed by *in silico* studies that introduction of these three mutations disrupted coiled-coil dimerization.

Biochemical assay studies, performed using rVP35TM, also showed that this protein has a reduce ability to bind dsRNA, confirming the importance of VP35 dimerization for VP35-dsRNA binding. However, when the VP35TM was expressed in a cellular system, it mainly maintained the ability to inhibit the IFN induction, showing only a limited reduction of the wild-type VP35 potency of RLR cascade inhibition. Overall, these results seem to confirm the hypothesis that VP35 binding to dsRNA is not the main interaction needed for VP35 inhibition of the IFN production and suggested that the VP35 interactions with cellular components do not require VP35 dimerization.

In conclusion, we demonstrated that small molecules interacting with VP35 can subvert its inhibition of the IFN production, possibly inhibiting its interactions with cellular components of RLR pathway and suggested that VP35 binding to dsRNA is not the driving for VP35 inhibition RLR cascade activation.

ACKNOWLEDGEMENTS

REFERENCES

Abraham, M.J., Van Der Spoel, D., Lindahl, E., Hess, B., and the GROMACS, Team, D., Manual, R., 2016. GROMACS User Manual version 5.1.3, www. gromacs. org.

Adams, M.J., Lefkowitz, E.J., King, a M.Q., Carstens, E.B., 2014. Ratification vote on taxonomic proposals to the International Committee on Taxonomy of Viruses (2014). Arch. Virol. 159, 2831–41. doi:10.1007/s00705-014-2114-3

Afonso, C.L., Amarasinghe, G.K., B??nyai, K., B??o, Y., Basler, C.F., Bavari, S., Bejerman, N., Blasdell, K.R., Briand, F.X., Briese, T., Bukreyev, A., Calisher, C.H., Chandran, K., Ch??ng, J., Clawson, A.N., Collins, P.L., Dietzgen, R.G., Dolnik, O., Domier, L.L., D??rrwald, R., Dye, J.M., Easton, A.J., Ebihara, H., Farkas, S.L., Freitas-Ast??a, J., Formenty, P., Fouchier, R.A.M., F??, Y., Ghedin, E., Goodin, M.M., Hewson, R., Horie, M., Hyndman, T.H., Ji??ng, D., Kitajima, E.W., Kobinger, G.P., Kondo, H., Kurath, G., Lamb, R.A., Lenardon, S., Leroy, E.M., Li, C.X., Lin, X.D., Li??, L., Longdon, B., Marton, S., Maisner, A., M??hlberger, E., Netesov, S. V., Nowotny, N., Patterson, J.L., Payne, S.L., Paweska, J.T., Randall, R.E., Rima, B.K., Rota, P., Rubbenstroth, D., Schwemmle, M., Shi, M., Smither, S.J., Stenglein, M.D., Stone, D.M., Takada, A., Terregino, C., Tesh, R.B., Tian, J.H., Tomonaga, K., Tordo, N., Towner, J.S., Vasilakis, N., Verbeek, M., Volchkov, V.E., Wahl-Jensen, V., Walsh, J.A., Walker, P.J., Wang, D., Wang, L.F., Wetzel, T., Whitfield, A.E., Xi??, J., Yuen, K.Y., Zhang, Y.Z., Kuhn, J.H., 2016. Taxonomy of the order Mononegavirales: update 2016. Arch. Virol. 161, 2351–2360. doi:10.1007/s00705-016-2880-1

Akira, S., Uematsu, S., Takeuchi, O., 2006. Pathogen Recognition and Innate Immunity. Cell 124, 783–801. doi:10.1016/j.cell.2006.02.015

Amman, B.R., Carroll, S.A., Reed, Z.D., Sealy, T.K., Balinandi, S., Swanepoel, R., Kemp, A., Erickson, B.R., Comer, J.A., Campbell, S., Cannon, D.L., Khristova, M.L., Atimnedi, P., Paddock, C.D., Kent Crockett, R.J., Flietstra, T.D., Warfield, K.L., Unfer, R., Katongole-Mbidde, E., Downing, R., Tappero, J.W., Zaki, S.R., Rollin, P.E., Ksiazek, T.G., Nichol, S.T., Towner, J.S., 2012. Seasonal Pulses of Marburg Virus Circulation in Juvenile Rousettus aegyptiacus Bats Coincide with Periods of Increased Risk of Human Infection. PLoS Pathog. 8. doi:10.1371/journal.ppat.1002877

Aniya, Y., Miyagi, C., Nakandakari, a, Kamiya, S., Imaizumi, N., Ichiba, T., 2002. Free radical scavenging action of the medicinal herb Limonium wrightii from the Okinawa islands. Phytomedicine 9, 239–244. doi:10.1078/0944-7113-00112

Atanasov, A.G., Waltenberger, B., Pferschy-Wenzig, E.M., Linder, T., Wawrosch, C., Uhrin, P., Temml, V., Wang, L., Schwaiger, S., Heiss, E.H., Rollinger, J.M., Schuster, D., Breuss, J.M., Bochkov, V., Mihovilovic, M.D., Kopp, B., Bauer, R., Dirsch, V.M., Stuppner, H., 2015. Discovery and resupply of pharmacologically active plant-derived natural products: A review. Biotechnol. Adv. 33, 1582–1614. doi:10.1016/j.biotechadv.2015.08.001

Atzei, A.D., 2009. Le piante nella tradizione popolare della Sardegna. Carlo Delfino Editore.

Bacchetta, G., Brullo, S., Salmeri, C., 2010. Hypericum scruglii sp. nov. (Guttiferae) from Sardinia. Nord. J. Bot. 28, 469–474. doi:10.1111/j.1756-1051.2009.00736.x

Baize, S., Leroy, E.M., Georges, A.J., Georges-Courbot, M.C., Capron, M., Bedjabaga, I., Lansoud-Soukate, J., Mavoungou, E., 2002. Inflammatory responses in Ebola virus-infected patients. Clin. Exp. Immunol. 128, 163–168. doi:10.1046/j.1365-2249.2002.01800.x

Bale, S., Julien, J.-P., Bornholdt, Z. a, Krois, A.S., Wilson, I. a, Saphire, E.O., 2013. Ebolavirus VP35 coats the backbone of double-stranded RNA for interferon antagonism. J. Virol. 87, 10385–8. doi:10.1128/JVI.01452-13

Bale, S., Julien, J.P., Bornholdt, Z.A., Kimberlin, C.R., Halfmann, P., Zandonatti, M.A., Kunert, J., Kroon, G.J.A., Kawaoka, Y., MacRae, I.J., Wilson, I.A., Saphire, E.O., 2012. Marburg Virus VP35 Can Both Fully Coat the Backbone and Cap the Ends of dsRNA for Interferon Antagonism. PLoS Pathog. 8, 1–12. doi:10.1371/journal.ppat.1002916

Basler, C.F., 2015. Innate immune evasion by filoviruses. Virology 479–480, 122–130. doi:10.1016/j.virol.2015.03.030

Basler, C.F., Mikulasova, A., Martinez-Sobrido, L., Paragas, J., Mühlberger, E., Bray, M., Klenk, H.-D., Palese, P., García-Sastre, A., 2003. The Ebola virus VP35 protein inhibits activation of interferon regulatory factor 3. J. Virol. 77, 7945–56.

Basler, C.F., Wang, X., Mühlberger, E., Volchkov, V., Paragas, J., Klenk, H.-D., Garcia-Sastre, A.,

Palese, P., 2000. The Ebola virus VP35 protein functions as a type I IFN antagonist. Proc. Natl. Acad. Sci. 97, 12289–12294. doi:10.1073/pnas.220398297

Baum, A., Garcia-Sastre, A., 2011. Differential recognition of viral RNA by RIG-I. Virulence 2, 166–169. doi:10.1073/

Baum, A., García-Sastre, A., 2010. Induction of type i interferon by RNA viruses: Cellular receptors and their substrates. Amino Acids 38, 1283–1299. doi:10.1007/s00726-009-0374-0

Baz-Martínez, M., El Motiam, A., Ruibal, P., Condezo, G.N., de la Cruz-Herrera, C.F., Lang, V., Collado, M., San Martín, C., Rodríguez, M.S., Muñoz-Fontela, C., Rivas, C., 2016. Regulation of Ebola virus VP40 matrix protein by SUMO. Sci. Rep. 6, 37258. doi:10.1038/srep37258

Beniac, D.R., Melito, P.L., DeVarennes, S.L., Hiebert, S.L., Rabb, M.J., Lamboo, L.L., Jones, S.M., Booth, T.F., 2012. The organisation of Ebola virus reveals a capacity for extensive, modular polyploidy. PLoS One 7, e29608. doi:10.1371/journal.pone.0029608

Bharat, T.A.M., Noda, T., Riches, J.D., Kraehling, V., Kolesnikova, L., Becker, S., Kawaoka, Y., Briggs, J.A.G., 2012. Structural dissection of Ebola virus and its assembly determinants using cryo-electron tomography. Proc. Natl. Acad. Sci. U. S. A. 109, 4275–80. doi:10.1073/pnas.1120453109

Bharat, T.A.M., Riches, J.D., Kolesnikova, L., Welsch, S., Krähling, V., Davey, N., Parsy, M.L., Becker, S., Briggs, J.A.G., 2011. Cryo-electron tomography of marburg virus particles and their morphogenesis within infected cells. PLoS Biol. 9. doi:10.1371/journal.pbio.1001196

Biedenkopf, N., Hartlieb, B., Hoenen, T., Becker, S., 2013. Phosphorylation of ebola virus VP30 influences the composition of the viral nucleocapsid complex: Impact on viral transcription and replication. J. Biol. Chem. 288, 11165–11174. doi:10.1074/jbc.M113.461285

Biedenkopf, N., Schlereth, J., Grünweller, A., Becker, S., Hartmann, R.K., 2016. RNA-binding of Ebola virus VP30 is essential for activating viral transcription. J. Virol. 90, 7481–7496. doi:10.1128/JVI.00271-16

Bilyk, A., Cooper, P.L., Sapers, G.M., 1984. Varietal differences in distribution of quercetin and kaempferol in onion (Allium cepa L.) tissue. J. Agric. Food Chem. 32, 274–276. doi:10.1021/jf00122a024

Blocquel, D., Habchi, J., Durand, E., Sevajol, M., Ferron, F., Erales, J., Papageorgiou, N., Longhi, S., 2014. Coiled-coil deformations in crystal structures: the Measles virus phosphoprotein multimerization domain as an illustrative example. Acta Crystallogr. Sect. D Biol. Crystallogr. 70, 1589–1603. doi:10.1107/S139900471400234X

Booth, T.F., Rabb, M.J., Beniac, D.R., 2013. How do filovirus filaments bend without breaking? Trends Microbiol. 21, 583–593. doi:10.1016/j.tim.2013.08.001

Bowie, A., O'Neill, L.A., 2000. The interleukin-1 receptor/Toll-like receptor superfamily: signal generators for pro-inflammatory interleukins and microbial products. J. Leukoc. Biol. 67, 508–14.

Bray, M., Geisbert, T.W., 2005. Ebola virus: the role of macrophages and dendritic cells in the pathogenesis of Ebola hemorrhagic fever. Int. J. Biochem. Cell Biol. 37, 1560–1566.

Bray, M., Hatfill, S., Hensley, L., Huggins, J.W., 2001. Haematological, biochemical and coagulation changes in mice, guinea-pigs and monkeys infected with a mouse-adapted variant of Ebola Zaire virus. J. Comp. Pathol. 125, 243–253. doi:10.1053/jcpa.2001.0503

Brubaker, S.W., Bonham, K.S., Zanoni, I., Kagan, J.C., 2015. Innate immune pattern recognition: a cell biological perspective., Annual review of immunology. doi:10.1146/annurev-immunol-032414-112240

Bruhn, J.F., Barnett, K.C., Bibby, J., Thomas, J.M.H., Keegan, R.M., Rigden, D.J., Bornholdt, Z.A., Saphire, E.O., 2014. Crystal structure of the nipah virus phosphoprotein tetramerization domain. J. Virol. 88, 758–62. doi:10.1128/JVI.02294-13

Bussi, G., Donadio, D., Parrinello, M., 2007. Canonical sampling through velocity rescaling. J. Chem. Phys. 126, 14101. doi:10.1063/1.2408420

Bylund, D.B., Murrin, L.C., 2000. Radioligand saturation binding experiments over large concentration ranges. Life Sci. 67, 2897–2911. doi:10.1016/S0024-3205(00)00877-8

Cannas, V., Daino, G.L., Corona, A., Esposito, F., Tramontano, E., 2015. A Luciferase Reporter Gene Assay to Measure Ebola Virus Viral Protein 35-Associated Inhibition of Double-Stranded RNA-Stimulated, Retinoic Acid-Inducible Gene 1-Mediated Induction of Interferon β. J. Infect. Dis. 212, S277–S281. doi:10.1093/infdis/jiv214

Cárdenas, W.B., Loo, Y.-M., Gale, M., Hartman, A.L., Kimberlin, C.R., Martínez-Sobrido, L., Saphire, E.O., Basler, C.F., 2006. Ebola virus VP35 protein binds double-stranded RNA and

inhibits alpha/beta interferon production induced by RIG-I signaling. J. Virol. 80, 5168–78. doi:10.1128/JVI.02199-05

Cardile, A.P., Downey, L.G., Wiseman, P.D., Warren, T.K., Bavari, S., 2016. Antiviral therapeutics for the treatment of Ebola virus infection. Curr. Opin. Pharmacol. 30, 138–143. doi:10.1016/j.coph.2016.08.016

Carette, J.E., Raaben, M., ..., 2011. Ebola virus entry requires the cholesterol transporter Niemann-Pick C1. Nature 477, 340–343. doi:10.1038/nature10348.Ebola

Centers for Disease Control and Prevention, 2016. Outbreaks Chronology: Ebola Virus Disease [WWW Document]. URL http://www.cdc.gov/vhf/ebola/outbreaks/history/chronology.html (accessed 3.5.17).

Chang, T., Kubota, T., Matsuoka, M., Jones, S., Bradfute, S.B., 2009. Ebola Zaire Virus Blocks Type I Interferon Production by Exploiting the Host SUMO Modification Machinery 5. doi:10.1371/journal.ppat.1000493

Chimenti, F., Cottiglia, F., Bonsignore, L., Casu, L., Casu, M., Floris, C., Secci, D., Bolasco, A., Chimenti, P., Granese, A., Befani, O., Turini, P., Alcaro, S., Ortuso, F., Trombetta, G., Loizzo, A., Guarino, I., 2006. Quercetin as the active principle of Hypericum hircinum exerts a selective inhibitory activity against MAO-A: Extraction, biological analysis, and computational study. J. Nat. Prod. 69, 945–949. doi:10.1021/np060015w

Cote, M., Masasi, J., Ren, T., Bruchez, A., Lee, K., Filone, M., Hensley, L., Li, Q., Ory, D., Chandran, K., Hospital, W., Hospital, C., Division, V., Louis, S., 2011. Small molecule inhibotor reveal Niemann-Pick C1 is essential for Ebolavirus infection. Nature 477, 344–348. doi:10.1038/nature10380.Small

Cox, R., Green, T.J., Purushotham, S., Deivanayagam, C., Bedwell, G.J., Prevelige, P.E., Luo, M., 2013. Structural and functional characterization of the mumps virus phosphoprotein. J. Virol. 87, 7558–68. doi:10.1128/JVI.00653-13

Cragg, G.M., Newman, D.J., 2013. Natural products: A continuing source of novel drug leads. Biochim. Biophys. Acta - Gen. Subj. 1830, 3670–3695. doi:10.1016/j.bbagen.2013.02.008

Cushnie, T.P.T., Lamb, A.J., 2005. Antimicrobial activity of flavonoids. Int. J. Antimicrob. Agents 26, 343–356. doi:10.1016/j.ijantimicag.2005.09.002

de Jong, D.H., Singh, G., Bennett, W.F.D., Arnarez, C., Wassenaar, T.A., Schäfer, L. V, Periole, X., Tieleman, D.P., Marrink, S.J., 2013. Improved Parameters for the Martini Coarse-Grained Protein Force Field. J. Chem. Theory Comput. 9, 687–97. doi:10.1021/ct300646g

de La Vega, M.A., Stein, D., Kobinger, G.P., 2015. Ebolavirus Evolution: Past and Present. PLoS Pathog. 11, 1–10. doi:10.1371/journal.ppat.1005221

DeBlasi, a, O'Reilly, K., Motulsky, H.J., 1989. Calculating receptor number from binding experiments using same compound as radioligand and competitor. Trends Pharmacol. Sci. 10, 227–229. doi:10.1016/0165-6147(89)90266-6

Deen, G.F., Knust, B., Broutet, N., Sesay, F.R., Formenty, P., Ross, C., Thorson, A.E., Massaquoi, T.A., Marrinan, J.E., Ervin, E., Jambai, A., McDonald, S.L.R., Bernstein, K., Wurie, A.H., Dumbuya, M.S., Abad, N., Idriss, B., Wi, T., Bennett, S.D., Davies, T., Ebrahim, F.K., Meites, E., Naidoo, D., Smith, S., Banerjee, A., Erickson, B.R., Brault, A., Durski, K.N., Winter, J., Sealy, T., Nichol, S.T., Lamunu, M., Ströher, U., Morgan, O., Sahr, F., 2015. Ebola RNA Persistence in Semen of Ebola Virus Disease Survivors — Preliminary Report. N. Engl. J. Med. 151014140118009. doi:10.1056/NEJMoa1511410

Dube, D., Brecher, M.B., Delos, S.E., Rose, S.C., Park, E.W., Schornberg, K.L., Kuhn, J.H., White, J.M., 2009. The primed ebolavirus glycoprotein (19-kilodalton GP1,2): sequence and residues critical for host cell binding. J. Virol. 83, 2883–91. doi:10.1128/JVI.01956-08

Dube, D., Schornberg, K.L., Shoemaker, C.J., Delos, S.E., Stantchev, T.S., 2010. Cell adhesion-dependent membrane traf fi cking of a binding partner for the ebolavirus glycoprotein is a determinant of viral entry 107, 16637–16642. doi:10.1073/pnas.1008509107

Elshabrawy, H.A., Erickson, T.B., Prabhakar, B.S., 2015. Ebola virus outbreak, updates on current therapeutic strategies. Rev. Med. Virol. 25, 241–253. doi:10.1002/rmv.1841

Elston, J.W.T., Cartwright, C., Ndumbi, P., Wright, J., 2017. The health impact of the 2014–15 Ebola outbreak. Public Health 143, 60–70. doi:10.1016/j.puhe.2016.10.020

Esposito, F., Sanna, C., Del Vecchio, C., Cannas, V., Venditti, A., Corona, A., Bianco, A., Serrilli, A.M., Guarcini, L., Parolin, C., Ballero, M., Tramontano, E., 2013. Hypericum hircinum L. Components as new single-molecule inhibitors of both HIV-1 reverse transcriptase-associated DNA polymerase and ribonuclease H activities. Pathog. Dis. 68, 116–124. doi:10.1111/2049-

632X.12051

Feldmann, H., Geisbert, T.W., 2011. Ebola haemorrhagic fever. Lancet 377, 849–862. doi:10.1016/S0140-6736(10)60667-8

Fitzgerald, K.A., McWhirter, S.M., Faia, K.L., Rowe, D.C., Latz, E., Golenbock, D.T., Coyle, A.J., Liao, S.-M., Maniatis, T., 2003. IKKε and TBK1 are essential components of the IRF3 signaling pathway. Nat. Immunol. 4, 491–496. doi:10.1038/ni921

Florescu, D.F., Kalil, A.C., Hewlett, A.L., Schuh, A.J., Stroher, U., Uyeki, T.M., Smith, P.W., 2015. Administration of Brincidofovir and Convalescent Plasma in a Patient with Ebola Virus Disease. Clin. Infect. Dis. 61, 969–973. doi:10.1093/cid/civ395

Folayan, M.O., Yakubu, A., Haire, B., Peterson, K., 2016. Ebola vaccine development plan: ethics, concerns and proposed measures. BMC Med. Ethics 1–8. doi:10.1186/s12910-016-0094-4

Formenty, P., 2014. Ebola Virus Disease, in: Emerging Infectious Diseases. Elsevier, pp. 121–134. doi:10.1016/B978-0-12-416975-3.00009-1

Formisano, C., Sanna, C., Ballero, M., Chianese, G., Sirignano, C., Rigano, D., Mill??n, E., Mu??oz, E., Taglialatela-Scafati, O., 2017. Anti-inflammatory sesquiterpene lactones from Onopordum illyricum L. (Asteraceae), an Italian medicinal plant. Fitoterapia 116, 61–65. doi:10.1016/j.fitote.2016.11.006

Gebhardt, R., 1998. Inhibition of cholesterol biosynthesis in primary cultured rat hepatocytes by artichoke (Cynara scolymus L.) extracts. J. Pharmacol. Exp. Ther. 286, 1122–8.

Gebhardt, R., Fausel, M., 1997. Antioxidant and hepatoprotective effects of artichoke extracts and constituents in cultured rat hepatocytes. Toxicol. Vitr. 11, 669–672. doi:10.1016/S0887-2333(97)00078-7

Geisbert, T.W., Hensley, L.E., Larsen, T., Young, H. a., Reed, D.S., Geisbert, J.B., Scott, D.P., Kagan, E., Jahrling, P.B., Davis, K.J., 2003. Pathogenesis of Ebola Hemorrhagic Fever in Cynomolgus Macaques. Am. J. Pathol. 163, 2347–2370. doi:10.1016/S0002-9440(10)63591-2

Glanzer, J.G., Byrne, B.M., McCoy, A.M., James, B.J., Frank, J.D., Oakley, G.G., 2016. In silico and in vitro methods to identify ebola virus VP35-dsRNA inhibitors. Bioorg. Med. Chem. doi:10.1016/j.bmc.2016.08.065

Goeijenbier, M., van Kampen, J.J.A., Reusken, C.B.E.M., Koopmans, M.P.G., van Gorp, E.C.M., 2014. Ebola virus disease: a review on epidemiology, symptoms, treatment and pathogenesis. Neth. J. Med. 72, 442–8.

Grigorian, A.L., Bustamante, J.J., Hernandez, P., Martinez, A.O., Haro, L.S., 2005. Extraordinarily stable disulfide-linked homodimer of human growth hormone 902–913. doi:10.1110/ps.041048805.Pituitary

Haasnoot, J., de Vries, W., Geutjes, E.-J., Prins, M., de Haan, P., Berkhout, B., 2007. The Ebola virus VP35 protein is a suppressor of RNA silencing. PLoS Pathog. 3, e86. doi:10.1371/journal.ppat.0030086

Han, Z., Boshra, H., Sunyer, J.O., Zwiers, S.H., Paragas, J., Harty, R.N., 2003. Biochemical and Functional Characterization of the Ebola Virus VP24 Protein: Implications for a Role in Virus Assembly and Budding. J. Virol. 77, 1793–1800. doi:10.1128/JVI.77.3.1793-1800.2003

Hartlieb, B., Modrof, J., Muhlberger, E., Klenk, H.-D., Becker, S., 2003. Oligomerization of Ebola Virus VP30 Is Essential for Viral Transcription and Can Be Inhibited by a Synthetic Peptide. J. Biol. Chem. 278, 41830–41836. doi:10.1074/jbc.M307036200

Hartlieb, B., Muziol, T., Weissenhorn, W., Becker, S., 2007. Crystal structure of the C-terminal domain of Ebola virus VP30 reveals a role in transcription and nucleocapsid association. Proc. Natl. Acad. Sci. 104, 624–629. doi:10.1073/pnas.0606730104

Hartman, A.L., Dover, J.E., Towner, J.S., Nichol, S.T., 2006. Reverse Genetic Generation of Recombinant Zaire Ebola Viruses Containing Disrupted IRF-3 Inhibitory Domains Results in Attenuated Virus Growth In Vitro and Higher Levels of IRF-3 Activation without Inhibiting Viral Transcription or Replication. J. Virol. 80, 6430–6440. doi:10.1128/JVI.00044-06

Hartman, A.L., Ling, L., Nichol, S.T., Hibberd, M.L., 2008. Whole-genome expression profiling reveals that inhibition of host innate immune response pathways by Ebola virus can be reversed by a single amino acid change in the VP35 protein. J. Virol. 82, 5348–5358. doi:10.1128/JVI.00215-08

Hartman, A.L., Towner, J.S., Nichol, S.T., 2004. A C-terminal basic amino acid motif of Zaire ebolavirus VP35 is essential for type I interferon antagonism and displays high identity with the RNA-binding domain of another interferon antagonist, the NS1 protein of influenza A virus. Virology 328, 177–84. doi:10.1016/j.virol.2004.07.006

Heeney, J.L., 2015. Ebola: Hidden reservoirs. Nature 527, 453–455. doi:10.1038/527453a

Henao-Restrepo, A.M., Longini, I.M., Egger, M., Dean, N.E., Edmunds, W.J., Camacho, A., Carroll, M.W., Doumbia, M., Draguez, B., Duraffour, S., Enwere, G., Grais, R., Gunther, S., Hossmann, S., Kondé, M.K., Kone, S., Kuisma, E., Levine, M.M., Mandal, S., Norheim, G., Riveros, X., Soumah, A., Trelle, S., Vicari, A.S., Watson, C.H., Kéïta, S., Kieny, M.P., Rottingen, J.-A., 2015. Efficacy and effectiveness of an rVSV-vectored vaccine expressing Ebola surface glycoprotein: interim results from the Guinea ring vaccination cluster-randomised trial. Lancet 386, 857–866. doi:10.1016/S0140-6736(15)61117-5

Hensley, L.E., Young, H.A., Jahrling, P.B., Geisbert, T.W., 2002. Proinflammatory response during Ebola virus infection of primate models: Possible involvement of the tumor necrosis factor receptor superfamily. Immunol. Lett. 80, 169–179. doi:10.1016/S0165-2478(01)00327-3

Herrmann, K.M., Weaver, L.M., 1999. THE SHIKIMATE PATHWAY. Annu. Rev. Plant Physiol. Plant Mol. Biol. 50, 473–503. doi:10.1146/annurev.arplant.50.1.473

Heymann, D.L., Barakamfitiye, D., Szczeniowski, M., Muyembe-Tamfum, J., Bele, O., Rodier, G., 1999. Ebola Hemorrhagic Fever: Lessons from Kikwit, Democratic Republic of the Congo. J. Infect. Dis. 179, S283–S286. doi:10.1086/514287

Hoenen, T., Groseth, A., Kolesnikova, L., Theriault, S., Ebihara, H., Hartlieb, B., Bamberg, S., Feldmann, H., Ströher, U., Becker, S., 2006. Infection of naive target cells with virus-like particles: implications for the function of ebola virus VP24. J. Virol. 80, 7260–4. doi:10.1128/JVI.00051-06

Hoenen, T., Shabman, R.S., Groseth, A., Herwig, A., Weber, M., Schudt, G., Dolnik, O., Basler, C.F., Becker, S., Feldmann, H., 2012. Inclusion Bodies Are a Site of Ebolavirus Replication. J. Virol. 86, 11779–11788. doi:10.1128/JVI.01525-12

Hoshino, K., Sugiyama, T., Matsumoto, M., Tanaka, T., Saito, M., Hemmi, H., Ohara, O., Akira, S., Kaisho, T., 2006. IκB kinase-α is critical for interferon-α production induced by Toll-like receptors 7 and 9. Nature 440, 949–953. doi:10.1038/nature04641

Huang, Y., Xu, L., Sun, Y., Nabel, G.J., 2002. The Assembly of Ebola Virus Nucleocapsid Requires Virion-Associated Proteins 35 and 24 and Posttranslational Modification of Nucleoprotein. Mol. Cell 10, 307–316. doi:10.1016/S1097-2765(02)00588-9

Hunt, C.L., Kolokoltsov, A. a, Davey, R. a, Maury, W., 2011. The Tyro3 receptor kinase Axl enhances macropinocytosis of Zaire ebolavirus. J. Virol. 85, 334–347. doi:10.1128/JVI.01278-09

ICTV, 2011. Filoviridae - ICTV 9th Report [WWW Document]. Int. Comm. Taxon. Viruses Reports. URL https://talk.ictvonline.org/ictv-reports/ictv_9th_report/negative-sense-rna-viruses-2011/w/negrna_viruses/197/filoviridae (accessed 3.8.17).

John, S.P., Wang, T., Steffen, S., Longhi, S., Schmaljohn, C.S., Jonsson, C.B., 2007. Ebola virus VP30 is an RNA binding protein. J. Virol. 81, 8967–76. doi:10.1128/JVI.02523-06

Kabsch, W., Sander, C., 1983. Dictionary of protein secondary structure: pattern recognition of hydrogen-bonded and geometrical features. Biopolymers 22, 2577–637. doi:10.1002/bip.360221211

Kaisho, T., Akira, S., 2001. Dendritic-cell function in Toll-like receptor- and MyD88-knockout mice. Trends Immunol. 22, 78–83. doi:10.1016/S1471-4906(00)01811-1

Kajihara, M., Takada, A., 2015. Host Cell Factors Involved in Filovirus Infection. Curr. Trop. Med. Reports 2, 30–40. doi:10.1007/s40475-015-0039-x

Kawai, T., Akira, S., 2007. TLR signaling. Semin. Immunol. 19, 24–32. doi:10.1016/j.smim.2006.12.004

Kawai, T., Takahashi, K., Sato, S., Coban, C., Kumar, H., Kato, H., Ishii, K.J., Takeuchi, O., Akira, S., 2005. IPS-1, an adaptor triggering RIG-I- and Mda5-mediated type I interferon induction. Nat. Immunol. 6, 981–988. doi:10.1038/ni1243

Khiar, S., Pietrancosta, N., Vidalain, P.-O., 2015. Stimuler la réponse interféron de type I avec des petites molécules : le renouveau d'une vieille idée. Biol. Aujourdhui. 209, 145–159. doi:10.1051/jbio/2015015

Kimberlin, C.R., Bornholdt, Z. a, Li, S., Woods, V.L., MacRae, I.J., Saphire, E.O., 2010. Ebolavirus VP35 uses a bimodal strategy to bind dsRNA for innate immune suppression. Proc. Natl. Acad. Sci. U. S. A. 107, 314–9. doi:10.1073/pnas.0910547107

Kirchdoerfer, R.N., Moyer, C.L., Abelson, D.M., Saphire, O., 2016. The Ebola Virus VP30-NP Interaction Is a Regulator of Viral RNA Synthesis 1–22. doi:10.1371/journal.ppat.1005937

Kondratowicz, A.S., Lennemann, N.J., Sinn, P.L., Davey, R. a, Hunt, C.L., Moller-Tank, S., Meyerholz, D.K., Rennert, P., Mullins, R.F., Brindley, M., Sandersfeld, L.M., Quinn, K., Weller,

M., McCray, P.B., Chiorini, J., Maury, W., 2011. T-cell immunoglobulin and mucin domain 1 (TIM-1) is a receptor for Zaire Ebolavirus and Lake Victoria Marburgvirus. Proc. Natl. Acad. Sci. U. S. A. 108, 8426–31. doi:10.1073/pnas.1019030108

Ksouri, R., Ksouri, W.M., Jallali, I., Debez, A., Magné, C., Hiroko, I., Abdelly, C., 2011. Medicinal halophytes: potent source of health promoting biomolecules with medical, nutraceutical and food applications. Crit. Rev. Biotechnol. 32, 1–38. doi:10.3109/07388551.2011.630647

Kuhn, J.H., 2008. Filovirses: A compendium of 40 years of epidemiological, clinical, and laboratory studies. SpringerWeinNew York.

Kuhn, J.H., Becker, S., Ebihara, H., Geisbert, T.W., Johnson, K.M., Kawaoka, Y., Lipkin, W.I., Negredo, A.I., Netesov, S. V., Nichol, S.T., Palacios, G., Peters, C.J., Tenorio, A., Volchkov, V.E., Jahrling, P.B., 2010. Proposal for a revised taxonomy of the family Filoviridae: Classification, names of taxa and viruses, and virus abbreviations. Arch. Virol. 155, 2083–2103. doi:10.1007/s00705-010-0814-x

Le Guenno, B., Formenty, P., Wyers, M., Gounon, P., Walker, F., Boesch, C., 1995. Isolation and partial characterisation of a new strain of Ebola virus. Lancet 345, 1271–1274. doi:10.1016/S0140-6736(95)90925-7

Lee, J.E., Fusco, M.L., Hessell, A.J., Oswald, W.B., Burton, D.R., Saphire, E.O., 2008. Structure of the Ebola virus glycoprotein bound to an antibody from a human survivor. Nature 454, 177–82. doi:10.1038/nature07082

Lee, J.E., Saphire, E.O., 2009. Ebolavirus glycoprotein structure and mechanism of entry. Future Virol. 4, 621–635. doi:10.2217/fvl.09.56

Leung, D.W., Ginder, N.D., Fulton, D.B., Nix, J., Basler, C.F., Honzatko, R.B., Amarasinghe, G.K., 2009a. Structure of the Ebola VP35 interferon inhibitory domain. Proc. Natl. Acad. Sci. 106, 411–416. doi:10.1073/pnas.0807854106

Leung, D.W., Ginder, N.D., Nix, J.C., Basler, C.F., Honzatko, R.B., Amarasinghe, G.K., 2009b. Expression, purification, crystallization and preliminary X-ray studies of the Ebola VP35 interferon inhibitory domain. Acta Crystallogr. Sect. F Struct. Biol. Cryst. Commun. 65, 163–165. doi:10.1107/S1744309108044187

Leung, D.W., Prins, K.C., Borek, D.M., Farahbakhsh, M., Tufariello, J.M., Ramanan, P., Nix, J.C., Helgeson, L. a, Otwinowski, Z., Honzatko, R.B., Basler, C.F., Amarasinghe, G.K., 2010a. Structural basis for dsRNA recognition and interferon antagonism by Ebola VP35. Nat. Struct. Mol. Biol. 17, 165–172. doi:10.1038/nsmb.1765

Leung, D.W., Shabman, R.S., Farahbakhsh, M., Prins, K.C., Borek, D.M., Wang, T., M??hlberger, E., Basler, C.F., Amarasinghe, G.K., Mühlberger, E., Basler, C.F., Amarasinghe, G.K., 2010b. Structural and functional characterization of Reston Ebola virus VP35 interferon inhibitory domain. J. Mol. Biol. 399, 347–357. doi:10.1016/j.jmb.2010.04.022

Luthra, P., Ramanan, P., Mire, C.E., Weisend, C., Tsuda, Y., Yen, B., Liu, G., Leung, D.W., Geisbert, T.W., Ebihara, H., Amarasinghe, G.K., Basler, C.F., 2013. Mutual antagonism between the ebola virus VP35 protein and the RIG-I activator PACT determines infection outcome. Cell Host Microbe 14, 74–84. doi:10.1016/j.chom.2013.06.010

Mahanty, S., Bray, M., 2004. Pathogenesis of filoviral haemorrhagic fevers. Lancet Infect. Dis. 4, 487–498. doi:10.1016/S1473-3099(04)01103-X

Martin, B., Canard, B., Decroly, E., 2017. Filovirus proteins for antiviral drug discovery: Structure/function bases of the replication cycle. Antiviral Res. 141, 48–61. doi:10.1016/j.antiviral.2017.02.004

Martin, B., Hoenen, T., Canard, B., Decroly, E., 2016. Filovirus proteins for antiviral drug discovery: A structure/function analysis of surface glycoproteins and virus entry. Antiviral Res. 135, 1–14. doi:10.1016/j.antiviral.2016.09.001

Mate, S.E., Kugelman, J.R., Nyenswah, T.G., Ladner, J.T., Wiley, M.R., Cordier-Lassalle, T., Christie, A., Schroth, G.P., Gross, S.M., Davies-Wayne, G.J., Shinde, S.A., Murugan, R., Sieh, S.B., Badio, M., Fakoli, L., Taweh, F., de Wit, E., van Doremalen, N., Munster, V.J., Pettitt, J., Prieto, K., Humrighouse, B.W., Ströher, U., DiClaro, J.W., Hensley, L.E., Schoepp, R.J., Safronetz, D., Fair, J., Kuhn, J.H., Blackley, D.J., Laney, A.S., Williams, D.E., Lo, T., Gasasira, A., Nichol, S.T., Formenty, P., Kateh, F.N., De Cock, K.M., Bolay, F., Sanchez-Lockhart, M., Palacios, G., 2015. Molecular Evidence of Sexual Transmission of Ebola Virus. N. Engl. J. Med. 373, 2448–2454. doi:10.1056/NEJMoa1509773

McCartney, S.A., Colonna, M., 2009. Viral sensors: Diversity in pathogen recognition. Immunol. Rev. 227, 87–94. doi:10.1111/j.1600-065X.2008.00726.x

Medini, F., Ksouri, R., Falleh, H., Megdiche, W., Trabelsi, N., Abdelly, C., 2011. Effects of physiological stage and solvent on polyphenol composition, antioxidant and antimicrobial activities of Limonium densiflorum. J. Med. Plants Res. 5, 6719–6730. doi:10.5897/JMPR11.684

Mehedi, M., Falzarano, D., Seebach, J., Hu, X., Carpenter, M.S., Schnittler, H.-J., Feldmann, H., 2011. A new Ebola virus nonstructural glycoprotein expressed through RNA editing. J. Virol. 85, 5406–5414. doi:10.1128/JVI.02190-10

Messaoudi, I., Amarasinghe, G.K., Basler, C.F., 2015. Filovirus pathogenesis and immune evasion: insights from Ebola virus and Marburg virus. Nat. Rev. Microbiol. 13, 663–76. doi:10.1038/nrmicro3524

Meylan, E., Curran, J., Hofmann, K., Moradpour, D., Binder, M., Bartenschlager, R., Tschopp, J., 2005. Cardif is an adaptor protein in the RIG-I antiviral pathway and is targeted by hepatitis C virus. Nature 437, 1167–1172. doi:10.1038/nature04193

Miller, E.H., Obernosterer, G., Raaben, M., Herbert, A.S., Deffieu, M.S., Krishnan, A., Ndungo, E., Sandesara, R.G., Carette, J.E., Kuehne, A.I., Ruthel, G., Pfeffer, S.R., Dye, J.M., Whelan, S.P., Brummelkamp, T.R., Chandran, K., 2012. Ebola virus entry requires the host-programmed recognition of an intracellular receptor. EMBO J. 31, 1947–60. doi:10.1038/emboj.2012.53

Modrof, J., Becker, S., Mühlberger, E., 2003. Ebola Virus Transcription Activator VP30 Is a Zinc-Binding Protein. J. Virol. 77, 3334–3338. doi:10.1128/JVI.77.5.3334–3338.2003

Moller-Tank, S., Kondratowicz, A.S., Davey, R.A., Rennert, P.D., Maury, W., 2013. Role of the phosphatidylserine receptor TIM-1 in enveloped-virus entry. J. Virol. 87, 8327–41. doi:10.1128/JVI.01025-13

Motulsky, H.J., Neubig, R.R., 2010. Analyzing binding data. Curr. Protoc. Neurosci. doi:10.1002/0471142301.ns0705s19

Mühlberger, E., 2007. Filovirus replication and transcription. Future Virol. 2, 205–215. doi:10.2217/17460794.2.2.205.

Mühlberger, E., Weik, M., Volchkov, V.E., Klenk, H.D., Becker, S., 1999. Comparison of the transcription and replication strategies of marburg virus and Ebola virus by using artificial replication systems. J. Virol. 73, 2333–42.

Murray, A.P., Rodriguez, S., Frontera, M.A., Tomas, M.A., Mulet, M.C., 2004. Antioxidant Metabolites from Limonium brasiliense (Boiss.) Kuntze. Zeitschrift für Naturforsch. C 59, 5–8. doi:10.1515/znc-2004-7-804

Negredo, A., Palacios, G., Vázquez-Morón, S., González, F., Dopazo, H., Molero, F., Juste, J., Quetglas, J., Savji, N., de la Cruz Martínez, M., Herrera, J.E., Pizarro, M., Hutchison, S.K., Echevarría, J.E., Lipkin, W.I., Tenorio, A., 2011. Discovery of an Ebolavirus-Like Filovirus in Europe. PLoS Pathog. 7, e1002304. doi:10.1371/journal.ppat.1002304

Neumann, G., Feldmann, H., Watanabe, S., Lukashevich, I., 2002. Reverse Genetics Demonstrates that Proteolytic Processing of the Ebola Virus Glycoprotein Is Not Essential for Replication in Cell Culture Reverse Genetics Demonstrates that Proteolytic Processing of the Ebola Virus Glycoprotein Is Not Essential for Repli. J. Virol. 76, 406–410. doi:10.1128/JVI.76.1.406

Neumann, G., Geisbert, T.W., Ebihara, H., Geisbert, J.B., Daddario-DiCaprio, K.M., Feldmann, H., Kawaoka, Y., 2007. Proteolytic processing of the Ebola virus glycoprotein is not critical for Ebola virus replication in nonhuman primates. J. Virol. 81, 2995–8. doi:10.1128/JVI.02486-06

Neumann, G., Watanabe, S., Kawaoka, Y., 2009. Characterization of Ebolavirus regulatory genomic regions. Virus Res. 144, 1–7. doi:10.1016/j.virusres.2009.02.005

Newman, D.J., Cragg, G.M., 2012. Natural Products As Sources of New Drugs over the 30 Years from 1981 to 2010. J. Nat. Prod. 75, 311–335. doi:10.1021/np200906s

Nie, L.-D., Shi, X.-X., Ko, K.H., Lu, W.-D., 2009. A Short and Practical Synthesis of Oseltamivir Phosphate (Tamiflu) from (−)-Shikimic Acid [†]. J. Org. Chem. 74, 3970–3973. doi:10.1021/jo900218k

Noda, T., Ebihara, H., Muramoto, Y., Fujii, K., Takada, A., Sagara, H., Jin, H.K., Kida, H., Feldmann, H., Kawaoka, Y., 2006. Assembly and budding of Ebolavirus. PLoS Pathog. 2, 0864–0872. doi:10.1371/journal.ppat.0020099

Olejnik, J., Ryabchikova, E., Corley, R.B., Mühlberger, E., 2011. Intracellular events and cell fate in filovirus infection. Viruses 3, 1501–1531. doi:10.3390/v3081501

Ong, K.C., Khoo, H.-E., 1997. Biological effects of myricetin. Gen. Pharmacol. Vasc. Syst. 29, 121–126. doi:10.1016/S0306-3623(96)00421-1

Ono, K., Nakane, H., 1990. Mechanisms of Inhibition of Various Cellular DNA and RNA Polymerases

by Several Flavonoids. J Biochem 108, 609–613.

Palombo, E.A., 2011. Traditional Medicinal Plant Extracts and Natural Products with Activity against Oral Bacteria: Potential Application in the Prevention and Treatment of Oral Diseases. Evidence-Based Complement. Altern. Med. 2011, 1–15. doi:10.1093/ecam/nep067

Panne, D., Maniatis, T., Harrison, S.C., 2007. An Atomic Model of the Interferon-beta Enhanceosome. Cell 129, 1111–1123. doi:10.1016/j.cell.2007.05.019

Parkin, J., Cohen, B., 2001. An overview of the immune system. Lancet 357, 1777–1789. doi:10.1016/S0140-6736(00)04904-7

Parrinello, M., Rahman, A., 1981. Polymorphic transitions in single crystals: A new molecular dynamics method. J. Appl. Phys. 52, 7182–7190. doi:10.1063/1.328693

Pistelli, L., Bertoli, A., Zucconelli, S., Morelli, I., Panizzi, L., Menichini, F., 2000. Antimicrobial activity of crude extracts and pure compounds of Hypericum hircinum. Fitoterapia 71, 138–140. doi:10.1016/S0367-326X(00)00189-1

Prins, K.C., Binning, J.M., Shabman, R.S., Leung, D.W., Amarasinghe, G.K., Basler, C.F., 2010a. Basic Residues within the Ebolavirus VP35 Protein Are Required for Its Viral Polymerase Cofactor Function. J. Virol. 84, 10581–10591. doi:10.1128/JVI.00925-10

Prins, K.C., Cárdenas, W.B., Basler, C.F., 2009. Ebola virus protein VP35 impairs the function of interferon regulatory factor-activating kinases IKKepsilon and TBK-1. J. Virol. 83, 3069–3077. doi:10.1128/JVI.01875-08

Prins, K.C., Delpeut, S., Leung, D.W., Reynard, O., Volchkova, V. a, Reid, S.P., Ramanan, P., Cárdenas, W.B., Amarasinghe, G.K., Volchkov, V.E., Basler, C.F., 2010b. Mutations Abrogating VP35 Interaction with Double-Stranded RNA Render Ebola Virus Avirulent in Guinea Pigs. J. Virol. 84, 3004–3015. doi:10.1128/JVI.02459-09

Qiu, X., Wong, G., Audet, J., Bello, A., Fernando, L., Alimonti, J.B., Fausther-Bovendo, H., Wei, H., Aviles, J., Hiatt, E., Johnson, A., Morton, J., Swope, K., Bohorov, O., Bohorova, N., Goodman, C., Kim, D., Pauly, M.H., Velasco, J., Pettitt, J., Olinger, G.G., Whaley, K., Xu, B., Strong, J.E., Zeitlin, L., Kobinger, G.P., 2014. Reversion of advanced Ebola virus disease in nonhuman primates with ZMapp. Nature 514, 47–53. doi:10.1038/nature13777

Quassinti, L., Lupidi, G., Maggi, F., Sagratini, G., Papa, F., Vittori, S., Bianco, A., Bramucci, M., 2013. Antioxidant and antiproliferative activity of Hypericum hircinum L. subsp. majus (Aiton) N. Robson essential oil. Nat. Prod. Res. 27, 862–8. doi:10.1080/14786419.2012.677044

Ramanan, P., Shabman, R.S., Brown, C.S., Amarasinghe, G.K., Basler, C.F., Leung, D.W., 2011. Filoviral immune evasion mechanisms. Viruses 3, 1634–1649. doi:10.3390/v3091634

Randall, R.E., Goodbourn, S., 2008. Interferons and viruses: An interplay between induction, signalling, antiviral responses and virus countermeasures. J. Gen. Virol. 89, 1–47. doi:10.1099/vir.0.83391-0

Reid, S.P., Cárdenas, W.B., Basler, C.F., 2005. Homo-oligomerization facilitates the interferon-antagonist activity of the ebolavirus VP35 protein. Virology 341, 179–189. doi:10.1016/j.virol.2005.06.044

Reid, S.P., Leung, L.W., Hartman, A.L., Martinez, O.., Shaw, M.L., Carbonnelle, C.., Volchkov, V.E., Nichol, S.T., Basler, C.F., 2006. Ebola Virus VP24 Binds Karyopherin 1 and Blocks STAT1 Nuclear Accumulation. J. Virol. 80, 5156–5167. doi:10.1128/JVI.02349-05

Reikine, S., Nguyen, J.B., Modis, Y., 2014. Pattern recognition and signaling mechanisms of RIG-I and MDA5. Front. Immunol. 5, 1–7. doi:10.3389/fimmu.2014.00342

Rid, A., Emanuel, E.J., 2014. Ethical considerations of experimental interventions in the Ebola outbreak. Lancet 384, 1896–1899. doi:10.1016/S0140-6736(14)61315-5

Sadler, A.J., Williams, B.R.G., 2008. Interferon-inducible antiviral effectors. Nat. Rev. Immunol. 8, 559–568. doi:10.1038/nri2314

Sagratini, G., Ricciutelli, M., Vittori, S., Öztürk, N., Öztürk, Y., Maggi, F., 2008. Phytochemical and antioxidant analysis of eight Hypericum taxa from Central Italy. Fitoterapia 79, 210–213. doi:10.1016/j.fitote.2007.11.011

Sali, A., Blundell, T.L., 1993. Comparative protein modelling by satisfaction of spatial restraints. J. Mol. Biol. 234, 779–815. doi:10.1006/jmbi.1993.1626

Sanchez, A., Geisbert, T.W., Feldmann, H., 2007. Filoviridae: Marburg and Ebola Viruses, in: Fields, B.N., Knipe, D.M., Howley, P.M. (Eds.), Fields Virology. Wolters Kluwer Health/Lippincott Williams & Wilkins, Philadelphia, pp. 1409–1448.

Sanchez, A., Kiley, M.P., Holloway, B.P., Auperin, D.D., 1993. Sequence analysis of the Ebola virus genome: organization, genetic elements, and comparison with the genome of Marburg virus.

Virus Res. 29, 215–240. doi:10.1016/0168-1702(93)90063-S

Sanchez, A., Lukwiya, M., Bausch, D., Mahanty, S., Sanchez, A.J., Wagoner, K.D., Rollin, P.E., 2004. Analysis of Human Peripheral Blood Samples from Fatal and Nonfatal Cases of Ebola (Sudan) Hemorrhagic Fever : Cellular Responses , Virus Load , and Nitric Oxide Levels Analysis of Human Peripheral Blood Samples from Fatal and Nonfatal Cases of Ebola (S. J. Morphol. 78, 10370–10377. doi:10.1128/JVI.78.19.10370

Satoh, T., Kato, H., Kumagai, Y., Yoneyama, M., Sato, S., Matsushita, K., Tsujimura, T., Fujita, T., Akira, S., Takeuchi, O., 2010. LGP2 is a positive regulator of RIG-I- and MDA5-mediated antiviral responses. Proc. Natl. Acad. Sci. U. S. A. 107, 1512–7. doi:10.1073/pnas.0912986107

Schornberg, K., Matsuyama, S., Kabsch, K., Delos, S., Bouton, A., White, J., 2006. Role of Endosomal Cathepsins in Entry Mediated by the Ebola Virus Glycoprotein Role of Endosomal Cathepsins in Entry Mediated by the Ebola Virus Glycoprotein. J. Virol. 80, 4174–4178. doi:10.1128/JVI.80.8.4174

Schümann, M., Gantke, T., Mühlberger, E., 2009. Ebola virus VP35 antagonizes PKR activity through its C-terminal interferon inhibitory domain. J. Virol. 83, 8993–7. doi:10.1128/JVI.00523-09

Sealy, T.K., Erickson, B.R., Taboy, C.H., Ströher, U., Towner, J.S., Andrews, S.E., Rose, L.E., Weirich, E., Lowe, L., Klena, J.D., Spiropoulou, C.F., Rayfield, M.A., Bird, B.H., 2016. Laboratory Response to Ebola - West Africa and United States. MMWR Suppl. 65, 44–49. doi:10.15585/mmwr.su6503a7

Seth, R.B., Sun, L., Ea, C.-K., Chen, Z.J., 2005. Identification and Characterization of MAVS, a Mitochondrial Antiviral Signaling Protein that Activates NF-κB and IRF3. Cell 122, 669–682. doi:10.1016/j.cell.2005.08.012

Siegal, F.P., Kadowaki, N., Shodell, M., Fitzgerald-bocarsly, P.A., Shah, K., Ho, S., 1999. The Nature of the Principal Type 1 Interferon – Producing Cells in Human Blood. Science (80-.). 284, 1835–1838. doi:10.1126/science.284.5421.1835

Stahelin, R. V., 2014. Membrane binding and bending in Ebola VP40 assembly and egress. Front. Microbiol. 5, 1–12. doi:10.3389/fmicb.2014.00300

Stein, R.A., 2015. What is Ebola? Int. J. Clin. Pract. 69, 49–58. doi:10.1111/ijcp.12593

Swietnicki, W., 2006. Folding aggregated proteins into functionally active forms. Curr. Opin. Biotechnol. 17, 367–372. doi:10.1016/j.copbio.2006.05.011

Takada, A., 2012. Filovirus tropism: Cellular molecules for viral entry. Front. Microbiol. 3, 1–9. doi:10.3389/fmicb.2012.00034

Tarbouriech, N., Curran, J., Ruigrok, R.W., Burmeister, W.P., 2000. Tetrameric coiled coil domain of Sendai virus phosphoprotein. Nat. Struct. Biol. 7, 777–81. doi:10.1038/79013

Thermo Fisher Scientific Inc, 2011. Pierce ® Nickel Coated Plates Instructions.

Thompson, J.M., Iwasaki, A., 2008. Toll-like receptors regulation of viral infection and disease ☆ 60, 786–794. doi:10.1016/j.addr.2007.11.003

Thompson, A.J. V, Locarnini, S. a, 2007. Toll-like receptors, RIG-I-like RNA helicases and the antiviral innate immune response. Immunol. Cell Biol. 85, 435–45. doi:10.1038/sj.icb.7100100

Topal, M., Gocer, H., Topal, F., Kalin, P., Köse, L.P., Gülçin, İ., Çakmak, K.C., Küçük, M., Durmaz, L., Gören, A.C., Alwasel, S.H., 2016. Antioxidant, antiradical, and anticholinergic properties of cynarin purified from the Illyrian thistle (Onopordum illyricum L.). J. Enzyme Inhib. Med. Chem. 31, 266–275. doi:10.3109/14756366.2015.1018244

Towner, J.S., Pourrut, X., Nichol, S.T., Leroy, E.M., 2007. Marburg Virus Infection Detected in a Common African. doi:10.1371/journal.pone.0000764

Towner, J.S., Sealy, T.K., Khristova, M.L., Albariño, C.G., Conlan, S., Reeder, S.A., Quan, P.L., Lipkin, W.I., Downing, R., Tappero, J.W., Okware, S., Lutwama, J., Bakamutumaho, B., Kayiwa, J., Comer, J.A., Rollin, P.E., Ksiazek, T.G., Nichol, S.T., 2008. Newly discovered Ebola virus associated with hemorrhagic fever outbreak in Uganda. PLoS Pathog. 4, e1000212. doi:10.1371/journal.ppat.1000212

Trad, M.A., Naughton, W., Yeung, A., Mazlin, L., O'sullivan, M., Gilroy, N., Fisher, D.A., Stuart, R.L., 2017. Ebola virus disease: An update on current prevention and management strategies. J. Clin. Virol. 86, 5–13. doi:10.1016/j.jcv.2016.11.005

Trunschke, M., Conrad, D., Enterlein, S., Olejnik, J., Brauburger, K., Mühlberger, E., 2013. The L-VP35 and L-L interaction domains reside in the amino terminus of the Ebola virus L protein and are potential targets for antivirals. Virology 441, 135–145. doi:10.1016/j.virol.2013.03.013

Venkataraman, T., Valdes, M., Elsby, R., Kakuta, S., Caceres, G., Saijo, S., Iwakura, Y., Barber, G.N., 2007. Loss of DExD/H box RNA helicase LGP2 manifests disparate antiviral responses. J

Immunol 178, 6444–6455. doi:178/10/6444 [pii]

Vilcek, J., 2003. Novel interferons. Nat. Immunol. 4, 8–9. doi:10.1038/ni0103-8

Volchkov, V.E., Volchkova, V.A., Chepurnov, A.A., Blinov, V.M., Dolnik, O., Netesov, S. V, Feldmann, H., 1999. Characterization of the L gene and 5' trailer region of Ebola virus. J. Gen. Virol. 80, 355–362. doi:10.1099/0022-1317-80-2-355

Volchkova, V.A., Klenk, H.-D., Volchkov, V.E., 1999. Delta-Peptide Is the Carboxy-Terminal Cleavage Fragment of the Nonstructural Small Glycoprotein sGP of Ebola Virus. Virology 265, 164–171. doi:10.1006/viro.1999.0034

Wang, Y.P., Zhang, X.E., Wei, H.P., 2011. Laboratory detection and diagnosis of filoviruses. Virol. Sin. 26, 73–80. doi:10.1007/s12250-011-3186-9

Watanabe, S., Noda, T., Kawaoka, Y., 2006. Functional Mapping of the Nucleoprotein of Ebola Virus Functional Mapping of the Nucleoprotein of Ebola Virus. Society 80, 3743–3751. doi:10.1128/JVI.80.8.3743

Weingartl, H.M., Embury-Hyatt, C., Nfon, C., Leung, A., Smith, G., Kobinger, G., 2012. Transmission of Ebola virus from pigs to non-human primates. Sci. Rep. 2, 811. doi:10.1038/srep00811

White, J.M., Schornberg, K.L., 2012. A new player in the puzzle of filovirus entry. Nat. Rev. Microbiol. 135, 612–615. doi:10.1038/nrmicro2764

Wool-Lewis, R.J., Bates, P., 1999. Endoproteolytic Processing of the Ebola Virus Envelope Glycoprotein : Cleavage Is Not Required for Function 73, 1419–1426.

World Health Organization, 2016a. Ebola Situation Report [WWW Document]. URL http://apps.who.int/ebola/current-situation/ebola-situation-report-30-march-2016 (accessed 3.13.17).

World Health Organization, 2016b. Clinical management of patients with viral haemorrhagic fever: A pocket guide for front-line workers.

World Health Organization, 2015. Categorization and prioritization of drugs for consideration for testing or use in patients infected with Ebola 1–8.

Xu, L.-G., Wang, Y.-Y., Han, K.-J., Li, L.-Y., Zhai, Z., Shu, H.-B., 2005. VISA Is an Adapter Protein Required for Virus-Triggered IFN-β Signaling. Mol. Cell 19, 727–740. doi:10.1016/j.molcel.2005.08.014

Yamamura, I.S., 1974. Muscarinic Cholinergic Binding in Rat Brain. Proc. Natl. Acad. Sci. U. S. A. 71, 1725–1729.

Zawilińska, B., Kosz-Vnenchak, M., 2014. General Introduction Into the Ebola Virus Biology and Disease. Folia Med. Cracov. 3, 57–65.

Zhang, A.P.P., Bornholdt, Z.A., Liu, T., Abelson, D.M., Lee, D.E., Li, S., Woods, V.L., Saphire, E.O., 2012. The Ebola Virus Interferon Antagonist VP24 Directly Binds STAT1 and Has a Novel, Pyramidal Fold. PLoS Pathog. 8, e1002550. doi:10.1371/journal.ppat.1002550

Zhang, J.-H., Chung, T.D.Y., Oldenburg, K.R., 1999. A Simple statistical parameter for use in evaluation and validation of high throughput screening assays.pdf, Journal of Biomolecular Screening. Sage PublicationsSage CA: Thousand Oaks, CA. doi:10.1177/108705719900400206

Zinzula, L., Esposito, F., Mühlberger, E., Trunschke, M., Conrad, D., Piano, D., Tramontano, E., 2009. Purification and functional characterization of the full length recombinant Ebola virus VP35 protein expressed in E. coli. Protein Expr. Purif. 66, 113–119. doi:10.1016/j.pep.2009.02.008

Zinzula, L., Esposito, F., Pala, D., Tramontano, E., 2012. DsRNA binding characterization of full length recombinant wild type and mutants Zaire ebolavirus VP35. Antiviral Res. 93, 354–363. doi:10.1016/j.antiviral.2012.01.005

Zinzula, L., Tramontano, E., 2013. Strategies of highly pathogenic RNA viruses to block dsRNA detection by RIG-I-like receptors: Hide, mask, hit. Antiviral Res. 100, 615–635. doi:10.1016/j.antiviral.2013.10.002